AD_____

Award Number: W81XWH-08-2-0207

TITLE: Measuring Intracranial Pressure and Correlation with Severity of Blast Traumatic Brain Injury

PRINCIPAL INVESTIGATOR: Pamela J. VandeVord, Ph.D.

CONTRACTING ORGANIZATION:

Metropolitan Detroit Research and Education Foundation
Detroit, MI 48201

REPORT DATE: January 2013

TYPE OF REPORT: Final Report

PREPARED FOR: U.S. Army Medical Research and Materiel Command
Fort Detrick, Maryland 21702-5012

DISTRIBUTION STATEMENT: Approved for Public Release;
Distribution Unlimited

The views, opinions and/or findings contained in this report are those of the author(s) and should not be construed as an official Department of the Army position, policy or decision unless so designated by other documentation.

REPORT DOCUMENTATION PAGE

Form Approved
OMB No. 0704-0188

Public reporting burden for this collection of information is estimated to average 1 hour per response, including the time for reviewing instructions, searching existing data sources, gathering and maintaining the data needed, and completing and reviewing this collection of information. Send comments regarding this burden estimate or any other aspect of this collection of information, including suggestions for reducing this burden to Department of Defense, Washington Headquarters Services, Directorate for Information Operations and Reports (0704-0188), 1215 Jefferson Davis Highway, Suite 1204, Arlington, VA 22202-4302. Respondents should be aware that notwithstanding any other provision of law, no person shall be subject to any penalty for failing to comply with a collection of information if it does not display a currently valid OMB control number. **PLEASE DO NOT RETURN YOUR FORM TO THE ABOVE ADDRESS.**

1. REPORT DATE	2. REPORT TYPE	3. DATES COVERED
January 2013	Final Report	16 September 2008-15 December 2012

4. TITLE AND SUBTITLE
Measuring Intracranial Pressure and Correlation with Severity of Blast Traumatic Brain Injury.

5a. CONTRACT NUMBER
W81XWH-08-2-0207

5b. GRANT NUMBER
W81XWH-08-2-0207

5c. PROGRAM ELEMENT NUMBER

6. AUTHOR(S)
VandeVord, Pamela, J.

E-Mail: pvord@vt.edu

5d. PROJECT NUMBER

5e. TASK NUMBER

5f. WORK UNIT NUMBER

7. PERFORMING ORGANIZATION NAME(S) AND ADDRESS(ES)
Metropolitan Detroit Research and Education Foundation

Detroit, MI 48201

8. PERFORMING ORGANIZATION REPORT NUMBER

9. SPONSORING / MONITORING AGENCY NAME(S) AND ADDRESS(ES)
U.S. Army Medical Research and Materiel Command
Fort Detrick, Maryland 21702-5012

10. SPONSOR/MONITOR'S ACRONYM(S)
US AMRMC

11. SPONSOR/MONITOR'S REPORT NUMBER(S)

12. DISTRIBUTION / AVAILABILITY STATEMENT
Approved for Public Release; Distribution Unlimited

13. SUPPLEMENTARY NOTES

14. ABSTRACT
A greater understanding of the mechanism(s) of TBI due from overpressure exposure is critical to develop effective protection and treatments. Fundamental, yet unresolved, questions concern the mode of blast energy transfer to the brain as well as the consequent damage or disruptive mechanisms at the cellular level. The ultimate goal of this research effort is to determine the intracranial pressure (ICP) responses to blast exposure. The objective of this research is to understand how pressure is transmitted through the brain and ascertain the relationship between levels of pressure transmission with severity of brain injury. Injury severity parameters were investigated during this year of the proposal. We used a shock tube model in which non-instrumented animals were be subjected to a single shock wave. Groups of animals were subjected to a different magnitude of overpressure. We present several neurological outcomes and neuropathologies that are unique to each pressure group. Overall, the large amount of data indicates molecular changes that occur depending on blast energy level.

15. SUBJECT TERMS
Blast, Overpressure, Traumatic Brain Injury, Animal Models

16. SECURITY CLASSIFICATION OF:			17. LIMITATION OF ABSTRACT	18. NUMBER OF PAGES	19a. NAME OF RESPONSIBLE PERSON
				62	USAMRMC
a. REPORT	b. ABSTRACT	c. THIS PAGE			19b. TELEPHONE NUMBER *(include area code)*
U	U	U	UU		

Table of Contents

Page

Introduction…….. 02

Body…….. 02

Key Research Accomplishments…….. 29

Reportable Outcomes…….. 30

Conclusion…….. 31

References…….. 31

Appendices…….. 34

Introduction:

A greater understanding of the mechanism(s) of TBI due from overpressure exposure is critical to develop effective protection and treatments. Fundamental, yet unresolved, questions concern the mode of blast energy transfer to the brain as well as the consequent damage or disruptive mechanisms at the cellular level. The ultimate goal of this research effort was to determine the intracranial pressure (ICP) responses to blast exposure. The objective of this research was to understand how pressure is transmitted through the brain and ascertain the relationship between levels of pressure transmission with severity of brain injury. The tasks of this proposal were to (1) map the transient ICP pressure as a function of blast magnitude (2) map the transient ICP as a function of head orientation and (3) ascertain injury severity as a function of ICP. We used an *in vivo* model in which animals were subjected to a series of systematic shock-tube studies of blast-stress transmission to the brain. The proposed research is *significant* because resolution of the mode of energy transfer and the induced stress states within the brain will allow for evaluations of mitigation/protective techniques, as well as design of experiments investigating live-cell response.

Body:

Blast-induced neurotrauma (BINT) is a hazardous condition developed after an exposure to a blast wave and is common in military, as well as civilian settings (1,2). Many debilitating effects are observed in individuals who have been exposed top this rapid overpressure, but there are still many gaps in the knowledge of the biomechanical and biomolecular mechanisms underlying BINT. There have been short-term deficits in cognitive function, such as decreased memory, attention, and intellectual effectiveness observed in addition to a delayed effect on mood and behavior (3,4). There has been a noticeable correlation in the long-term cognitive effects, like increased anxiety, and post-traumatic stress disorder (PTSD) (5-7). BINT has been underreported in the past due to the variable nature of when the most noticeable symptoms will reveal themselves (8,9). Understanding the mechanism of earlier biomarkers that could be associated with the presence of BINT will significantly catalyze diagnostics and treatment options for this disorder. In this study, the effects of exposure to blast waves with different peak pressures were analyzed in order to determine injury characteristics of varied blast exposure.

There are several variables that can be used to describe a blast wave, including peak pressure, positive phase duration, negative phase, rise time to peak and impulse. It is hypothesized that the crucial variable in determining injury is peak pressure, which can also be easily adjusted due to the action of the blast wave. The effects of exposure to varied peak overpressures have not been studied in depth and the mechanisms of molecular injury to induce BINT are likely different. ***Since the last progress report from 2011, we have completed several key experiments in order to accomplish our goals of this project.*** Since the first years of this award where focused on the biomechanical responses of the head to shock exposure, this past and final year are focused on investigating how the biomechanical responses are linked to injury severity. We further

identified key molecular and behavioral changes that are occurring and may contribute to the injury occurring from blast. During our testing we also discovered several challenges with respect to the blast model. A detailed description of our methodology, results and challenges are presented below.

Please note: We were granted a no-cost extension as the PI, Dr. Pamela VandeVord, moved to a new university (Virginia Tech) in July 2011. The project was only slightly delayed as new animal protocols were required. After the initial delay, the project continued quickly and results proved to be very interesting and important to the blast community.

SOW Task 1: Task 1: Determination of pressure wave through brain from blast exposure (Completed and Published)

SOW Task 2: Determination if an increase in overpressure magnitude affects pressure wave transmission (Completed and Published)

1.1 Animals and Testing Parameters.

This project began while the PI was faculty at Wayne State University (WSU) and a Health Scientist at the Detroit VAMC. Animals were purchased and housed at the WSU animal facility and all procedures were approved by the WSU Animal Investigation Committee prior to testing.

The first goal was to investigate how the blast energy was transmitted to the brain. A rodent model was used to measure ICP during blast exposure. Male Sprague Dawley rats 240-300g) were anesthetized with ketamine/xylazine (i.p. 100/20 mg/mL), their heads were shaved, and they were placed in a stereotaxic frame. A longitudinal incision allowed visualizing bregma and lambda. A 1mm hole was drilled in the skull for insertion of a guided cannula (18-gauge). The sites chosen for placement of the cannula was frontal cortex (+3AP/-2ML/-1DV). The cannula was anchored to the skull by using bone cement and two screws were used to reinforce the anchoring site. A dummy-cannula (cap) was screwed onto the cannula to close the opening while the animal was recovering. The scalp was sutured around the cannula, covering the screws and the bone cement. Seven days after surgery, the animal was anesthetized with ketamine/xylazine (i.p. 100/20 mg/mL) and a fiber optic sensor (FISO) was placed inside the brain cortex and then the cannula is sealed to provide a closed system. The animal was placed into a soft holder before exposure to shock waves. The holder positioned the rat's head at 44 inches from the open end of the tube, facing the shock wave frontally. By means of a long rod, the holder was connected to a trolley positioned outside the tube. The purpose of this moveable cart is to minimize stresses imparted to the specimen due to its restraint in the shock wave flow.

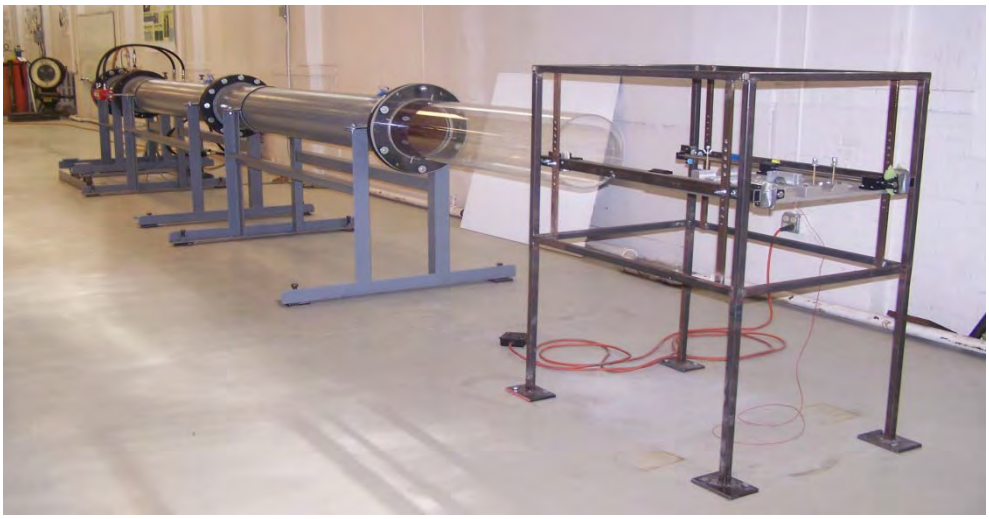

Figure 1. WSU Bioengineering Center Shock Tube.

Rats were subjected to a series of transient shock waves at 10 (68.95 kPa) and 14 psi peak pressures. Each pressure had triplicate tests conducted. ICP was measured, and then compared. After exposure, the anesthetized animals were immediately sacrificed by perfusion.

1.2 Results from ICP as a function of magnitude

A detail description of the results has been published by our group and is attached within the Appendix of this report (Leonardi et al 2010). To summarize, we were the first to recognize that ICP increased above the static pressure exposure. Another significant observation was that skull thickness contributed to ICP measurements. This is expected to have a significant impact in the biomechanical arena as we move forward on potential scaling rules for blast exposures. We hypothesized that the dynamic structural response modes of the skull, with the associated viscoelastic brain mass acting as a coupled mechanical system, controls the stress (pressure) waveform imparted to brain tissue under shock wave insult. The dynamic response modes of the skull, and hence imparted ICP, will relate to its particular geometry, material characteristics, physiology, and size. Thus, in order to better understand the biomechanics of the shock wave interaction with the rat skull, we conducted Computer Tomography (CT) analysis of the rat skull. CT scans were obtained for the rats by means of a microCT device (Scanco VivaCT, Scanco Medical). Variability of rat skull thickness throughout the skull was determined to help identify structural weaknesses that could be considered candidates for energy propagation. Skulls were scanned using a voltage of 70 kVp and current of 114 uA at a 30 um resolution with a 320 ms integration time. Thickness measurements were calculated by using MicroCT Analysis Software (Scanco Medical Inc.). Measurements were taken at the midpoint between the lambda and bregma sutures. Additionally, three-dimensional reconstruction of the skull was undertaken to study the overall skull geometry.

Figure 2 demonstrated an image that is representative of test subjects from this study in age and weight. Note the gaps, evident along the medial suture line between the lambda and bregma, and along the transverse dorsal suture crossing the bregma. Further anisotropic variation is derived from the ridges along the periphery of the skull. The superior-transverse and medial planar CT image of the brain case illustrates the locations of significant structural variation in the rat skull. The rostral terminus is a matrix of both bone and cartilage comprising the sinus cavities and orbital sockets while the caudal terminus is the occipital bone. Note the flat and unreinforced regions comprising the sagittal planes of the skull.

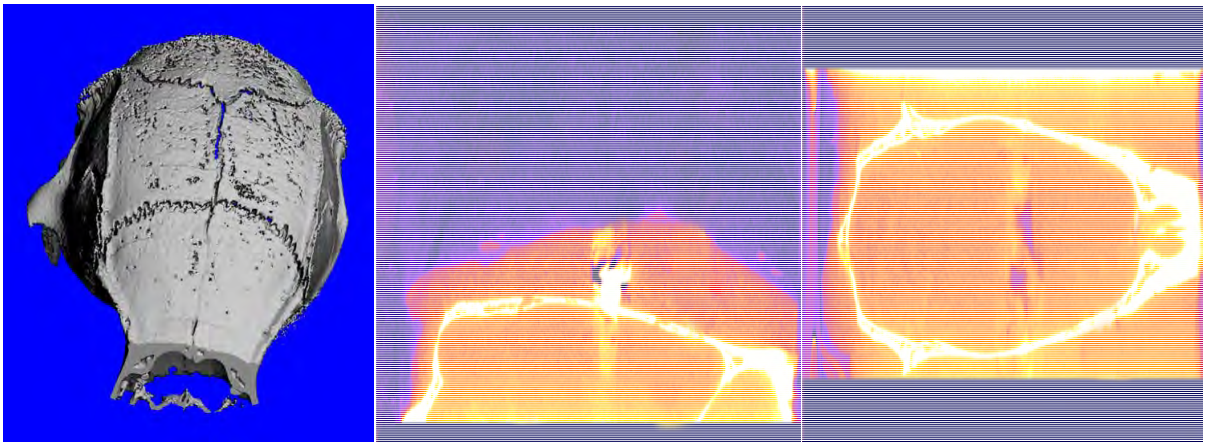

Figure 2. Micro-CT images collected from male rats.

Made clear by the series of tests conducted was the sensitivity of the brain-skull system to shock waves. With frontal exposure trials, the combination of structural elements, illustrated in Figure 2, including cranial sutures and sinus cavities in the rostral portion of the skull present a structure that is prone to protracted oscillatory behavior with independent rise times rivaling those of the initial insult. Since we have found that the rat skull is so thin and flexible, we had concerns that the addition of extra weight from the instrumentation may have an effect on the pressure recordings. We do not expect that one sensor should create much of an effect; however the proposed experiments state the use of several sensors mounted to the top of the skull which may have a significant effect. Because of this, we developed another route that was utilized for placing the sensor in the brain, which was entrance to the brain cavity via the occipital bones. We believe this methodology changes gave more realistic data on the ICP recordings, as noted in the next task.

Since the results from our previous experiments demonstrated that the rat skull is very thin and the addition of instrumentation to the top of the skull could potentially be influencing the data, we conducted an experiment to see if this was the case. The mounting of the fiber optic pressure sensor on the superior skull case may change the frequency response of the skull under shock wave loading. To address this concern a series of tests were developed to determine if mounting of the fiber optic pressure sensor on the occipital bone would report unique ICP profiles. Additionally, to investigate the effect of skull maturation on pressure recordings, older rats were

included in this study to determine if age affects the ICP response. Two different groups of rats were designated for this study. Group 1 consisted of male Sprague Dawley rats (N=12) that were instrumented with a cannula mounted to the superior aspect of skull (IC). Group 2 consisted of male Sprague Dawley rats (N=6) that were instrumented with a cannula mounted through the occipital bone (OIC). The superior mounted test set-up (IC) was similar to the methodology described prior and is demonstrated in Figure 3A. The installation procedure for the rats with the occipital mount (OIC) differed from the IC. In brief, rats were euthanized with an overdose of ketamine/xylazine. The scalp of the posterior region was removed. A small hole was then drilled into the bone to allow for the cannula to be placed. Screws were then drilled into the bone at four positions on the occipital bone to be used as anchor points. The cannula with its threaded cap was placed and bone cement was applied to hold the cannula system. Following curing of the cement (~ 10 minutes) the ICP sensor was then sealed within the cannula, with the sensor tip exposed beneath the region between the lambda and bregma (Figure 3B).

d

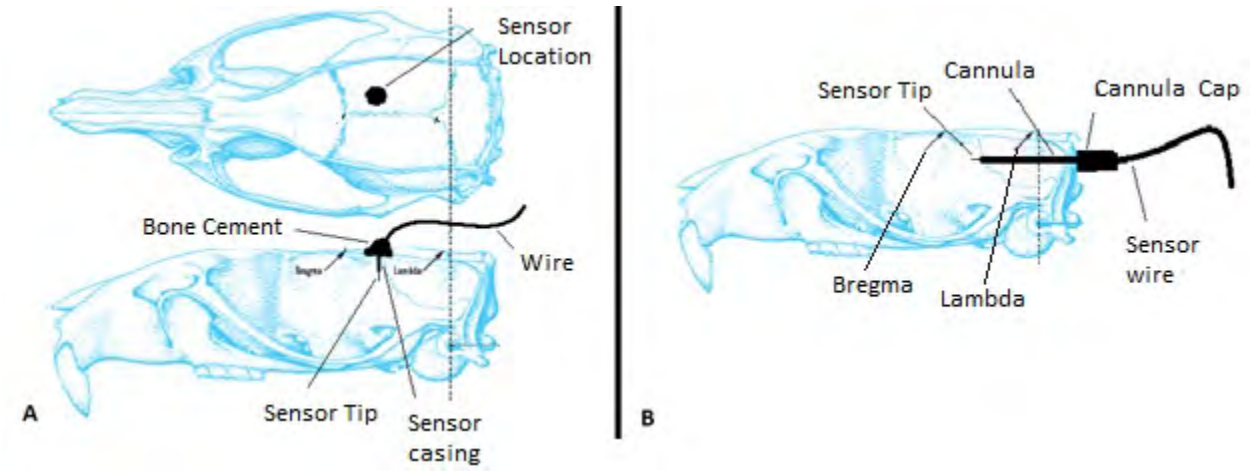

Figure 3. A schematic of the mounting procedures for the IC (A) and OIC (B) mounting positions of the rat skull. Drawings are not to scale.

Each rat was exposed to three shock wave exposures at a given intensity. The intensities ranged from 69 to 172 kPa peak static pressure shock wave intensities. The time in between each exposure was approximately two minutes. Following testing, rats from the IC group were euthanized. The purpose for euthanizing the OIC group prior to testing was undertaken due to the severity of the surgical technique. Pressure data were collected at 400 kHz by the DASH HF. The peak ambient pressure and peak ICP magnitudes were recorded. The peak ICP pressures were grouped by incident intensity and compared with ANOVA. This was also completed for the ratio of peak ICP/peak ambient, where following ANOVA, the *post hoc* Tukey HSD test was conducted to determine significance amongst each group.

For each rat, a unique frequency waveform was observed where first five cycles were counted for the response where the waveform oscillated the most harmonically. Approximate frequencies were then calculated from these cycles using simple wave form analysis. The relationships between weight of the rat, shock wave intensity, and calculated frequency were then described graphically using the contour map method where weight of the specimen and shock wave intensity were graphed on the x and y axes and "contour" of the frequency response was then created using DPLOT (Hydesoft Computing LLC).

A detail description of the results has been published by our group and is attached within the Appendix of this report (Bolander et al 2011). To summarize, we were the first to recognize the variable ICP profiles found from different magnitude exposures. Furthermore, the mounting system appeared to have an effect on the pressure recordings. It was demonstrated that the skull acts as an interface between the shock wave and the brain. This phenomenon has been demonstrated by the modification of either the superior or posterior brain case. For the IC group, it was shown that as a rat became heavier, the secondary signal would oscillate at lower frequencies and that greater incident shock wave intensities were required to invoke this oscillatory response. The response appeared to be similar to that of a damped harmonic oscillator. Where there would be an initial deflection and then a series of oscillations that would dampen out and return to pre-event conditions. Instrumentation placement appeared to alter the frequency of the pressure oscillations within the brain. Factors associated with those modifications included the additional mass and stiffness on the surface of the brain case from the application of bone cement and equipment for mounting the pressure sensor.

To address the issues associated with instrumenting the top of the skull, the fiber optic sensor was mounted into the occipital bone (OIC) to measure the intracranial pressure response without changing the native properties of the superior surface. The results indicated that mounting of instrumentation to the superior surface did have an effect on the observed oscillatory response. In both groups, intracranial pressure peaks increased with intensity, but the increase in the ratio of the ICP to ambient pressure peaks was specific to the IC group data.

SOW Task 3: Investigating the effects of head orientation on intracranial pressure wave transmission (Completed and Published)

After optimized our testing methodology, we continued investigating how head orientation effects the animal's ICP measurements. We further identified key biomechanical parameters that may contribute to the injury occurring form blast.

2.1 Animals and Testing Parameters.

Experiments were completed at WSU and were approved by the university animal committee.

The WSU shock tube (ORA Inc., Fredericksburg, VA) was used to produce simulated blast waves. It consists of two sections: the driver (0.76 m long; 0.31 m in diameter), filled with highly

pressurized helium; and the driven section open to ambient air. The sections are separated by a membrane, which is ruptured to generate a shock wave. The driven section had two distinct parts: a cylindrical part (2.46 m long; 0.31 m diameter), and a conical expansion (4.70 m long; expanding to 0.91 m in diameter at the open end). This expanded configuration is used so that the apparatus holding the specimen covers no more than 15% of the cross-sectional area of the conical driven. This is done to avoid disrupting the shockwave natural flow; otherwise, transverse reflections will affect the response and the restricted airflow would adversely affect the relationship between dynamic and static pressures loading the target. Thus, the tube ceases to simulate a free field shock wave environment and data would be corrupted.

The animal was placed inside the conical section and its head was consistently positioned at 1.25 m from the open end of the tube (Figure 4). This position assured that the air overpressure positive phase was not affected by the anomalous effect of the rarefaction wave coming from the open-end of the tube. Calibrations were performed to determine the shock wave profile in air using a side-on pressure sensor (PCB Piezotronics, Model 137A22) placed at the same location where the rat head was positioned. This side-on pressure sensor captured the static pressure changing in time and the peak pressure measured at 1.25 m from the open end of the tube was approximately 70kPa. An additional side-on pressure sensor (PCB Piezotronics, Model 102A06) was installed on the cylindrical driven section to monitor the development of the shock wave along the test section. This sensor (R-wall) was placed at 1.83 m from the frangible membrane and was utilized as the trigger for the event. The sampling rate for all pressure sensors was 500 kHz with an anti-aliasing filter at 200 kHz.

Eight male Sprague-Dawley rats were divided into two groups of four based on their ages. Group 1 was 68 days old on day of testing with an average weight of 274.8 g (Standard Deviation (SD) ± 1.7 g). Group 2 was 158 days old with an average weight of 453.5 g (SD ± 4.4 g). The difference in animal weight allowed for assessing the effects of skull maturity on ICP. Rats were anesthetized and an incision was made along the midline suture of the head to expose the superior and caudal portions of the skull. A 1-mm-diameter hole was drilled into the occipital bone 1-mm right of the midline to allow for insertion of a guided cannula (16-gauge with hypodermic steel tubing) to reach the right forebrain area (Fig 3). The occipital mounting method was necessary to preserve the physiological response of the skull top. Screws were placed around the cannula to help anchor it to the skull once bone cement was applied. For group 1, a 10 mm long cannula was mounted to the occipital bone; for group 2, the cannula length was increased to 14 mm in order to measure ICP in analogous locations in the brain. Once the cement had cured, the incision was sutured to minimize direct skull exposure.

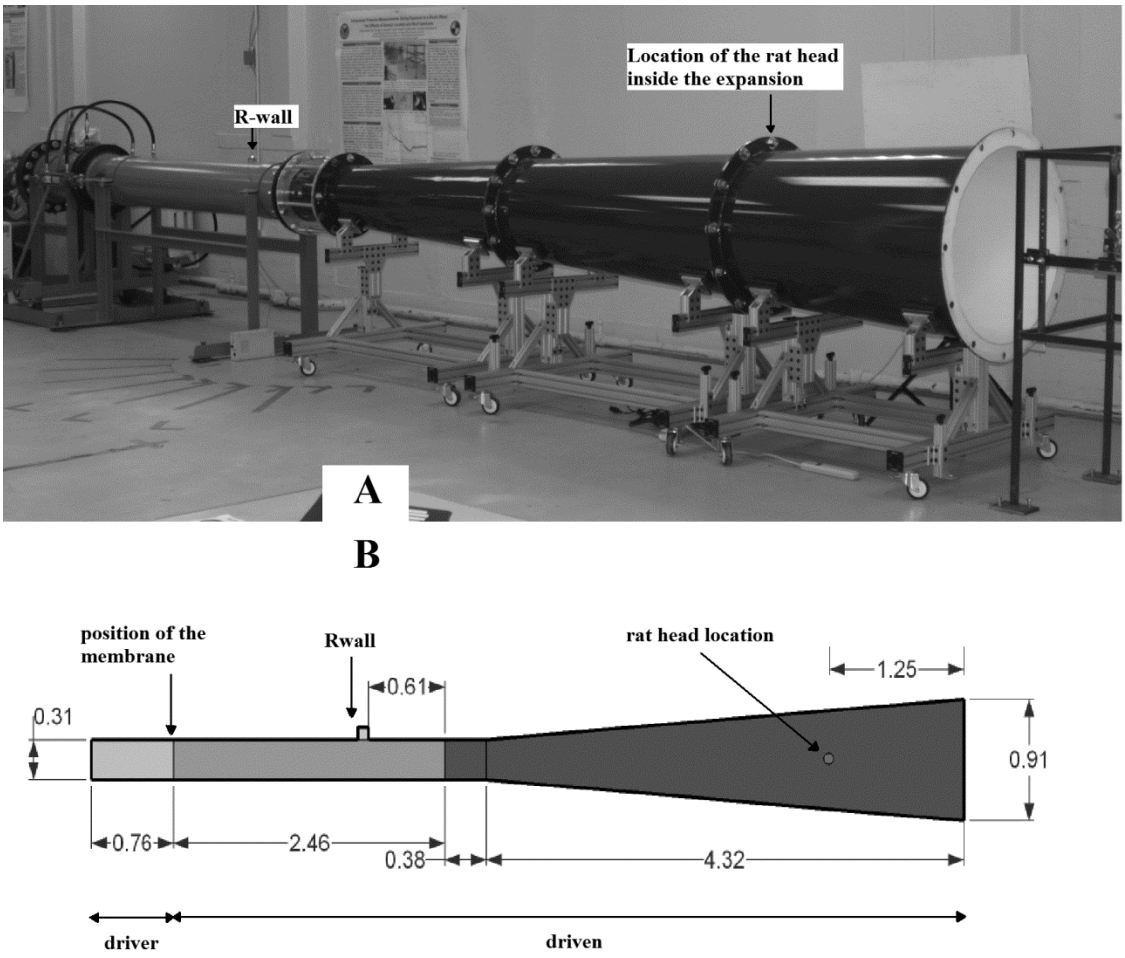

Figure 4. WSU Shock tube with expansion section attached.

Prior to testing, saline solution was administered into the cannula to reduce the possibility of introducing air in the system, which hampers the rise of ICP. Then an optic pressure sensor (FISO Technologies, model FOP-MIV-PK) was inserted into the cannula and locked into position. The sensor optic cable was adapted to screw into the cannula in order to seal the skull/brain system (Dal Cengio Leonardi et al., 2011).

Each rat was exposed to a series of shock waves with its head in one of four different orientations: front, side, top, and back. For each orientation the rat was placed in a custom-built restraint fixture that shielded the body and exposed only the head in each orientation. The animal's muzzle was secured to the fixture to prevent rotation of the head due to the blast wind. The animal was exposed to three separate shock waves of equal intensity; subsequently the orientation was changed. The frontal exposure was repeated at the end of the series to verify that the results remained consistent: this brought the total number of exposures to 13 trials per rat.

Importantly, the head remained at 1.25 m from the open end for all orientations. Fixtures were designed to maximize the aerodynamic profile in order to minimize the creation of anomalous turbulence and shock reflections (Fig. 5). For side and top orientations the same fixture was used. During side exposure, the left side of the rat head made the initial contact with the shock front.

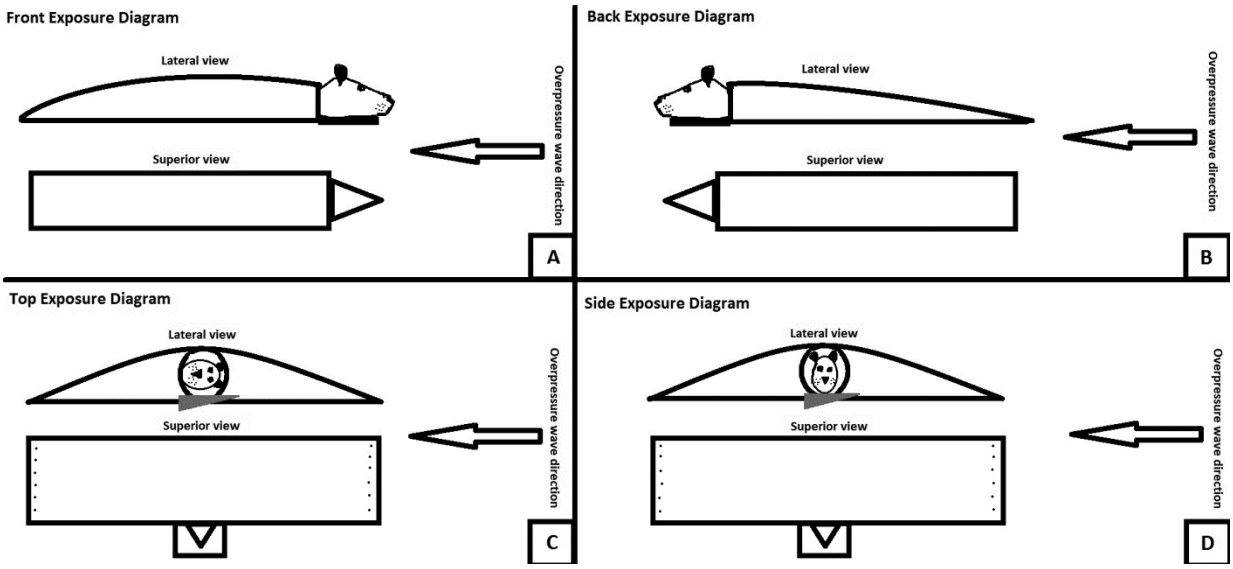

Figure 5. Orientation of animal during series of testing.

2.2 Results from ICP as a function of orientation.

A detail description of the results has been published by our group and is attached within the Appendix of this report (Leonardi et al 2012). To summarize, we demonstrated a significant increase in ICP for larger rats in all orientations. It also showed a relation between ICP and orientation of the head due to geometry of the skull and location of sutures. Varying the skull's orientation to the transient shock wave results in dramatic changes to the energy landscape associated with intracranial pressure. These findings accentuate the importance of skull dynamics in explaining the possible injury mechanism during blast. Furthermore, the rate of pressure change confirmed that the initial biomechanical response of the superior rat skull is distinctive compared to other areas of the skull. How the pressure response observed in the rat brain will translate to the human injury is still unknown. Nevertheless, this data provides clues as to how geometry, bone thickness and skull sutures play a role in the pressure transfer. This knowledge can ultimately help understand the injury occurring to the human brain and help design strategies to protect against it.

SOW Task 4: Correlate histological injury with intracranial pressure (Completed and Publication Pending)

SOW Task 5: Correlate CSF injury biomarkers with intracranial pressure (Completed and Publication Pending)

The last component of the project was to investigate how magnitude of pressure correlated with injury. Tasks 4 and 5 were conducted after the PI's laboratory was moved. Dr. VandeVord became faculty at Virginia Tech University (VT) and a Health Scientist at the Salem Virginia VAMC in Aug 2011. There was a slight delay as new animal protocols were required, but quickly were approved and research was conducted. The Virginia Tech Institutional Animal Care and Use Committee approved experimental protocols described herein

3.1 Animals and Testing Parameters.

In order to accomplish Tasks 4 and 5, male Sprague Dawley rats were acquired (~250 g, Harlan Labs, San Diego) and acclimated for at least three days (12 hr light/dark) and food and water provided ad lib. The shock front and dynamic overpressure was generated by a custom-built shock tube (driving compression chamber attached to rectangular tube with wave eliminator, ORA Inc. Fredericksburg, VA.) located at the VT Center of Injury Biomechanics (CIB). A peak static overpressure was produced with compressed helium and calibrated acetate sheets (Grafix Plastics, Cleveland, OH). Exposure pressures were determined by three sensors placed along the wall within the tube (1232 mm, 1537 mm, and 1842 mm from the driver). The middle sensor was positioned coincident with the animal's head, so the static pressure measured at that point would represent the exposure on the animal.

Pressure measurements were collected at 250 kHz using a Dash 8HF data acquisition system (Astro-Med, Inc, West Warwick, RI) and shock wave profiles were verified to maintain consistent exposure pressures between subjects. The animals were anesthetized with 3% isoflurane before being placed in a sling with a rostral cephalic orientation towards the shock wave. The animals were exposed to a single incident pressure profile resembling a 'free-field' blast exposure, which was made possible by utilizing a wave eliminator device at the end of the tube. The animals were exposed to peak overpressures of 10 psi, 14 psi, and 24 psi to account for three distinct pressure groups represented in the biomechanical testing series (Figure 6). Each group included 5 animals including the control group that was anesthetized with 3% isoflurane but did not experience the overpressure. The representative curves are seen below from the 1537 mm sensor, which represents the exposed absolute overpressure on the subject.

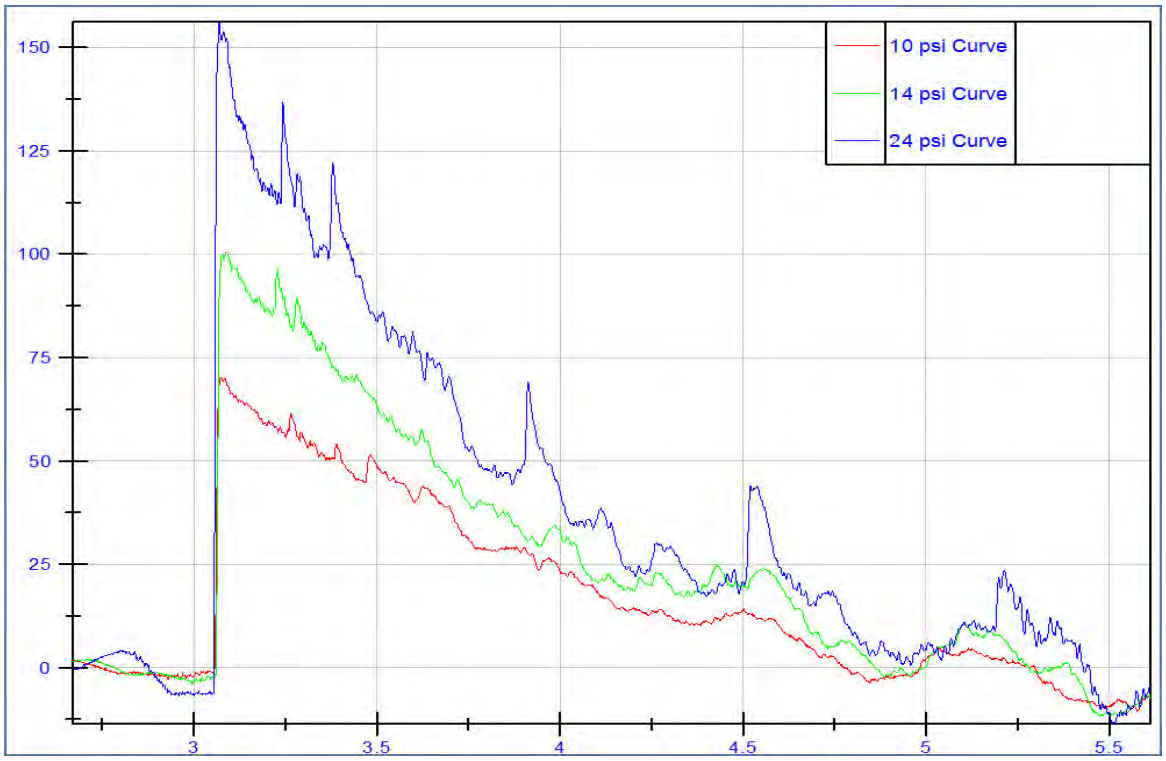

Figure 6. Static overpressure (kPa) vs. time (msec) profiles for the 10, 14, and 24 psi blast exposure

Behavioral assessment following blast exposure. Animal were assessed for behavioral deficits following blast exposure. Since anxiety is a common outcome following blast exposure, animals were evaluated for anxiety-like behavior. The light/dark box is a characteristic tool used in the assessment of anxiety. The basic measure is the animal's preference for dark, enclosed places over bright, exposed places. Time spent in the lit (light) half of the arena, and the related exploratory behavior, are reliable parameters for assessing anxiolytic effects that may be useful in identifying and/or screening of anxiolytic and anxiogenic agents. There have been many other light/dark box studies to test anxiety in animal models (10). These studies determined that animals supposed exhibiting anxiety-like behavior spent a significant amount of time in the dark side compared to a control group. Animals that display less anxiety have a longer duration in the light side compartment (11). This test has been widely used in identifying anxiety after brain injury and neurological disorders in animal models.

The apparatus consisted of two equal acrylic compartments, one dark side closed with a lid and one light side. Each rat was tested by placing it in the light area, facing away from the dark one, and was allowed to explore the novel environment for 5 min. The number of transfers from one compartment to the other along with the time spent in the light and dark side was measured. In order to avoid any environmental bias, the animal was left alone in the testing room for the duration of the exploratory time, so the behavior measurements were obtained from video

analysis. This test exploited the conflict between the animal's tendency to explore an open environment (non-anxiety like effect) and to stay in a defensive mode (anxiety like effect).

Immunohistochemistry of brain section for neuropathology. Brains were collected following euthanizing animals at specific time points following injury. Tissue sections (20 μm) were fixed in 4% paraformaldehyde for 15 min at room temperature, rinsed with PBS, and incubated in 0.5% Triton X-100+ 0.5% gelatin blocking buffer for one hour. After being washed with PBS, nonspecific binding sites were blocked with 3% bovine serum albumin (BSA) in PBS for 1 hour at room temperature and incubated with the primary antibody. Sections from ***hippocampus and amygdala*** were stained for glial fibrillary acidic protein (GFAP; an astrocyte specific cell activation indicator), Iba 1 (microglial), cleaved caspase-3 (apoptosis) or CuZn SOD (oxidative stress). Sections were then incubated with a primary antibody (anti-GFAP, anti-Iba1, anti-cleaved caspase-3 or anti-CuZn SOD at 1:200) overnight at 4ºC. After a PBS wash, the samples were incubated for 1.5 hours with fluorescence-tagged fluorescein isothiocyanate (FITC)-secondary anti-rat IgG antibodies (1:200; Vector Laboratories, Burlingame, CA) or Alexa flour-555 anti-rabbit IgG antibody (1:200; Cell Signaling, Danvers, MA). After a PBS wash, samples were mounted on slides, air dried, and coverslipped with prolong antifade gold antifade reagent with 6-diamidino-2-phenylindole (DAPI;Invitrogen). Sections were examined under Zeiss fluorescence microscope at 20X magnification under appropriate fluorescent filters. An observer blinded to the experimental conditions carried out cell counting.

Gene expression changes evaluated in key injury pathways. Real time PCR (RT-PCR) was used to measure gene expression from blasted samples relative to the internal housekeeping gene control. The total RNA from the tissues was extracted with Trizol (Invitrogen, Carlsbad, CA) following the manufacturer's protocol and homogenized using Branson Ultrasonicator (Fisher Scientific, Hampton, NH). The RNA was then purified using RNeasy MinElute Cleanup kit (Qiagen, Valencia, CA). The RNA concentration and purity was determined using a spectrophotometer through UV absorbance at 260nm and 280nm. Reverse transcriptase using the random primers converted the mRNA to a cDNA template using a thermal cycler (Mastercycler Gradient, Eppendorf, Hauppauge, NY). For PCR analysis, we used cDNA equivalent to 40ng of total RNA. Specific primer pairs (Table 1) for reactivity: GFAP, MAP2k1, Bax, Bcl2, Piezo2; survival: Bcl-2, IL-3, GDNF, BDNF; and superoxides: CuZn-SOD1 and Mn-SOD2 were used. As an internal control, we used the house-keeping gene glyceraldehyde-3-phosphate dehydrogenase (GAPDH). The PCR master mix included 1×SYBR® Green (Applied Biosystems, Foster City, CA), and forward and reverse primers (0.4μM each). cDNA templates and master mix were read in a 96-well optical plate using a 7500 Fast Real-Time PCR System (Applied Biosystems, Foster City, CA). The following profile was used: 50◦C for 2 min, 95◦C for 10 min, and 40 cycles of 95◦C for 15s and 60◦C for 1 minute. Threshold cycle (Ct) values for each sample and primer pair were obtained and analyzed with the delta (Δ) Ct method [12, 13](Livak and Schmittgen, 2001; Schmittgen and Livak, 2008) in order to calculate the fold change (R) in each target gene.

The following equations were used: $\Delta Ct = Ctblast - CtGAPDH$; $R = 2^{-\Delta Ct}$

Table 1. Primer sequences for real-time PCR.

Category	Gene	Primer Sequence
Housekeeping gene	GAPDH	5'-TGGCCTTCCGTGTTCCTACC-3' (F)
		5'-AGCCCAGGATGCCCTTTAGTG-3' (R)
Reactivity	GFAP	5'-GTTGTGTTCAAGCAGCCTGG-3' (F)
		5'-CGTGTCCACGTCAGCAATCATC -3'(F)
	MAP2k1	5'-TTCAAGGTCTCCCACAAGCCATCT-3' (F)
		5'-TTGATCCAAGGACCCACCATCCAT-3' (R)
	Piezo2	5'- GCTGGGCACCTGATTGGA -3' (F)
		5'-CGGGACCGCTTCTTGGA-3' (R)
	GLAST	5'- CATCCAGGCCAACGAAACA -3' (F)
		5'-GAGTCTCCATGGCCTCTGACA-3' (R)
Survival	IL-3	5'- CGCTCCTGATGCTCTTCCA -3' (F)
		5'- GGCATCTGAGCCCCTGTCT -3' (R)
	GDNF	5'- ACTTGGGTTTGGGCTACGAA -3' (F)
		5'- CAGGAACCGCTACAATATCGAAA-3' (R)
	BDNF	5'- TTGGAGCCTCCTCTGCTCTTT -3' (F)
		5'- GTTTGCGGCATCCAGGTAAT-3' (R)
Oxidative Stress	Mn-SOD2	5'- GGGCTGGCTTGGCTTCA -3' (F)
		5'- AGCAGGCGGCAATCTGTAA-3' (R)
	CuZn-SOD1	5'- CATTCCATCATTGGCCGTACT -3' (F)
		5'- CCACCTTTGCCCAAGTCATC-3' (R)

Statistical Analysis. Effects of blast exposure were measured in separate experiments (i.e. 10, 14 and 24 psi blast overpressure exposure). In each experiment, separate sham-treated animals served as respective comparison groups for unknown influences (e.g. residual effects of isoflurane, which was used in histology but not spectroscopy studies). Thus, for neurological experiments statistical differences between sham and blast-exposed rats were assessed with independent two-tailed Student's t-test with $p < 0.05$ considered significant. A two-factorial repeated measured ANOVA was used for the behavioral testing with $p<0.05$ considered statistically significant. Unless indicated otherwise, data are presented as mean ± standard error of the mean (SEM).

3.2 Results of Injury Study

Neurological assessments were conducted on each pressure group following blast exposure and several significant observations were found as described below.

Animal Weights. Animals were weighed after blast in order to assess physical changes. No significant differences in weights were observed at 3 and 7 day time point between the groups (Table 2).

Table 2. Raw values of the weights at 3 and 7 days after blast exposure

	Time Point (Post Blast)	
	3 days	**7 days**
Pressure	**Weight (grams)**	
Sham	310.8 $\pm$ 4.72	319.8 $\pm$ 5.85
10 psi	307.4 $\pm$ 4.79	315.4 $\pm$ 7.36
14psi	312.2 $\pm$ 5.24	325.2 $\pm$ 5.45
24psi	309.8 $\pm$ 5.67	321.7 $\pm$ 5.95

Wake-up time after anesthesia induction. After blast exposure, the time it took for the animal to awake from anesthesia was measured. Difference in the wake-up time of the blast groups compared to the sham group after anesthesia was observed. The mean wake times in addition to the standard error of the mean are presented below (Table 3). The significant values are denoted by the same convention as the graph (Figure 7).

Table 3. Raw Values of the Wake Times after Anesthetization

Pressure Group	**Wake Time (seconds)**
Sham	555.3 $\pm$ 14.43
10 psi	*484.0 $\pm$ 26.55
14psi	*421.6 $\pm$ 6.81
24psi	#513.3 $\pm$ 38.25

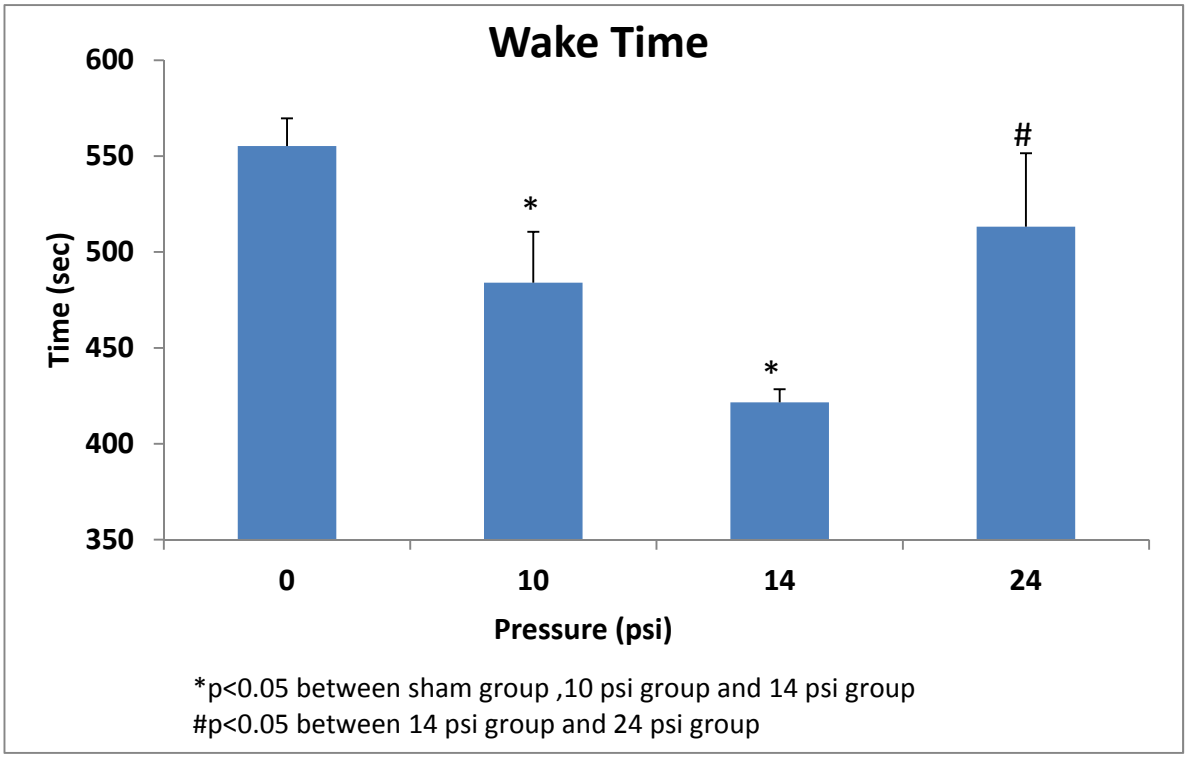

Figure 7. Significant difference in wake time following blast

2.2 Anxiety-like behavior increased with blast exposure.

At the one week time point, there is a significant difference in time spent on the light side of the box in the sham group (no exposure to blast) and the exposed groups of lower peak overpressures (Figure 8). There is less difference in the higher pressure group as compared to the control group. The same result was seen below in the latency of the different groups (Figure 9).

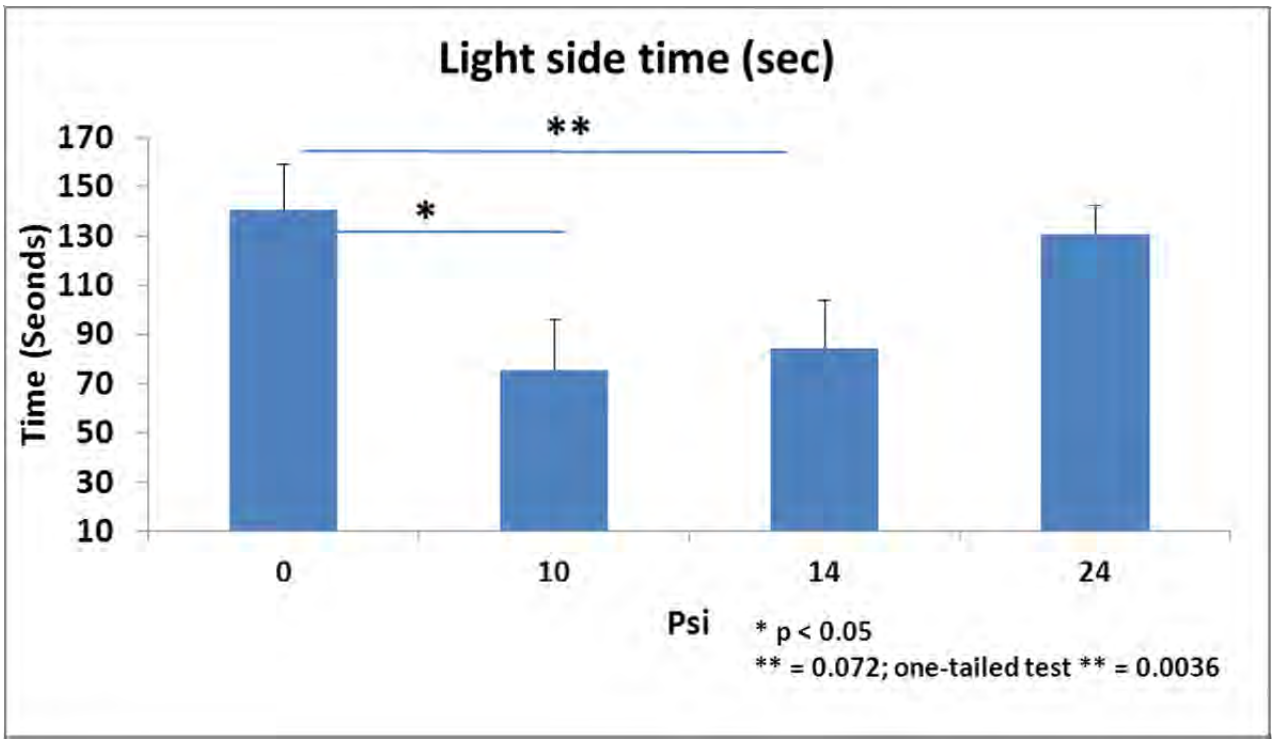

Figure 8. Time spent in light was significantly less for the 10 and 14 psi groups. No difference was found between sham and 24 psi groups.

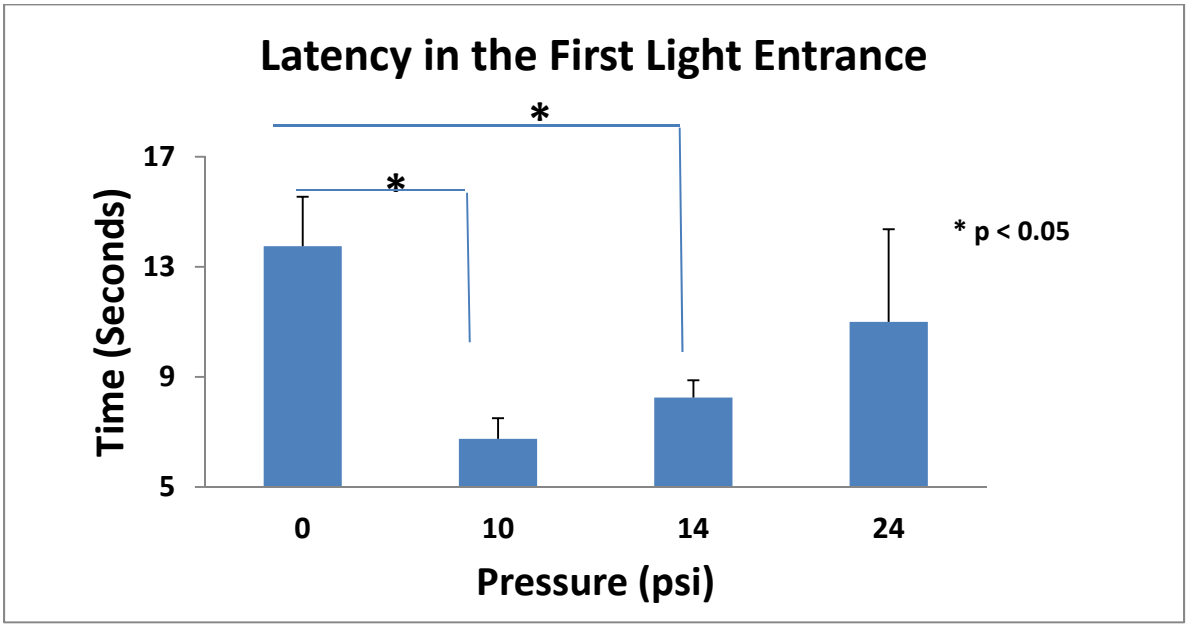

Figure 9. Time spent until first light entrance was found to be significantly lower in 10 and 14 psi groups.

Immunohistochemistry.

Cleaved caspase-3 was found to be significantly higher in blast groups, yet to varying levels. Cleaved caspase-3 is considered as a marker of apoptotic cell death. A significant increase of cleaved caspase-3 positive cells was found in hippocampus at 10, 14 and 24 psi following blast overpressure at 7 days following blast. While a significant increase in all pressure groups was found within the amygdala compared to sham group, *p<0.05., the 10 psi was significantly higher than the other pressure groups (Figures 10 and 11).

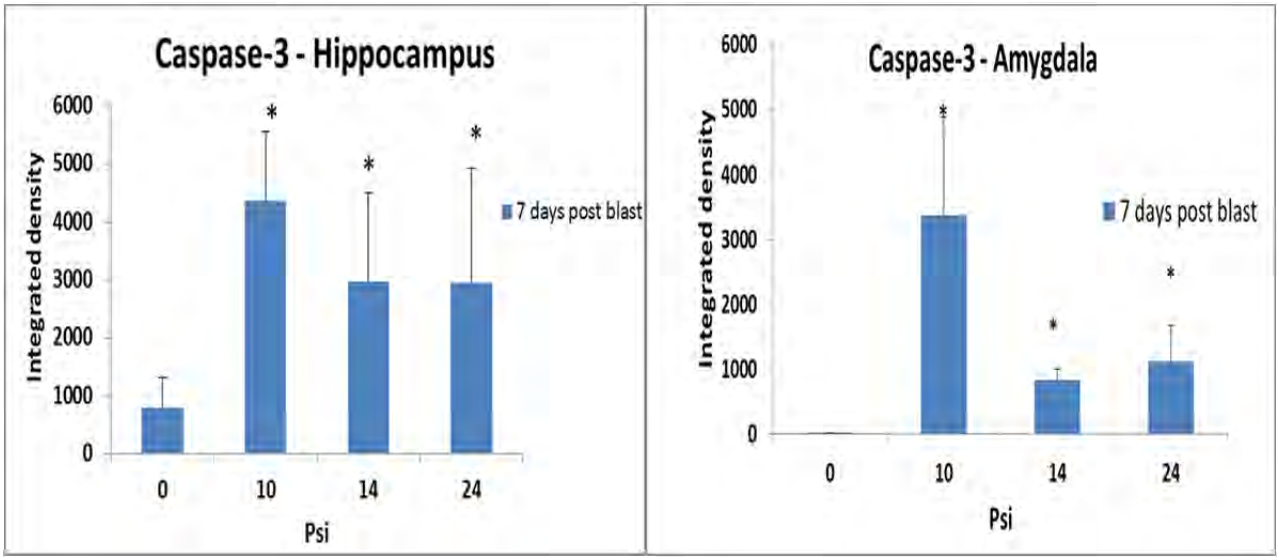

Figure 10. Cleaved capase-3 expression in different pressure groups at 7 days following blast over pressure in hippocampus and amygdala compared to sham group.

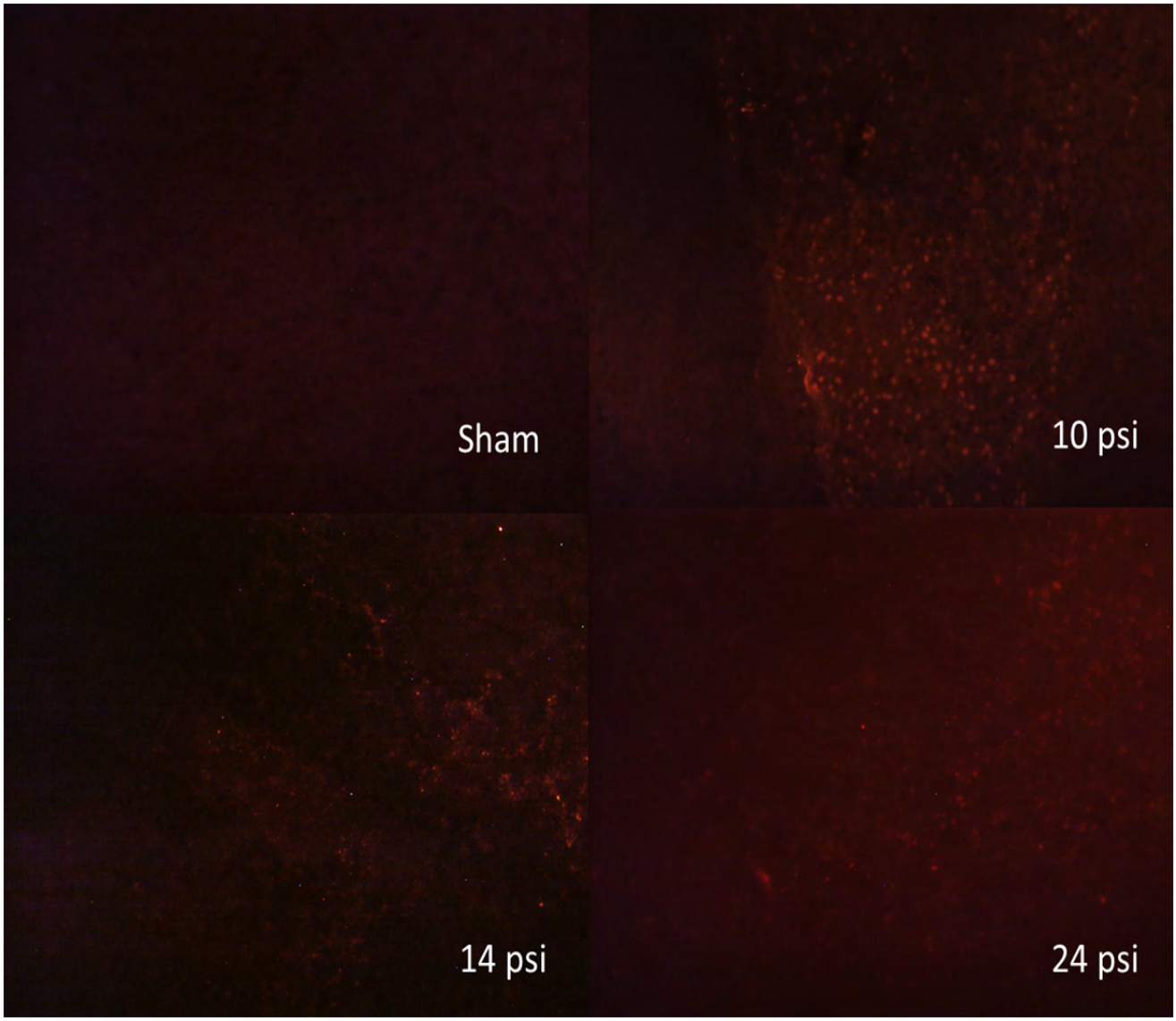

Figure 11. Representative figures of cleaved caspase-3 levels at different pressure groups following 7 days following blast overpressure. Red color indicates caspase-positive cells.

Increased levels of GFAP were found in blast animals. A significant increase in GFAP in hippocampus at 14 and 24 psi following blast overpressure, while a significant increase in all pressure groups was observed in amygdala exposure compared to sham group, *p<0.05. (Figures 12 and 13).

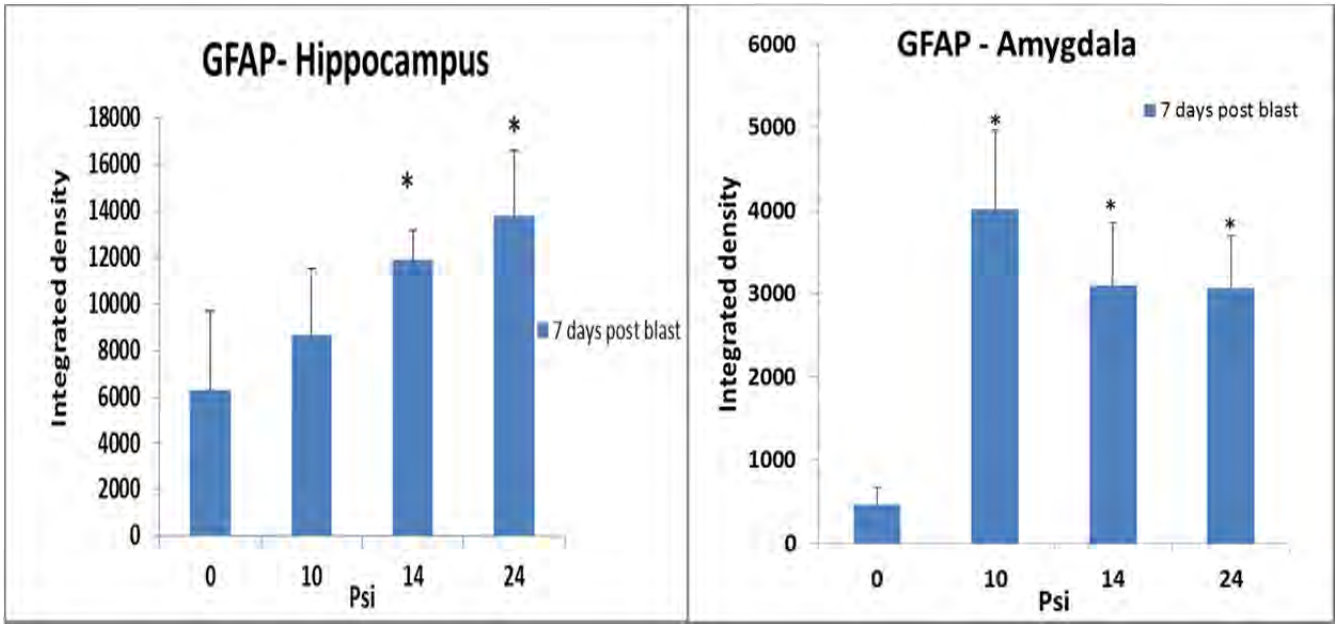

Figure 12. GFAP expression (astrocyte marker) in different pressure groups at 7 days following blast over pressure in hippocampus and amygdala compared to sham group *p<0.05.

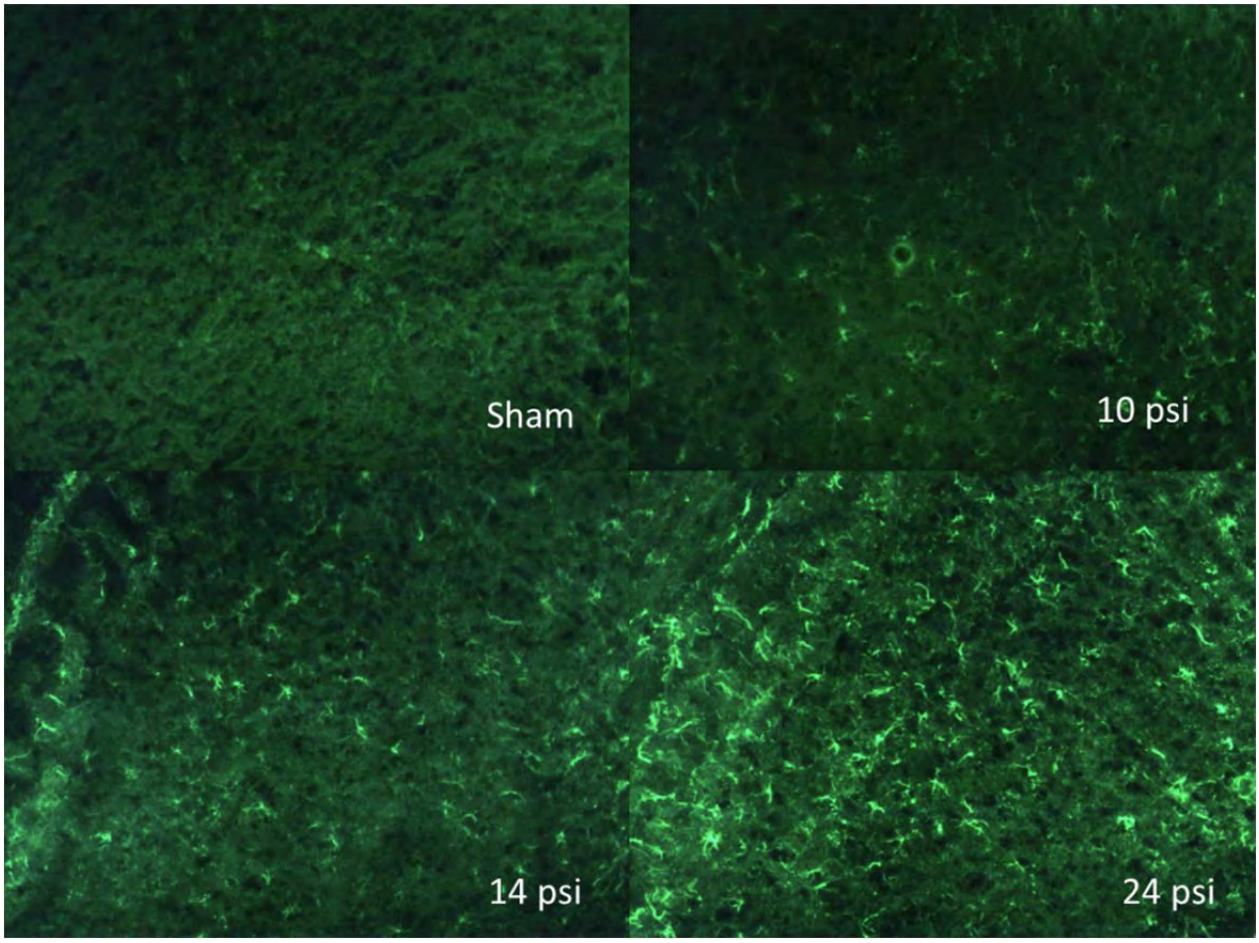

Figure 13. Representative figures of GFAP levels (astrocyte marker) at different pressure groups following 7 days following blast overpressure. Green indicated GFAP positive cells.

Elevated levels of Iba1 were only found in low pressure group. A significant increase in Iba1, marker of microglia, in hippocampus and amygdala was found only in the 10 psi group following blast overpressure compared to sham group, *$p<0.05$ (Figures 14 and 15).

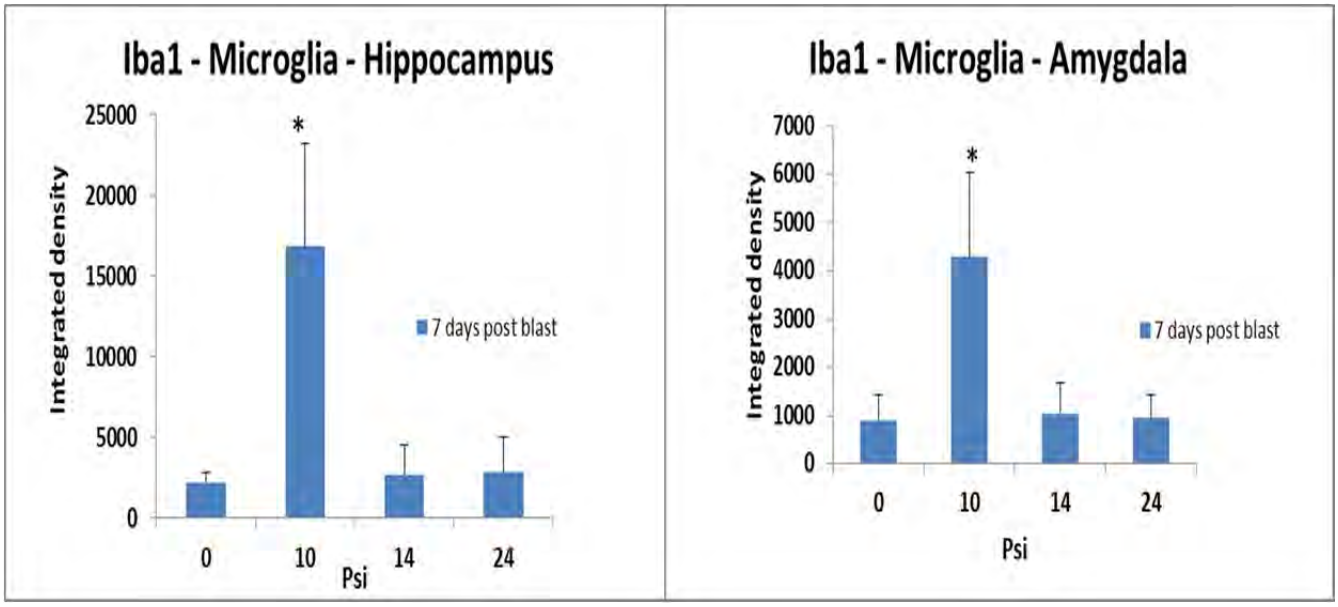

Figure 14. Iba1 (microglia marker) in different pressure groups at 7 days following blast over pressure in hippocampus and amygdala compared to sham group *p<0.05.

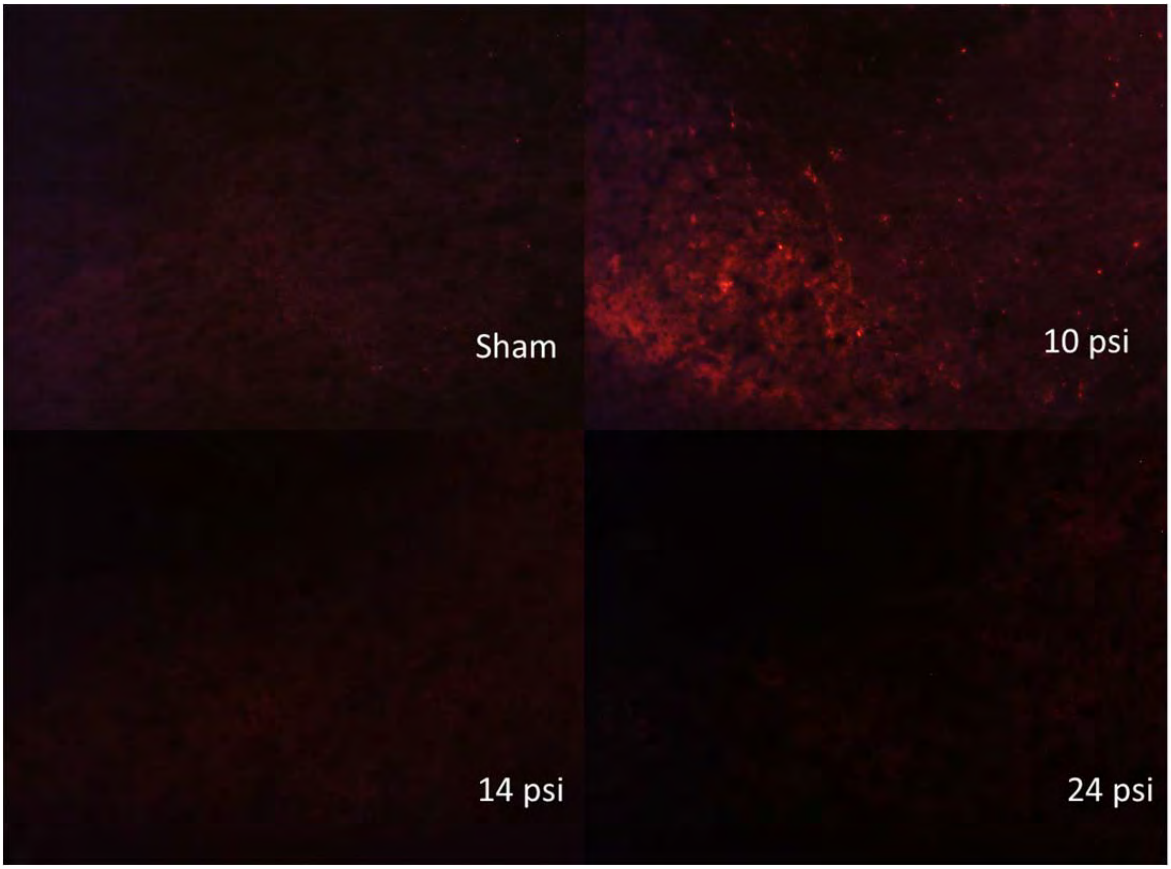

Figure 25. Representative figures of Iba1 levels (microglia marker) at different pressure groups following 7 days following blast overpressure. Red indicates Iba1 positive cells.

Levels of CuZn Super oxide dismutase (***SOD1) which indicates oxidative stress are high in blast animals.*** A significant increase in SOD1, a major anti-oxidant, in hippocampus and amygdala was found at 10,14 psi following blast overpressure and SOD1 levels was reduced in 24 psi compared to sham group, *p<0.05. (Figures 16 and 17).

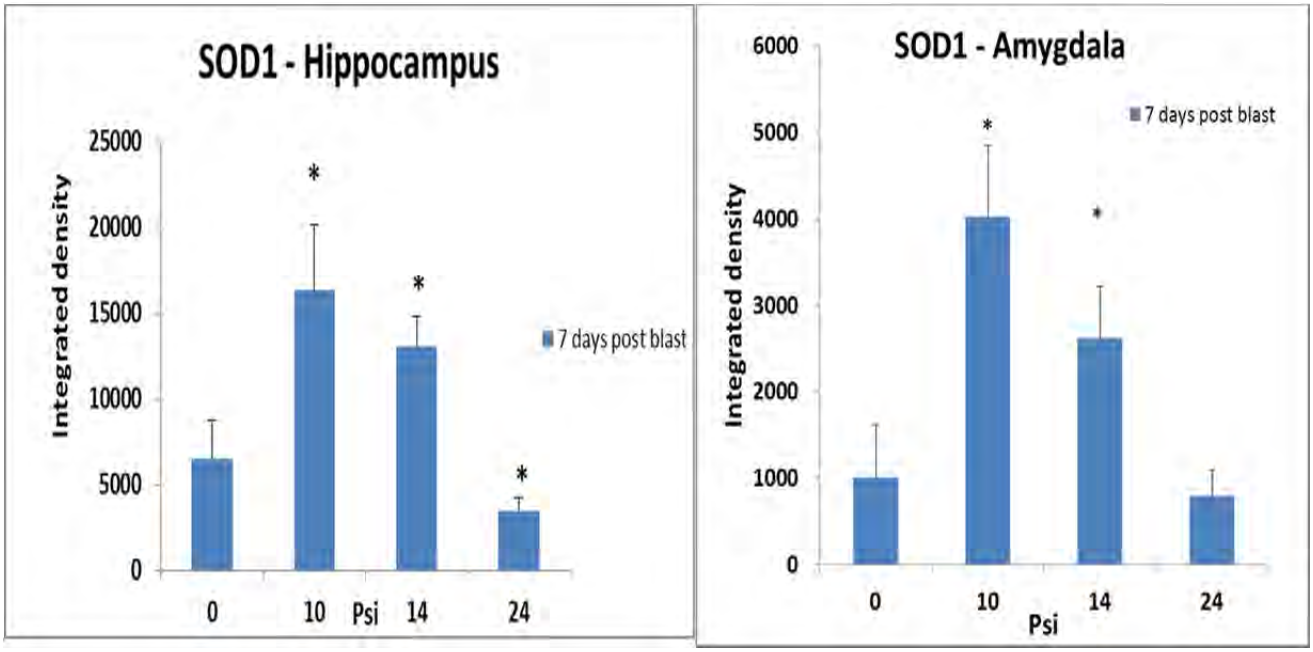

Figure 16. SOD1 levels in different pressure groups at 7 days following blast over pressure in hippocampus and amygdala compared to sham group , *p<0.05.

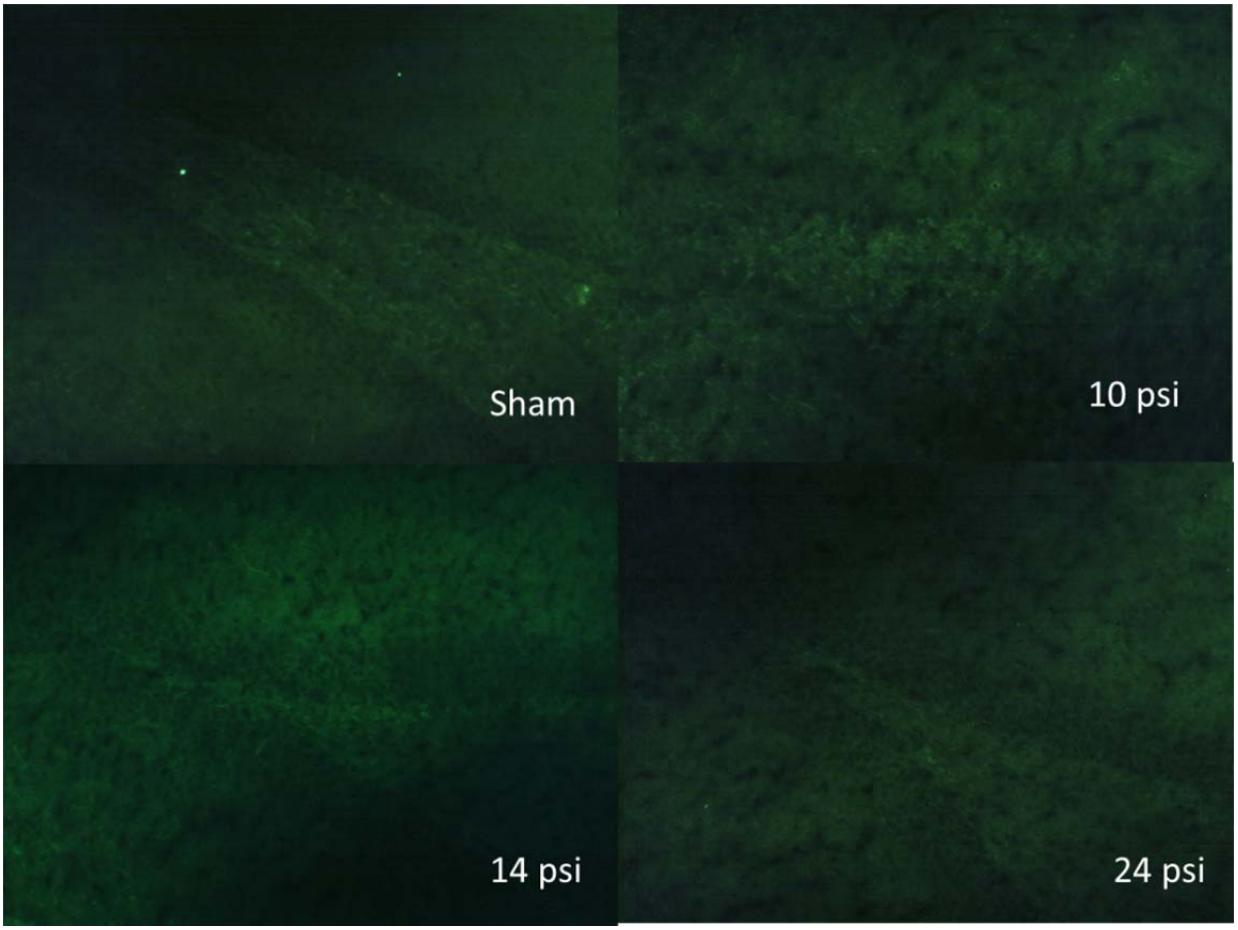

Figure 17. Representative figures of SOD1 levels at different pressure groups following 7 days following blast overpressure. Green color indicate SOD1 positive cells.

Levels of neuronal staining (Neu-N) are decreased in blast animals. A significant decrease in Neu-N, a neuronal marker, in hippocampus was found in all pressure groups following blast overpressure as compared to sham group, *$p<0.05$. Within the amygdala, only 14 and 24 psi groups demonstrated a decrease in number of neurons (Figures 18 and 19).

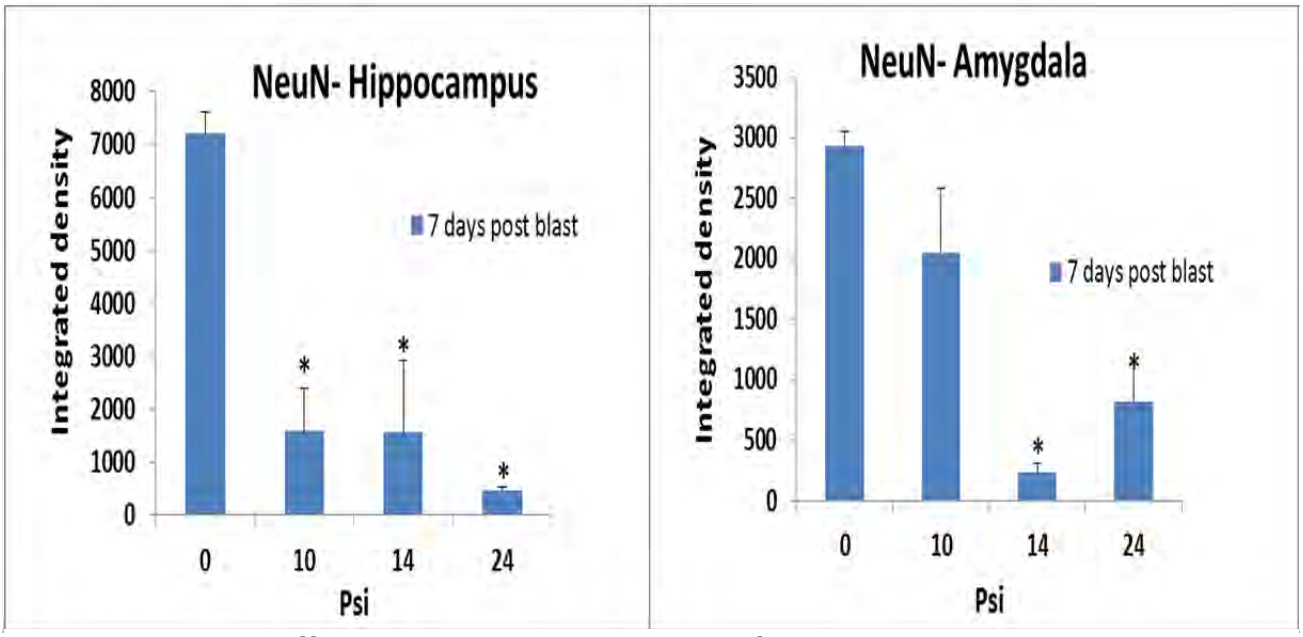

Figure 18. levels in different pressure groups at 7 days following blast over pressure in hippocampus and amygdala compared to sham group , *p<0.05.

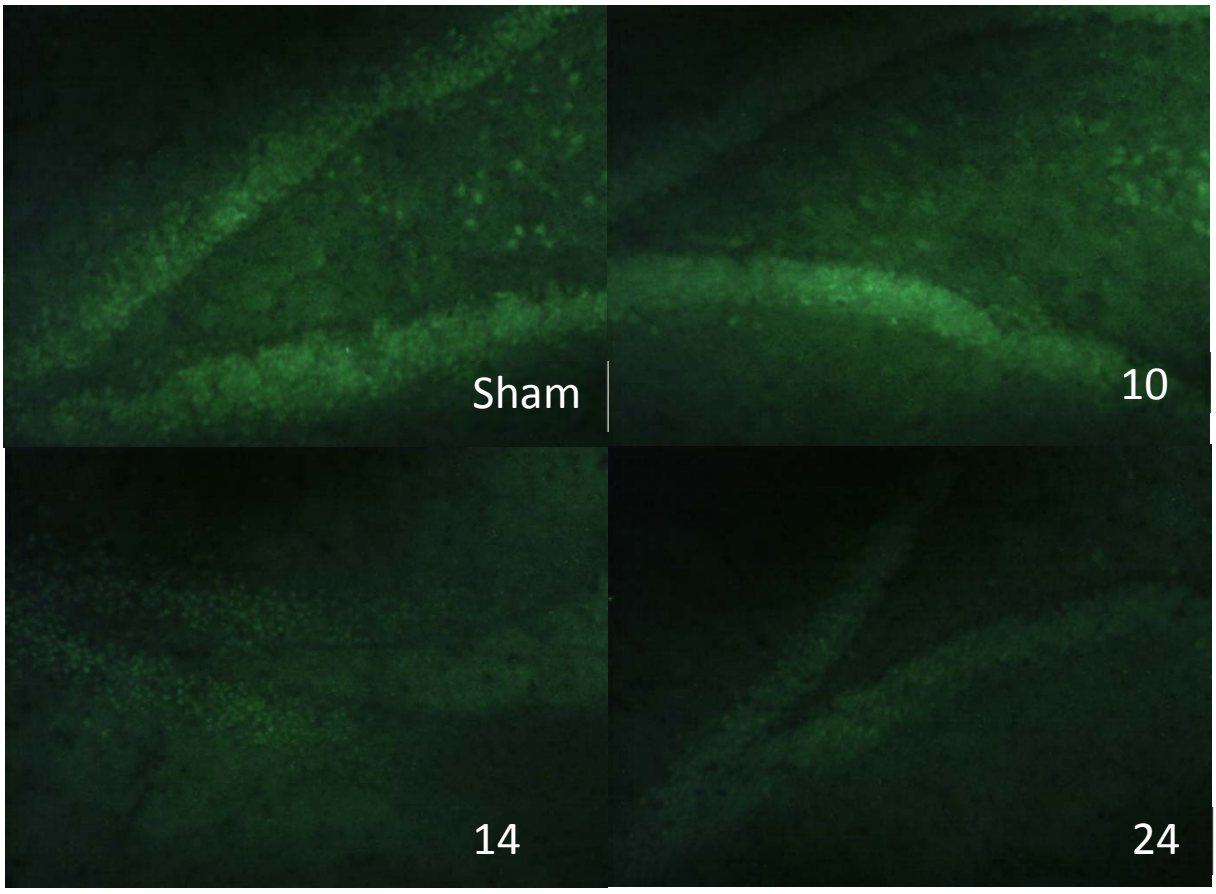

Figure 19. Representative figures of NeuN levels at different pressure groups following 7 days following blast overpressure. Green color indicated neurons.

2.4 Gene Expression changes are significant depending on pressure level.

A significant increase in mRNA expression of superoxide dismutase (CuZnSOD1 and MnSOD2), glial cell line derived neurotropic factor (GDNF), brain derived neurotropic factor (BDNF), excitatory amino acid transporter (GLAST) was observed in 10 psi following BOP. Significant increase in GFAP, Piezo 2, and MAP2k1 was observed in 14 psi following BOP. Significant reduction in expression of GLAST was observed in 24 psi following BOP (Figure 20).

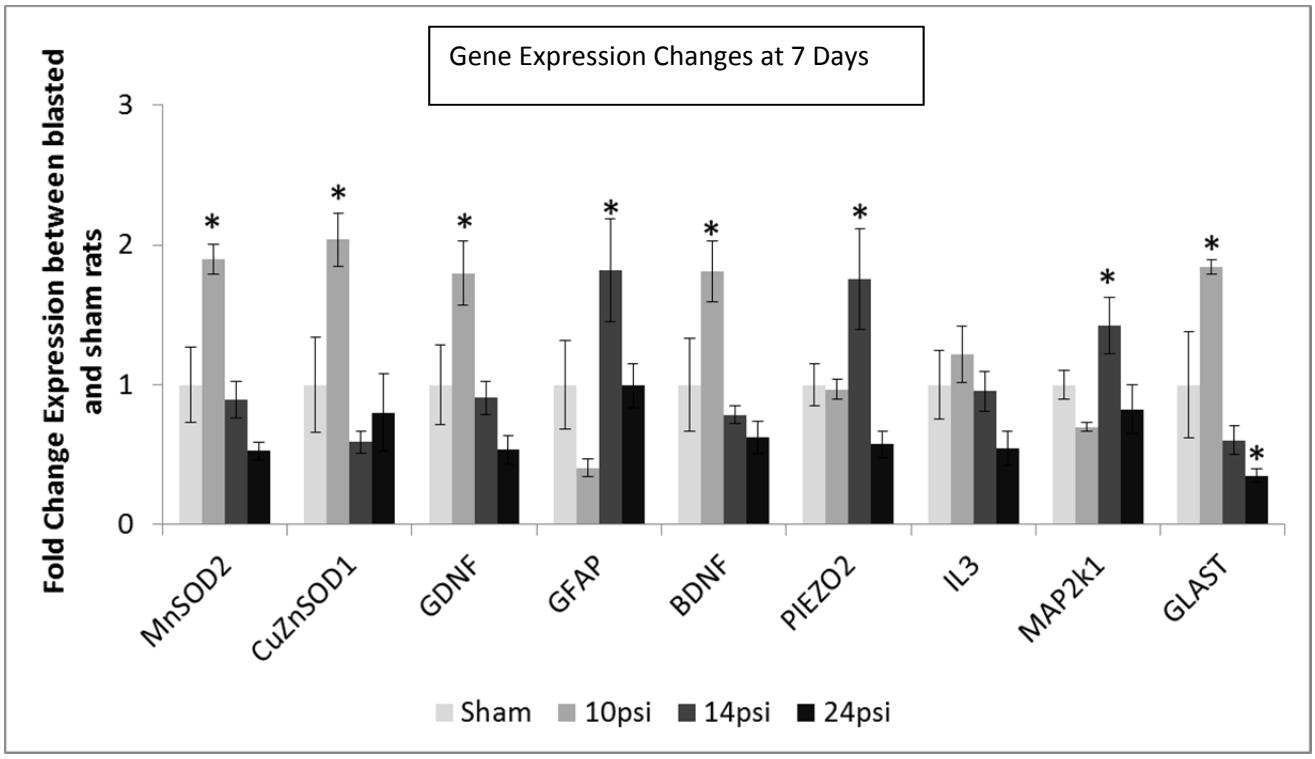

Figure 20. Gene expression changes were significant depending on pressure group at 7 days following blast *p<0.05.

4.0 Discussion:

The 'time to awake' data demonstrated a significant difference between blast and sham animals. It was determined that blasted animals awoke faster than the controls. Since anesthesia induces a "reversible coma" by inhibiting certain neurons (involved in the cortex), the blast wave could induce neuronal activity to counter the effects of the isoflurane. The GABA receptor is a known target for many anesthetics, such as isoflurane, because this GABA inhibition can inactivate large regions of the brain leading to unconsciousness. [14] If the blast wave somehow affects these GABA receptors, the difference in wake time could be explained.

When evaluating anxiety-like behavior in the animals, the blast-induced neurotrauma was shown to induce anxiety. From the light and dark box behavior data, it seems that the low and medium blast groups experienced some degree of anxiety compared to the control group. High anxiety levels can be correlated to longer durations in the dark compartment and also a lower latency to the light compartment compared to the control group. Contrary to previous hypotheses, it seems that animals exposed to lower peak overpressures show more anxiety-like behavior than the animals in the higher peak overpressure group, at least at a seven day time point. Differences in histology could give a potential explanation of the causes of varied levels of anxiety-like behavior in the different groups after blast exposure.

Glial response and cell death

A varied glial response was observed when the distinct pressure groups (10 psi, 14 psi, and 24 psi) compared to the sham. Elevated levels of GFAP, an astrocyte marker, was observed in the 14 and 17 psi groups compared to the sham for the hippocampus while elevated levels of GFAP were found in all blast overpressure groups compared to the sham in the amygdala. In addition, levels of Iba1, a microglial marker, was found to be elevated in the 10 psi group compared to the sham group in both the hippocampus and the amygdala. Astrocytes typically play a prominent role in supporting the nutrient supply during a disrupted homeostasis due to energy deficits and clearance of debris during the cell death and injury progression [15]. In previous studies, at the acute stage (6-72 hours following blast overpressure exposure) there is neurodegeneration and cell death in the hippocampus and the amygdala at higher pressure (>14psi) [16-18]. In addition, increased levels of apoptotic cells (cleaved caspase-3 positive cells) and decreased levels of neuronal (NeuN staining) were found 7 days following the blast overpressure exposure in all pressure groups. Delayed cell death was observed only in the low pressure groups (10psi) while increase in apoptosis was observed as early as 6 hours following BOP higher pressure groups (>14psi). Furthermore, elevated levels of microglia were observed only in the 10 psi group compared to the sham. Microglial is one of the first responders after injury towards injury progression [19], which may explain the delayed onset of apoptosis and injury progression in 10 psi group.

Oxidative stress

Previous studies have shown that oxidative stress was observed at different pressure groups in the hippocampus following BOP [17,20]. An increased level of SOD1 in the 10 psi and 14 psi groups explains the counteractive oxidative stress against apoptosis mechanism following BOP in both the hippocampus and the amygdala. However, decreased levels of SOD1 could be due to substantial loss of microglia by 7 days following BOP in the 24 psi group. Overall, ongoing injury progression due to increased apoptotic levels is caused by an inadequate anti-oxidant system, which serves to stop the injury from progressing.

Gene Expression

Results of the gene expression analysis demonstrated opposing cell responses to the different blast pressures exposed to the animals. We found significantly higher gene expression of superoxides and growth factors compared to shams at 10psi pressures which indicate an attempt for cell survival. Studies have shown oxidative stress to play a pivotal role in the pathology of TBI [21-23]. Oxidative stress handling enzymes, Cu/Zn- and Mn-superoxide dismutases (CuZn-SOD1 and Mn-SOD2), act as a defense system to prevent an excessive accumulation of reactive oxygen species (ROS) in the cell, which assist in the cells' ability to resist prooxidant attack and delay apoptosis [24, 25]. Specifically, damages to the cytoskeleton, mitochondrial dysfunction, and altered signal transduction have been shown to result from oxidative stress-related cascades due to TBI [23, 25]. We found at 10psi blast pressure there was an increase in both CuZn-SOD1 and Mn-SOD2, suggesting an attempt for the cells to prevent an accumulation of ROS thus preventing cell death. Increased levels of extracellular glutamate concentration in the brain may lead to neuronal cell damage and eventual death [26, 27]. The reuptake of glutamate is regulated via glial excitatory amino acid transporters (EAATs); (EAAT1 is the human homologue of the rodent glutamate/aspartate transporter-1 (GLAST/GLAST1)) [26, 27]. Therefore, an increase of the GLAST expression found in our study at 10psi blast pressure, suggests there was an increase in extracellular glutamate, consequently astrocytes are working to take it up and avoid neuronal cell damage. Brain derived neurotropic factor (BDNF) and glial cell line derived neurotropic factor (GDNF) are both known neuroprotective neurotrophins [28, 29]. Studies have shown following TBI, GDNF and BDNF treatment served as a neuroprotective for damaged neurons [28-30]. Our results showed an increase in both GDNF and BDNF expression after 10psi blast exposure therefore implying cells are trying to protect the damaged neurons.

At 14psi pressure exposure there was a significant increase in glial fibrillary acidic protein (GFAP) and Piezo2 gene expression compared to shams. Astrocytes are characterized by their intermediate filaments made up of polymerized GFAP [31]. Studies have shown after injury, astrocytes become activated and GFAP levels are increased [31-33]. Piezo2 is a transmembrane protein that is expressed in neurons [34]. Elevated expression of both GFAP and Piezo2 suggest possible membrane damage to the cell. Results at 24psi depicted a significant down-regulation of GLAST and Mn-SOD2 in blasted rats compared to the shams. Similarly, a study done by Rao et al, found that after traumatic brain injury, there was a down-regulation of GLAST in rat brains [35]. Reduced levels of GLAST may lead to an accumulation of glutamate in the extracellular

space, which subsequently results in neuronal damage due to glutamate-mediated excitotoxicity [26, 27, 35]. Furthermore, reduced levels of Mn-SOD2 may result in excess ROS and consequent in cell death.

Summary

Overall, different exposed peak overpressures show varied responses for the expression in genes of survival and glial activation cascades with a delayed effect (7 days following BOP exposure) on 10psi and 14psi compared to higher pressure groups (>14 psi) as demonstrated in VandeVord et al [16]. Despite ongoing protective effects, increased apoptosis could trigger a delayed defect in the hippocampus and the amygdala on 10 psi and 14 psi can explain the anxiety associated effects in contrast to 24 psi. While this study has significantly advance the knowledge of molecular changes that occur with blast exposure, further studies are vital to provide a more complete molecular picture of the temporal response of the brain to blast exposure. The results lead to further questions that need to be accomplished at the cellular level. It is likely that the different cells of the brain response and acquires injury at different levels. We would like to pursue this research at the cellular level to expand and thoroughly examine the cell membrane responses to blast energy.

KEY RESEARCH ACCOMPLISHMENTS

- We demonstrated that the skull acts as an interface between the shock wave and the brain.
- Front facing measurements demonstrate an increase over the incident shock wave magnitude.
- As a rat became heavier/more mature, the secondary signal would oscillate at lower frequencies and that greater incident shock wave intensities were required to invoke this oscillatory response.
- Instrumentation placement appeared to alter the frequency of the pressure oscillations within the brain. Factors associated with those modifications included the additional mass and stiffness on the surface of the brain case from the application of bone cement and equipment for mounting the pressure sensor.
- We developed a new method for ICP recordings to address the issues associated with instrumenting the top of the skull. The new method includes a fiber optic sensor which is mounted into the occipital bone to measure the intracranial pressure response without changing the native properties of the superior surface.
- New instrumentation method indicated that mounting of instrumentation to the superior surface did have an effect on the observed oscillatory response.
- The results from the strain gage data further substantiates the hypothesis that the incident shock wave is causing the skull to flex. The rapid compression that increases in magnitude with the intensity of the incident shock is believed to be the direct result of the shock wave compressing the skull surface.

- Different exposed peak overpressure showed varied responses for the expression in genes of survival and glial activation cascades with a delayed effect.
- Increased apoptosis may contribute to the delayed defect in the hippocampus and the amygdala on 10psi and 14psi which may explain the anxiety associated effects in contrast to 24psi.
- Hippocampus and Amygdala are significantly affected by blast.

REPORTABLE OUTCOMES

Publications:

1. Leonardi AC, Bir CA, Ritzel D, VandeVord PJ. Intracranial pressure increases during exposure to a shock wave. *J Neurotrauma*. Jan;28(1):85-94 (2011) (Impact factor = 4.25)
2. Bolander R, Mathie BA, Bir CA, Ritzel D, VandeVord PJ. The Contribution of Skull Flexure as a Possible Mechanism for Neurotrauma in the Rat when Exposed to a Shock Wave. *Annals of Biomedical Engineering*; Oct;39(10):2550-9. (2011) (Impact factor = 2.4)
3. Leonardi AC, Keene, N. Bir CA, VandeVord PJ. Head Orientation Affects the Intracranial Pressure Response Resulting from Shock Wave Loading in the Rat, Journal of Biomechanics; Oct 11;45(15):2595-602 (2012) (Impact factor = 2.4)
4. Sajja VS, Hubbard WB, Hall C, Hampton C, VandeVord PJ. Anxiety-like behavior and cellular response varies with blast pressure. *In preparation*.

Poster Presentations:

1. *Bolander R, Bir CA, VandeVord PJ. Maturation related changes may explain a range specific response in the rat model to shock wave induced neurotrauma**.** *The Eight World Congress on Brain Injury,* Washington DC. March 2010.

   Awarded first place poster presentation.

2. Dal Cengio AL, Ritzel D, VandeVord PJ. Cranial Flexure as a Primary Mechanism for Blast-TBI. *Proceedings for the National Neurotrauma Society*. Las Vegas, NV, July 2010.
3. Mathie BM, VandeVord PJ. Variances in the Blast-Induced Intracranial Pressure Response Due to Subject Orientation. *Advanced Technology Applications for Combat Casualty Care*, St. Petersburg, FL, August 2010.
4. Mathie BM, VandeVord PJ. Variances in the Blast-Induced Intracranial Pressure Response Due to Subject Orientation. *Biomedical Engineering Society Annual Meeting,* Austin, TX, October, 2010.
5. Sajja S, Galloway M, Ghoddoussi F, VandeVord PJ. Neurochemical Profiles of Blast Induced Traumatic Brain Injury in Rat Hippocampus and Nucleus Accumbens. *Society for Neuroscience Annual Meeting,* San Diego, CA, 2011

6. Dal Cengio AL, Keane N, Bir C, VandeVord PJ. Effects of Head Orientation on the Intracranial Pressure of Rats Exposed to Shock Waves. *Proceedings of the ASME 2012 Summer Bioengineering Conference*, Puerto Rico, 2012.
7. Hubbard WB, Sajja S, Hampton C, VandeVord PJ. The behavioral, histological, and molecular effects of exposure to blast waves with different peak pressures. Submitted to *Biomedical Engineering Society Annual Meeting,* Seattle 2013.

CONCLUSIONS

There is a pressing need for a comprehensive explanation of the mechanism of traumatic brain injury after exposure to blast. Understanding the biomechanical response and its relationship to the injury outcomes is vital to helping personnel affected by blast TBI. The progression we made these past years will have a large impact in the area of blast neurotrauma. Made clear by the series of publications from our work is the sensitivity of the brain-skull system to shock waves. The data has provided key evidence that skull flexure is a likely candidate for the development of ICP gradients within the rat brain and that these ICP gradients contribute to the neurological deficits found in the animals following blast. We expect that this knowledge will be of significant value to computational models of blast and the future design of protective gear for military personnel.

REFERENCES

1. Okie S. Traumatic Brain Injury in the War Zone. *N. Engl. J. Med.* 2005; 352:2043-2047.
2. Leung LY, VandeVord PJ, Dal Cengio AL, Bir C, Yang KH, King AI. Blast related neurotrauma: a review of cellular injury. *Mol. Cell. Biomech*. 2008; 5:155–168.
3. Fausti SA, Wilmington DJ, Gallun FJ, Myers PJ, Henry JA. Auditory and vestibular dysfunction associated with blast-related traumatic brain injury. *J. Rehabil. Res. Dev*. 2009; **46:**97–810.
4. Trudeau DL, Anderson J, Hansen LM, Shagalov DN, Schmoller, J, Nugent S, Barton S. Findings of Mild Traumatic Brain Injury in Combat Veterans With PTSD and a History of Blast Concussion. *J. Neuropsychiatry Clin. Neurosci*. 1998; 10:308-313.
5. Svetlov SI, Larner SF, Kirk DR, Atkinson J, Hayes RL, Wang KK. Biomarkers of Blast-Induced Neurotrauma: Profiling Molecular and Cellular Mechanisms of Blast Brain Injury. *J. Neurotrauma* 2009; 26:913-921.
6. Warden D. Military TBI During the Iraq and Afghanistan Wars. *J. Head Trauma Rehabil*. 2006; 21:398-402.
7. Jeffrey VR, Nick LF. Bomb blast, mild traumatic brain injury and psychiatric morbidity: A review. *Injury* 2010; 41:437-443.
8. Kochanek PM, Bauman AR, Long JB, Dixon CE, Jenkins LW. Blast-induced traumatic brain injury and polytrauma--a critical problem begging for new insight and new therapies. *J. Neurotrauma* 2009; N/A

9. Säljö A, Svensson B, Mayorga M, Hamberger A, Bolouri H. Low-level blasts raise intracranial pressure and impair cognitive function in rats. *J. Neurotrauma* 2009; 26:1345-1352.
10. Kliethermes CL., et al. Anxiety-like behavior in mice in two apparatuses during withdrawal from chronic ethanol vapor inhalation. *Alcohol Clinical Experiment Research* 2004 Jul; 28(7):1012-9.
11. Chaouloff F., et al. Anxiety- and activity-related effects of diazepam and chlordiazepoxide in the rat light/dark and dark/light tests. *Behavioral Brain Research* 1997 Apr; 85(1):27-35.
12. Schmittgen, T.D. and K.J. Livak, *Analyzing real-time PCR data by the comparative C(T) method.* Nat Protoc, 2008. **3**(6): p. 1101-8.
13. Livak, K.J. and T.D. Schmittgen, *Analysis of relative gene expression data using real-time quantitative PCR and the 2(-Delta Delta C(T)) Method.* Methods, 2001. **25**(4): p. 402-8.
14. Brown E.N., et al. General Anesthesia, Sleep, and Coma. *New England Jounral of Medicine* 2010; 363:2638-2650
15. Sofroniew, M.V., Molecular dissection of reactive astrogliosis and glial scar formation. *Trends Neurosci*, 2009. 32(12): 638-647.
16. VandeVord, P.J., et al., Mild neurotrauma indicates a range-specific pressure response to low level shock wave exposure. *Ann Biomed Eng*, 2012. 40(1): 227-36.
17. Sajja, V.S.S.S., et al., Blast-induced neurotrauma leads to neurochemical changes and neuronal degeneration in the rat hippocampus. *NMR Biomed*, 2012. 25(12): p. 1331-1339.
18. Cernak, I., et al., The pathobiology of blast injuries and blast-induced neurotrauma as identified using a new experimental model of injury in mice. *Neurobiol Dis*, 2011. 41(2): 538-551.
19. Davalos, D et al., ATP mediates rapid microglial response to local brain injury in vivo. *Nat Neurosci*. 2005. 8(6):752-758.
20. Cernak, I., et al., Ultrastructural and Functional Characteristics of Blast Injury-Induced Neurotrauma. *J Trauma Acute Care Surg*, 2001. 50(4): 695-706.
21. Zhang, Q.G., et al., *Critical role of NADPH oxidase in neuronal oxidative damage and microglia activation following traumatic brain injury.* PLoS One, 2012. **7**(4): p. e34504.
22. Ansari, M.A., K.N. Roberts, and S.W. Scheff, *A time course of contusion-induced oxidative stress and synaptic proteins in cortex in a rat model of TBI.* J Neurotrauma, 2008. **25**(5): p. 513-26.
23. Ansari, M.A., K.N. Roberts, and S.W. Scheff, *Oxidative stress and modification of synaptic proteins in hippocampus after traumatic brain injury.* Free Radic Biol Med, 2008. **45**(4): p. 443-52.

24. Michael Y. Aksenov, H.M.T., Prakash Nair, Marina V. Aksenova, D. Allan Butterfield, Steven Estus,and William R. Markesbery, *The Expression of Key Oxidative Stress-Handling Genes in Different Brain Regions in Alzheimer's Disease.* Journal of Molecular Neuroscience, 1998. **11**: p. 151-164.
25. Bayir, H., et al., *Neuronal NOS-mediated nitration and inactivation of manganese superoxide dismutase in brain after experimental and human brain injury.* J Neurochem, 2007. **101**(1): p. 168-81.
26. Yi, J.H. and A.S. Hazell, *Excitotoxic mechanisms and the role of astrocytic glutamate transporters in traumatic brain injury.* Neurochem Int, 2006. **48**(5): p. 394-403.
27. R. Beschorner, K.D., N. Schauer, M. Mittelbronn, H.J. Schluesener, K. Trautmann, R. Meyermann and P. Simon, *Expression of EAAT1 reflects a possible neuroprotective function of reactive astrocytes and activated microglia following human traumatic brain injury.* Histol Histopathol 2007. **22**: p. 515-526.
28. Minnich, J.E., et al., *Glial cell line-derived neurotrophic factor (GDNF) gene delivery protects cortical neurons from dying following a traumatic brain injury.* Restor Neurol Neurosci, 2010. **28**(3): p. 293-309.
29. Kim, B.T., et al., *Protective effects of glial cell line-derived neurotrophic factor on hippocampal neurons after traumatic brain injury in rats.* J Neurosurg, 2001. **95**(4): p. 674-9.
30. Gao, X. and J. Chen, *Conditional knockout of brain-derived neurotrophic factor in the hippocampus increases death of adult-born immature neurons following traumatic brain injury.* J Neurotrauma, 2009. **26**(8): p. 1325-35.
31. Buffo, A., C. Rolando, and S. Ceruti, *Astrocytes in the damaged brain: molecular and cellular insights into their reactive response and healing potential.* Biochem Pharmacol, 2010. **79**(2): p. 77-89.
32. Yates, D., *Traumatic brain injury: Serum levels of GFAP and S100B predict outcomes in TBI.* Nat Rev Neurol, 2011. **7**(2): p. 63.
33. Vos, P.E., et al., *GFAP and S100B are biomarkers of traumatic brain injury: an observational cohort study.* Neurology, 2010. **75**(20): p. 1786-93.
34. Coste, B., et al., *Piezo1 and Piezo2 are essential components of distinct mechanically activated cation channels.* Science, 2010. **330**(6000): p. 55-60.
35. Rao, V.L., et al., *Traumatic brain injury down-regulates glial glutamate transporter (GLT-1 and GLAST) proteins in rat brain.* J Neurochem, 1998. **70**(5): p. 2020-7.

APPENDIX

1. Leonardi AC, Bir CA, Ritzel D, VandeVord PJ. Intracranial pressure increases during exposure to a shock wave. *J Neurotrauma*. Jan;28(1):85-94 (2011) (Impact factor = 4.25)
2. Bolander R, Mathie BA, Bir CA, Ritzel D, VandeVord PJ. The Contribution of Skull Flexure as a Possible Mechanism for Neurotrauma in the Rat when Exposed to a Shock Wave. *Annals of Biomedical Engineering*; Oct;39(10):2550-9. (2011) (Impact factor = 2.4)
3. Leonardi AC, Keene, N. Bir CA, VandeVord PJ. Head Orientation Affects the Intracranial Pressure Response Resulting from Shock Wave Loading in the Rat, Journal of Biomechanics; Oct 11;45(15):2595-602 (2012) (Impact factor = 2.4)

JOURNAL OF NEUROTRAUMA 28:85–94 (January 2011)
© Mary Ann Liebert, Inc.
DOI: 10.1089/neu.2010.1324

Intracranial Pressure Increases during Exposure to a Shock Wave

Alessandra Dal Cengio Leonardi,[1] Cynthia A. Bir,[1] Dave V. Ritzel,[2] Pamela J. VandeVord[1]

Abstract

Traumatic brain injuries (TBI) caused by improvised explosive devices (IEDs) affect a significant percentage of surviving soldiers wounded in Iraq and Afghanistan. The extent of a blast TBI, especially initially, is difficult to diagnose, as internal injuries are frequently unrecognized and therefore underestimated, yet problems develop over time. Therefore it is paramount to resolve the physical mechanisms by which critical stresses are inflicted on brain tissue from blast wave encounters with the head. This study recorded direct pressure within the brains of male Sprague-Dawley rats during exposure to blast. The goal was to understand pressure wave dynamics through the brain. In addition, we optimized *in vivo* methods to ensure accurate measurement of intracranial pressure (ICP). Our results demonstrate that proper sealing techniques lead to a significant increase in ICP values, compared to the outside overpressure generated by the blast. Further, the values seem to have a direct relation to a rat's size and age: heavier, older rats had the highest ICP readings. These findings suggest that a global flexure of the skull by the transient shockwave is an important mechanism of pressure transmission inside the brain.

Key words: blast; improvised explosive device; intracranial pressure; overpressure; traumatic brain injury

Introduction

Blast traumatic brain injuries (blast TBI) caused by improvised explosive devices (IED) affect a significant percentage of surviving soldiers wounded in Iraq and Afghanistan (Warden, 2006). There is a pressing need for a comprehensive explanation of the mechanism of injury of TBI after exposure to blast. Substantial resources have been spent on the IED problem with regard to methods to defeat this threat, deal with casualties, and develop countermeasures. Although little is known about the mechanism of trauma induced by blast waves, it is now known that blast TBI can occur without obvious external injuries, loss of consciousness, or visible findings on magnetic resonance imaging (Bhattacharjee, 2008; Cernak et al., 1999; Guy et al., 2000; Irwin et al., 1997). The extent of a blast TBI, especially initially, is difficult to diagnose, as internal injuries are frequently unrecognized and therefore underestimated, yet problems develop over time. It is essential to understand the physical mechanisms by which critical stresses are inflicted on brain tissue from blast wave encounters with the head. Only with a careful assessment of the physics of the blast/head interaction will it be possible to determine the modes by which injury is inflicted at the cellular level. Subsequently, effective treatments and protective technologies may be developed.

The precise mechanism of blast TBI is not well understood and several hypotheses have been suggested. Some have proposed that damage is due to transosteal propagation (Clemedson, 1956; Clemedson and Jonsson, 1961a), or the shockwave entering the brain by propagating directly through the skull. Others contend that blood vessels from the body can transmit the outside hydrostatic pressure to the brain, causing damage (Cernak et al., 2001; Courtney and Courtney, 2009; Young, 1945), or suggest that damage to the lungs can elicit a physiological response creating injury to the brain (Cernak et al., 1996). Still others propose that a pressure wave imparted to a different point in the body could have enough magnitude to be transmitted to the brain and cause histologically observable damage (Suneson et al., 1990). Recently, computational simulations using a finite-element model that has not yet been validated by experimental results, have shown that skull flexure, in the form of transverse waves, may be a mechanism of stress transfer and injury (Moss et al., 2009). Preliminary studies conducted by our group have led us to hypothesize that other modes of skull deformation, including "global" compression, may contribute

[1]Department of Biomedical Engineering, Wayne State University, Detroit Michigan.
[2]Dyn-FX Consulting Ltd., Amherstburg, Ontario, Canada.

to generating injurious stress waves within the head (Dal Cengio Leonardi et al., 2009).

Some animal tests have been designed and carried out in an attempt to learn more about the mechanism of shock-wave transmission to the brain, but only a few animal studies recorded direct pressure within the brain tissue during exposure to blast (Chavko et al., 2007; Clemedson, 1956; Clemedson and Jonsson, 1961b; Romba and Martin, 1961). Such experiments are challenging to conduct because the instrumentation technology, which measures the true *in vivo* pressure condition during shock exposure, has not yet been perfected and validated. These tests also carry the burden of the complex preparation of the animals, which must be carried out while adhering to strict guidelines for animal handling.

The objective of our research was to investigate shock-wave dynamics through the brain. In order to provide clues about the mechanism by which this pressure was being imparted, we set out to measure the transient intracranial pressure (ICP) in an animal model subjected to an air shockwave, in order to identify features of the pressure wave profile, such as wave shape, peak overpressure, and impulse and duration of the positive phase. In the process of performing this study some factors of the head anatomy and the measurement technique were explored that might affect the results.

Regarding head anatomy, the orbits provide a potential pathway for an external pressure wave to propagate into the brain. Thus, ICP measurements were compared with and without this pathway blocked. Since the thickness and stiffness of the skull increase with the age and size of the rat (Gefen et al., 2003), measurements were compared for rats of different ages. Regarding instrumentation, the effects of the location of the sensor in a fluid cavity (lateral ventricle) or tissue mass (frontal cortex) were compared. Since theory would suggest that any pressure leakage would diminish pressure developed within the skull, the sensitivity of the ICP measurement to sealing of the gauge at its penetration point of the skull was assessed. As these measurements are critical to understanding the processes by which the brain is stressed, it was important to devise experiments that reliably replicate those of actual blast injury. Certain requirements needed to be met in terms of generating the shock-wave pressure (both static and dynamic components), animal restraint, and sensor mounting.

Methods

Wayne State University shockwave generator

While we acknowledge that the mechanism of brain injury from an IED blast could involve several factors, which have traditionally been referred to as primary, secondary, and tertiary injuries, our goal was to focus on one of the hypotheses for primary brain injury due to blast: global skull flexure. In order to do this in a standard laboratory setting, a shock tube is the most practical instrument to generate the shock-wave. To simulate a free-field blast wave, a shock tube activated by compressed gas is commonly used. In this study, the simulated blast waves were generated by a helium-driven shock tube located at the Wayne State University Bioengineering Center. Our shock tube consists of two separate chambers: the driver section (30 inches long, 12 inches in diameter), which is filled with highly pressurized helium; this is separated by a Mylar membrane from the driven section (242 inches long, 12 inches in diameter), which is filled with ambient air, and where the specimen is placed (Celander and Clemedson, 1954). Upon rupture of the membrane, a shock-wave is propagated into the driven section by the rapid expansion of gases from the driver section.

The air shockwave developed in the test section evolves as a combination of waves, and approximates that from a chemical explosion, if care is taken in the location of the specimen within the tube. When the membrane bursts, a uniform shock front quickly develops and propagates down the test section. Since the cross-section of the shock tube is constant, the shockwave moves at a constant speed unattenuated down the tube until the reflected rarefaction from the closed end of the driver overtakes it. Prior to this overtaking, the shock waveform will feature a flat section after the peak. Following the overtaking, the waveform for static pressure, also called the incident pressure wave, will have a decaying profile similar to a blast wave. In this phase, the dynamic pressure component of the shockwave is similar to that of a free-field blast. It is important to note that any zone within the shock tube that is appropriate for blast simulation will eventually be affected by the arrival of disturbances and gas dynamic features entirely atypical of blast waves. Examples of such anomalous disturbances include the arrival of the contact surface with expanding driver gas, and the arrival of the strong rarefaction created by the open end of the tube. At some locations within the tube, the effects of these anomalous flow features are exaggerated, and will corrupt the experimental conditions much earlier. These factors were taken into consideration, and the animals were placed inside the tube at such a distance from the open end to optimize the shock-wave pressure. Our specimens were placed inside the driven section, and the head was positioned 198 inches downstream from the bursting membrane (44 inches from the open end of the tube).

Extremely adverse effects will result from experiments staged with a specimen near the end of the tube, where the end-rarefaction will quickly cause imbalance of high dynamic pressures, yet reduced static pressure conditions. The specimen in this regime would in fact be subjected to a nearly pure jet-stream outflow, with exaggerated underpressures or vacuum, or a shock propagating upstream.

Animal preparation

Approval from the Wayne State University Institutional Animal Care and Use Committee was obtained prior to testing. All animals were purchased from the same vendor and were kept under the same housing conditions at the WSU animal facilities. Twenty-five male Sprague-Dawley rats (245–395 g) were anesthetized with ketamine/xylazine (100/20 mg/mL IP), their heads were shaved, and they were placed in a stereotaxic frame. A longitudinal incision allowed visualization of the bregma and the lambda. A 1-mm hole was drilled in the skull for insertion of a guided cannula (18 gauge). Two sites were chosen for placement of the cannula: the ventricle (−1.3 AP, −1.8 ML, −3.2 DV), or the frontal cortex (+3 AP, −2 ML, −1 DV). The cannula was anchored to the skull by bone cement, and two screws were used to reinforce the anchoring site. A dummy-cannula (cap) was screwed onto the cannula to close the opening while the animal was recovering. The scalp was sutured around the cannula, covering the screws and the bone cement. Seven days after surgery, the animal was anesthetized with ketamine/xylazine (100/20 mg/mL IP) and placed in a soft holder before exposure to shockwaves (Fig. 1).

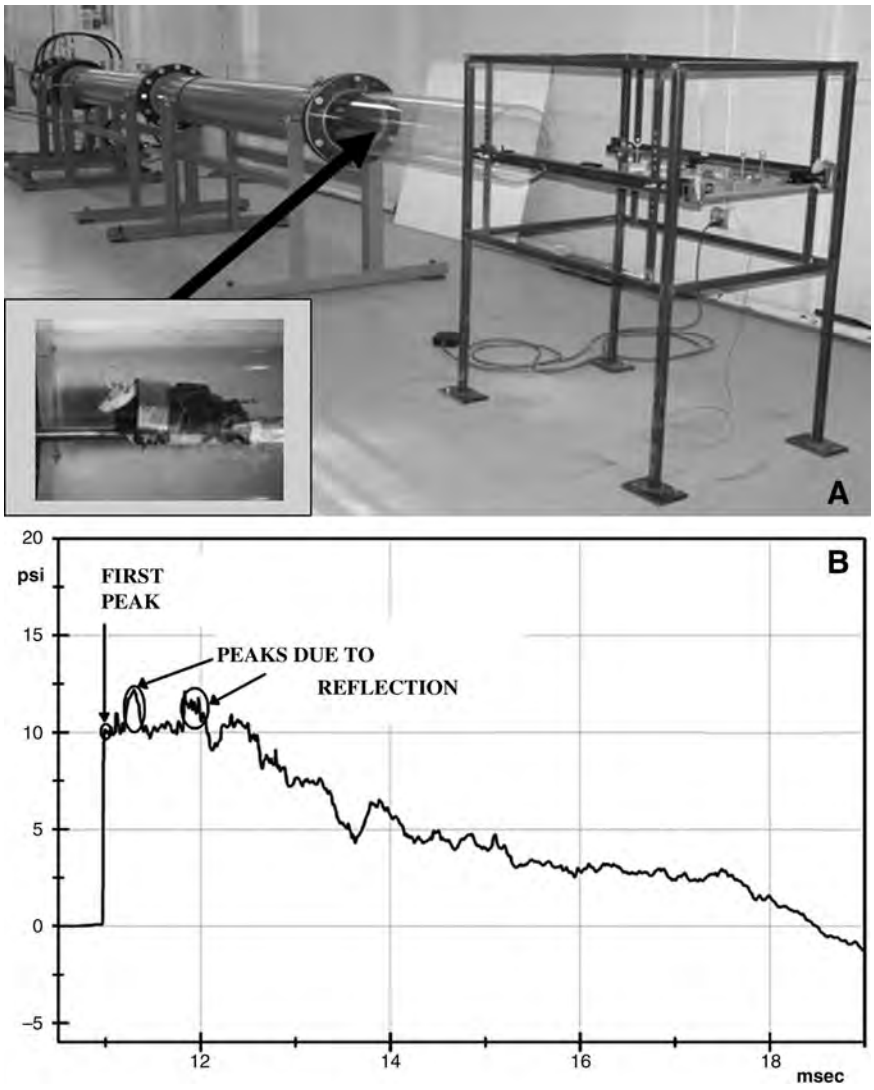

FIG. 1. (**A**) Photo of the Wayne State University shockwave generator; the arrow points to the position of the specimen's head, which is 44 inches from the end of the tube. The inset shows the rat holder in position. (**B**) An incident shockwave profile generated by the WSU shock tube. The graph shows the first peak, which is the true overpressure value, and a few later higher peaks, that are due to reflections of the shockwave off of the rat and rat holder. These later peaks are not present if the pressure sensor is placed at the same position without the presence of the rat and rat holder.

The holder was positioned so that the rat's head was 44 inches from the open end of the tube, facing the shockwave frontally. By means of a long rod, the holder was connected to a trolley positioned outside the tube. The purpose of this moveable trolley was to minimize mechanical stresses imparted to the specimen due to its restraint in the shockwave flow.

The rats were instrumented with a specially-adapted miniature optical ICP gauge and exposed to simulated blast waves of approximately 10 psi (68.95 kPa) in magnitude, and 7.5 msec in positive phase duration (Fig. 1). After exposure, all anesthetized animals were immediately sacrificed by perfusion with 4% paraformaldhyde; the brains were removed and collected for histological verification of sensor position.

Pressure sensors

Two PCB sensors (model 102A06; PCB Piezotronics, Inc., Depew, NY) were mounted on the inside wall of the shock tube at two separate locations to monitor the development of the shock front and measure its speed. The first wall sensor was placed 72 inches downstream from the bursting membrane, and the second wall sensor was 181 inches downstream from the membrane. A third PCB sensor (model 137A22; PCB Piezotronics, Inc.), commonly called "the pencil" because of its aerodynamic shape, was placed 1 inch in front of the animal's head (thus meeting the shock front slightly before the specimen) to record the static pressure delivered. A fourth sensor was used to record the ICP in the animal (model FOP-MIV; FISO Technologies, Quebec City, Quebec, Canada).

Multiple sensors were used in this study because they differ on several levels. First, the mechanism of measuring pressure is distinctive. The PCB sensors utilize a quartz piezoelectric element to convert strain created by a sudden change in ambient pressure into a voltage output, compared to the FISO sensors, that measure pressure by converting wavelength-modulated light into a voltage value. Additionally, the PCB

sensors are robust and designed to withstand the energy of the shockwave in open air. The FISO optic sensor, on the other hand, was designed for medical applications and is very fragile, weighing only 0.163 mg. The characteristics of these sensors are especially important when making *in vivo* measurements in small animals, since the sensor should approximate the density of the tissue surrounding it, and ideally move with the cells. Otherwise, the inertia of the sensor may affect the reading of *in vivo* pressure.

Experimental set-up

In order to obtain the most accurate ICP measurements, we investigated the effects of various sealing methods of the cannula. The rodents were divided into three groups: A, B, and C, according to the sealing method used during exposure to the simulated blast. In group A, the cannula opening was not sealed after insertion of the optic sensor. The sensor was simply held in place by duct tape that wrapped around the cannula and the head. In group B, modeling putty was placed around the optic cable, at the opening of the cannula, and taping was performed as for group A. Using a modeling compound was a rudimentary attempt to provide partial sealing of the system. In group C, an optic sensor was modified to provide complete sealing of the cannula during testing. The optic sensor fiber was glued onto the dummy-cannula with a two-part epoxy glue (drying time 5 min) after the stem had been removed. The optic sensor and fiber replaced the internal stem of the dummy-cannula, and this mount provided a durable and full mechanical seal once the dummy was screwed onto the cannula (Fig. 2). For group C, additional care was taken to ensure the removal of air bubbles. Saline solution was placed in the cannula through a syringe and petroleum jelly was added to the cap thread immediately prior to insertion of the optic sensor to ensure that no air was left in the cannula. Note that this procedure was not necessary for the other two groups because of the different types of installation. For group A, by design there was no seal, therefore ambient air was in contact with the fluid in the cannula. For group B, putty was applied at the cannula entrance, while care was taken to have CSF all the way to the cannula's edge. Unlike a rigid dummy-cannula, the modeling compound easily adapts to the cannula's contours, creating direct contact between the CSF and the putty.

Each anesthetized rat was subjected to a minimum of six shockwave tests with experimental conditions kept identical for three trials at a time. Group A was subjected to different incident overpressures to determine the optimal testing pressure. Groups B and C were exposed to only one incident overpressure, and in the first three trials the eyes were left exposed to the shockwave, while in the next three the eyes were protected by eyegear (to study the effects of the apertures in the skull on pressure transmission). A total of 129 exposures occurred at the chosen pressure of 10 psi (68.95 kPa). In all three groups two brain locations were randomly investigated. Each rat had the optic pressure sensor placed either in the frontal cortex or in the lateral ventricle (numbers in ventricle/cortex: group A 1/6; group B 3/2; group C 5/8). The lateral ventricle was chosen to compare with a previous study (Chavko et al., 2007), while the frontal cortex site was introduced to investigate if changes in depth with respect to the shockwave would have an effect on the measured pressure-wave profile results.

Histological assessment of cannular position

All animals survived testing and subsequently underwent transcardial perfusion with 4% paraformaldehyde. The brains were removed, processed for post-fixation, and embedded in embedding compound. Sections were cut and stained with hematoxylin and eosin (H&E) to inspect the area of the brain in which the cannula was placed (Fig. 3).

Statistical analysis

Statistical analyses were performed using the statistical package SPSS ver.18 (SPSS Inc., Chicago, IL). First, a paired samples *t*-test was run between the eyes-exposed and the eyes-protected means for both peak and impulse to determine the significant differences. Since differences were not significant and because they were measured from the same rats, those measures, either eye-protected or eye-exposed, were treated as homogeneous observations from the same subject. Therefore, all measures from each rat were used for the data analysis. A linear mixed model was run for the dependent variable "Impulse," assuming that the repeated observations within each rat would cause correlated error terms. A first-order autoregressive covariance structure was chosen for the repeated time factor. The factors "Seal" (groups A, B, and C) and "Position" (Cortex versus Ventricle) were taken as fixed, and the "rat ID" was treated as a random factor. The analysis

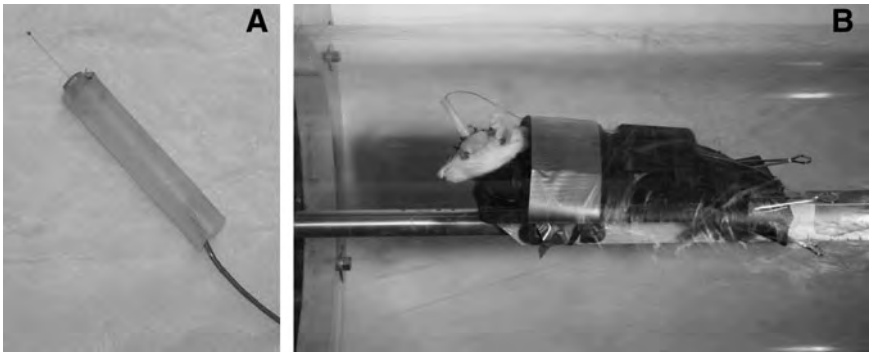

FIG. 2. Placement of the intracranial pressure sensor for group C, which is the sealed group. (**A**) A piece of plastic tubing is glued on top of the dummy cannula to protect the optic cable at its exit from the head. (**B**) The dummy-cannula is screwed onto the guided cannula cemented onto the rat's skull, and the rat is positioned inside the tube.

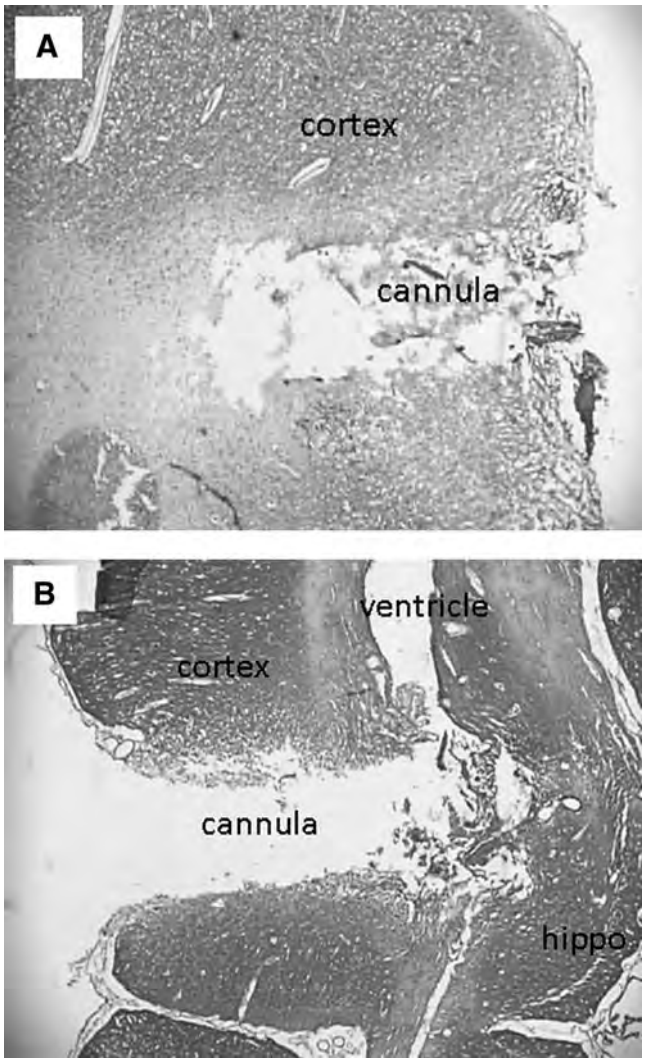

FIG. 3. Histological confirmation of cannula placement. (**A**) Hematoxylin and eosin section demonstrates that the cannula was placed within the cortical tissues. (**B**) Tissue section showing that the cannula pierced through the cortical tissue for placement in the ventricle (hippo, hippocampus).

was statistically significant for "Seal" ($p = 0.002$), but "Position" by itself or in relation to "Seal" was not significant. The variance of error terms was significant ($p = 0.000$), while the correlation of error terms was not significant. The random intercept for "Impulse" was not significant, and the random slopes value was significant ($p = 0.000$). The pair-wise comparison among the groups showed significance between groups A and C ($p = 0.005$), and between groups B and C ($p = 0.028$). A linear mixed model was run for the dependent variable "Peak" for group C only. A first-order autoregressive covariance structure was chosen for the repeated time factor in this case also. The factors "Age" and "Position" were taken as fixed, and the "rat ID" was treated as a random factor. The analyses were significant for "Age" ($p = 0.003$), and for "Position" ($p = 0.017$). The pair-wise comparison among the age groups indicated a significant difference between the "61-day-old" and the "95-day-old" groups ($p = 0.003$), and between the "67-day-old" and the "95-day-old" groups ($p = 0.048$). An alpha level of 0.05 was selected for significance in all statistical tests.

Results

A total of 25 rats were tested: 7 for group A (unsealed); 5 for group B (partially sealed); and 13 for group C (fully sealed). Table 1 shows an example of one rat from each group. Note the high consistency of the values extrapolated from the data collected from each individual rat during the six tests.

For each rat, we recorded 10 msec of pre-trigger data and 40 msec of post-trigger data: this allowed to log a brain pressure baseline (used later to zero each record) and to assure capture of the shockwave's entire positive and negative phase. However, the time duration shown in two of the columns of Table 1 is that of the positive phase only. We documented the weight of the rat before the commencement of testing, and the location of the intracranial (IC) optic pressure sensor. From the data collected, the area under the positive phase (impulse) for both the incident pressure wave recording (pencil sensor), and the intracranial pressure wave recording (optic sensor) was calculated. All IC pressure and impulse values were normalized to their associated value of incident pressure. This normalization is necessary to compare the relative differences in IC pressure to the incident blast, and it is shown in the last two columns of Table 1. The normalized impulse values were obtained by dividing each IC impulse (Impulse Optic) value by the respective incident impulse value (Impulse Pencil). The normalized IC peak pressure values were obtained by dividing each IC peak pressure value (Max Optic Pressure) by the respective incident first peak pressure (Pencil First Peak Pressure). Note that since normalization requires one to ratio two values that are expressed in the same units (psi/psi in the case of pressure, for example), the result is simply a number without unit. As it is not possible to produce an identical shockwave for each test, the significance of such normalized numbers are relative to the pressure and impulse that were provided for that particular test by the shock tube and measured by the pencil gauge. For each test, the first peak of the "pencil profile" (the plot that chronologically recorded the value of static overpressure in the air next to the specimen) was chosen as the representative value for the incident wave peak pressure. It should be noted that the record from the pencil probe shows a higher sharp peak within a millisecond following the shock front, which is a reflection from the specimen and its holder (Fig. 1). Therefore the pencil first peak more truly represents the peak value of the incident wave. Since the maximum value of the pencil profile is reached later on, and is due to a reflection wave coming from the opposite direction of the shock front, that maximum value on the plot can be considered an artifact, and it is not the actual pressure that will hit the specimen.

Statistical analysis showed a significant difference [$F(2,16.89) = 9.586$, $p = 0.002$] in normalized impulse values when examining group A versus group B versus group C, respectively (Fig. 4). This difference is attributable to the different sealing methods used. The mean normalized impulse values were 0.92 for group A, 1.06 for group B, and 1.21 for group C (Fig. 4). It is important to note that to compare the effects seen among the different groups we used the normalized impulse values. The normalized impulse, by representing an integration of the positive-phase pressure profile over time, better tells the story of what is happening to

Table 1. Example of Data Collected from Each Group

Rat/ group	*Weight (g)*	*Location*	*Test type*	*Pencil first peak pressure (psi)*	*Max optic pressure (psi)*	*Duration pencil (msec)*	*Duration optic (msec)*	*Impulse pencil (psi*msec)*	*Impulse optic (psi*msec)*	*Normalized IC peak pressure*	*Normalized IC impulse*
			#1 EE	10.61	20.87	7.56	7.18	41.56	47.78	1.97	1.15
			#2 EE	10.57	20.01	7.43	7.31	40.92	47.35	1.89	1.16
28/C	350	Cortex	#3 EE	10.14	18.44	7.54	7.4	41.84	48.56	1.82	1.16
			#4 EP	10.4	18.72	7.47	7.35	40.24	50.45	1.80	1.25
			#5 EP	10.56	18.14	7.47	7.39	39.8	49.32	1.72	1.24
			#6 EP	10.86	17.92	7.5	7.44	39.91	49.01	1.65	1.23
			#1 EP	9.61	15.51	7.5	6.99	37.7	31.68	1.61	0.84
			#2 EP	9.68	21.66	7.49	5.68	37.47	32.87	2.24	0.88
25/B	341	Cortex	#3 EP	9.98	19.42	7.46	4.96	37.98	30.32	1.95	0.80
			#4 EE	9.63	21.33	7.48	4.96	37.2	31.36	2.21	0.84
			#5 EE	9.68	22.51	7.5	5.12	38	28.84	2.33	0.76
			#6 EE	9.92	22.86	7.44	6.91	37.16	32.98	2.30	0.89
			#1 EE	8.99	9.99	7.54	7.28	37	29.79	1.11	0.81
223/A	NA	Cortex	#2 EE	9.13	9.14	7.54	7.32	36.76	30.65	1.00	0.83
			#3 EE	9.15	10.12	7.46	6.92	36.9	29.51	1.11	0.80

For groups C and B (rats 28 and 25, respectively), there were three tests performed with eyes exposed (EE), and three tests performed with eyes protected (EP). For group A, rat 223, three tests were conducted at one overpressure and three at another; the eyes were always exposed. For rat 223, the only tests presented are the ones at the same overpressure as for groups C and B. The duration in milliseconds for both the pencil and optic sensor refers to the positive phase only. The normalized columns were obtained by dividing the optic sensor value by the respective pencil value.

psi, pounds per square inch; IC, intracranial; NA, not available.

the seal, especially in the case of group B, for which there was a sudden pressure variation (Fig. 5). Figure 5 shows an example of three ICP profiles, one from each group, plotted against the incident wave profile at the specimen location. Comparing each ICP profile to the incident overpressure, we note that the curve from group A follows quite closely the overpressure measured near the animal. On the other hand, the curves from the other two groups greatly differentiate them from the incident overpressure, especially in the first 3 msec from the inception of the shock front. Group B (partially sealed) shows a sharp rise in pressure and a seemingly sharp decrease in pressure that goes even below the incident overpressure, which we attribute to failure of the seal. Likewise group C initially presents with a sharp rise in pressure, but contrary to group B, as the seal continues to hold, the IC pressure remains above the incident overpressure until near the end of the positive phase. Overall we found that proper sealing technique caused an average 30% increase in impulse value for fully sealed versus unsealed.

After we determined the appropriate sealing method (group C), we further investigated how age and weight affected ICP measurements in this group. The weight of group C ranged from 245 to 395 g, and the age ranged from 61 to 95 days. Figure 6 demonstrates the consequence of animal age when measuring ICP. There was a significant increase [$F(2,6.92) = 15.770$, $p = 0.003$] in ICP values in the

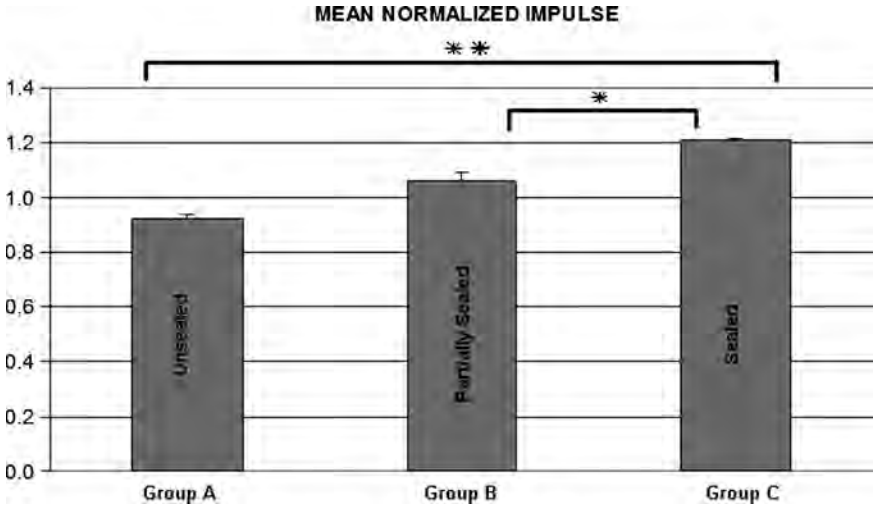

FIG. 4. Mean normalized impulse values with standard error for group A (unsealed), B (partially sealed), and C (completely sealed; *$p = 0.028$; **$p = 0.005$ for pair-wise comparisons).

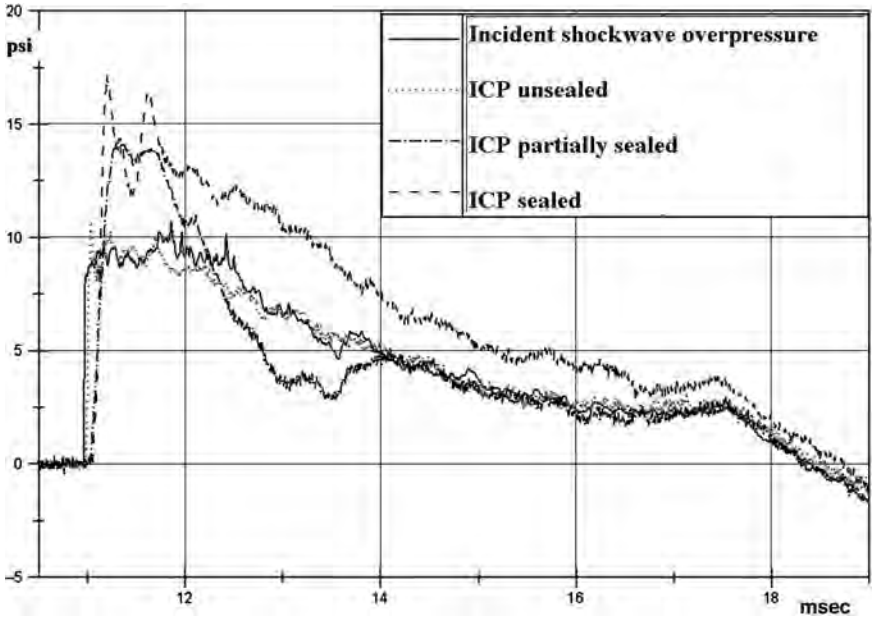

FIG. 5. This is one example of intracranial pressure (ICP) profiles when different types of cannula seal were used. All three specimens had ventricle placement. The incident shockwave overpressure is shown for reference. The ICP profiles show the development of the ICP over time, while the incident overpressure profile shows the chronological development of the hydrostatic pressure outside the head (psi, pounds per square inch).

older animals. Mean normalized IC peak pressure values were found to be 1.40 for the 61-day-old rats, 1.54 for the 67-day-old rats, and 1.68 for the 95-day-old rats. The mean weights for the 61-, 67-, and 95-day-old rats were 269, 280, and 365 g, respectively.

When evaluating sensor placement within the brains of the rats in the sealed group, we observed that ventricle placement provided readings that were slightly more consistent than those from the cortex. When comparing the results from the position of the ICP sensor, we found that the difference in positions was significant [$F(1,6.92) = 9.784$, $p = 0.017$], regardless of age (the interaction term between days and position was not significant). When comparing results for rats of the same age and weight, we observed that the results from the cortex had higher starting values than those from the ventricle, but that they decreased more with successive trials (Figs. 7 and 8). We hypothesize that this shift in the cortex measurements was due to a "well" of fluid developed at the sensor tip, such that the results eventually approached those for the fluid-filled ventricle. Placement of the optic sensor in the fluid of the ventricle appears to cause less interference between the liquid material surrounding the sensor and the device itself, explaining the more consistent results compared to the cortex. Also, when comparing rats having similar age and weight (within 6 g), and different sensor placement, 94% of the tests showed that cortex placement produced higher normalized peak pressure values than ventricle placement. Note that only tests without eyegear were used in this comparison. Since the sensor in the ventricle was positioned deeper in the brain, we hypothesize that the lower peak pressure value could be due to a pressure decrease caused by transmission via a longer path. Additional investigations are needed to examine this hypothesis.

To study the effects that orbits may have on pressure transmission within the brain, we protected the eyes with a custom-made device. This eyegear was a simple strip of

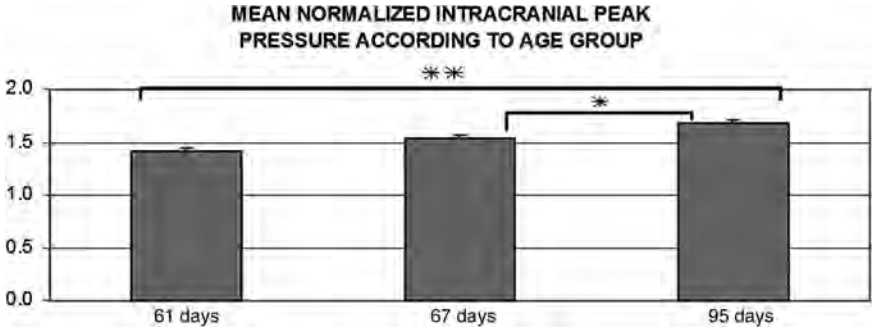

FIG. 6. Mean normalized intracranial peak pressure according to age group in rats from group C (the sealed group). Normalized values were 1.40 for the 61-day-old group, 1.54 for the 67-day-old group, and 1.68 for the 95-day-old group (*$p = 0.048$; **$p = 0.003$ by pair-wise comparisons).

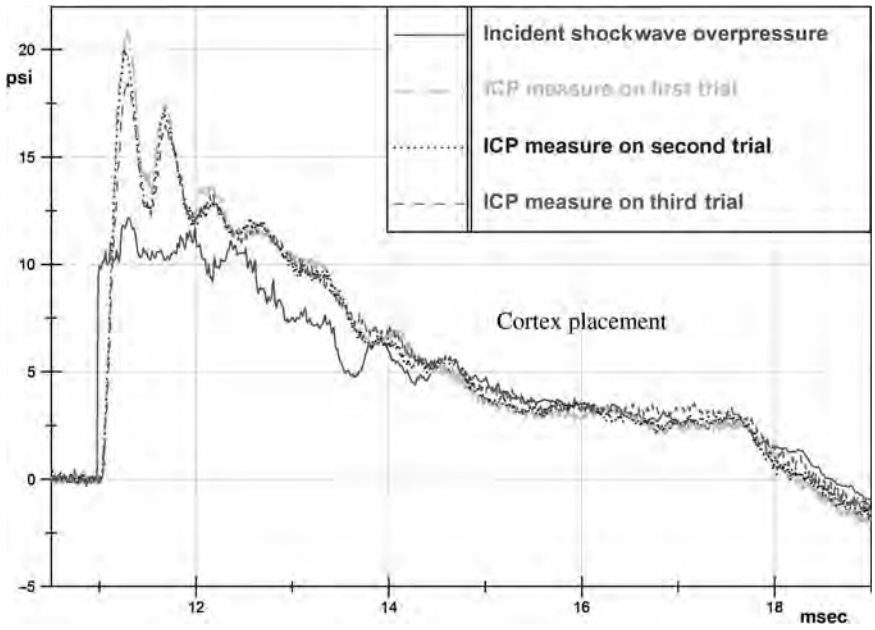

FIG. 7. Example of intracranial pressure (ICP) measures for three trials when the optic sensor was in the cortex. Notice the decrease in peak value from the first to the third trial.

1-mm-thick copper encased in fabric. Copper was chosen because it is lightweight, which added less mass to the rat's skull; it is also pliable, which helped adjust the fit to the rat's contours; and most significantly, it is able to reduce transmission of incident stress waves (Cooper et al., 1991), which we hypothesized would decrease the measured ICP value. Analyses of the transmission of the shockwaves when the orbits were protected found that 69% of the rats had higher ICP values when wearing the eyegear than when the eyes were exposed. Therefore protection of the eyes offered no mitigation of pressure transference to the brain in the sealed rat model. Ultimately, the changes in ICP values between eyes-exposed and eyes-protected animals were not statistically significant. However, the rise in ICP peak value between eyes-exposed and eyes-protected was consistent enough to be noted, and an example of this effect is shown in Figure 9. To explain this effect we suggest that the added mass of the eyegear probably caused an increase in energy transfer to the

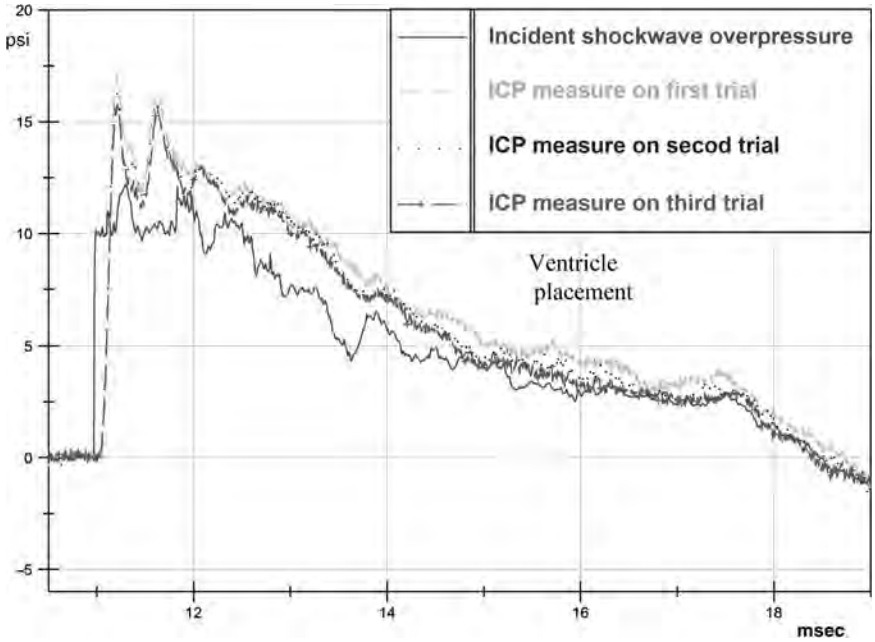

FIG. 8. Example of intracranial pressure (ICP) measures for three trials when the optic sensor was in the ventricle. Notice the decrease in peak value from the first to the third trial.

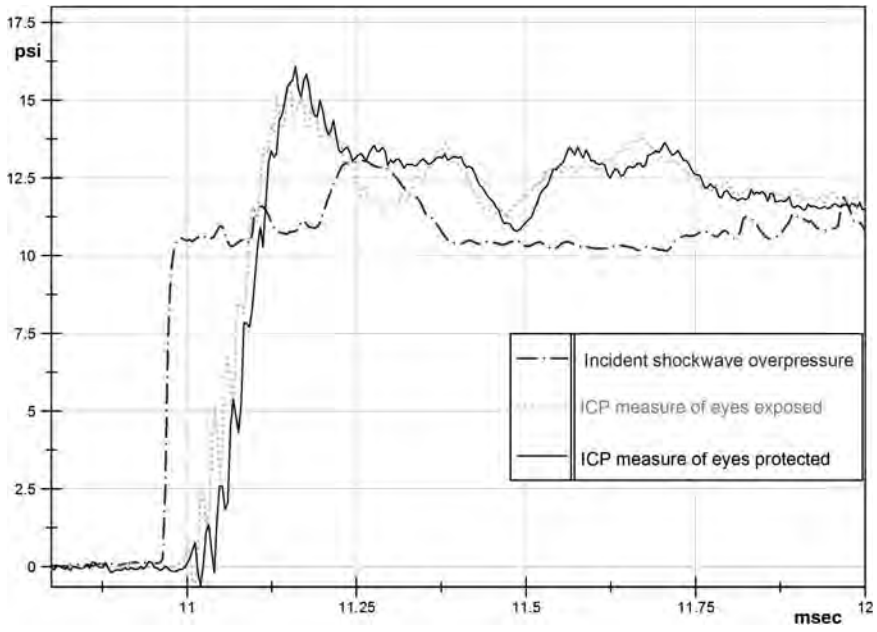

FIG. 9. Example of intracranial pressure (ICP) measures for the same rat with the eyes exposed and the eyes protected; 69% of the rats in group C had higher ICP values when wearing the eyegear; however, this change was not significant. To minimize variation between trials, we compared only the two trials next to each other (third and fourth trials) when determining these percentages. The added mass of the eyegear may have caused the difference in peak pressures seen with the eyes exposed and the eyes protected.

skull-brain system. This finding may be useful for the future development of protective headgear.

Discussion

Understanding the exact means by which stress is imparted to brain tissue from blast exposure to the head, and carefully resolving the spatial and temporal nature of these stress conditions, are fundamental to resolving the blast TBI problem. There is a pressing need for a comprehensive explanation of the mechanism of TBI after exposure to blast, and the testing of animals instrumented with pressure sensors in the brain is one step toward fulfilling this need. The results of the current study highlight two major findings, which will have a major impact on understanding the pressure wave dynamics seen during blast. First, we discovered that with proper sealing methods, there is a significant increase in ICP when the brain is exposed to a shockwave. Second, the physical maturity of the animals themselves has a considerable effect on the ICP measured within the brain.

The present study shows that the degree to which a test aperture is sealed can significantly affect ICP measurements. This is important because apertures must be created to obtain ICP readings with current sensor technologies. These findings demonstrate that without proper sealing of the skull, accurate measurements of ICP may not be obtained. Furthermore, when the cannula was left unsealed, the ICP values closely followed the incident shock-wave overpressure. This was not the case when the seal was engaged. When comparing the ICP profiles for the partially sealed group, the variations in the shapes of the ICP profiles were greater than those in the other two groups. This is probably because of the intrinsic variability of the partially sealed set-up. Finally, when looking more closely at the ICP profiles for the sealed group, there is an oscillation, which appears in the initial 2 msec from inception of the pressure front. We hypothesize that this oscillation is due to the specific material response of the rat skull that reveals itself at the ICP sensor. Because the sensor is anchored to the skull, it is impossible to avoid mapping skull motion if it occurs. Thus, global flexure of the skull, caused by the pressure-wave dynamics with the head, could translate into pressure oscillation within the tissues.

Additionally, the present study confirms that the weight and age of the animals are the most influential factors on pressure-wave transmission. The rat's weight and age directly determine the skull's overall size and maturity (Gefen et al., 2003), with older rats presumably possessing thicker, more rigid skulls. Transosteal propagation should cause the thicker skulls to have lower ICP values; therefore the higher pressures should be seen in the younger rats. Instead, global flexure may explain why the younger rats had lower ICP values. When pressure is exerted on the skull of a young rat, the more flexible, pliant structure is capable of deforming more easily than an older, more rigid skull. Since pressure is a force applied to a surface, the ability to increase even slightly the surface value due to a more flexible material (e.g., bones and suture lines), allows the younger rat to keep the ICP at a lower value. Thus, the deformation allows dissipation of some of the pressure that otherwise would build inside. Our results demonstrate a strong correlation between the ICP values and the rat's maturity, and such findings seem to suggest that global flexure of the skull by the transient shockwave is an important mechanism of pressure transmission inside the brain. Ongoing investigations are exploring these effects in more detail.

In conclusion, in this study we demonstrated that there are significant factors of paramount importance when investigating pressure-wave dynamics in an animal model of blast TBI. The results suggest that to obtain reliable and accurate measurements of intracranial pressurization, proper sealing of the skull needs to be achieved. When a seal is achieved, the results demonstrate that ICP values have a direct association to a rat's size and age, and are significantly higher compared to the overpressure outside the head. Consequently one must be aware that in order to translate the results of shockwave transmission in the rodent brain to a human model, one needs to take into consideration the animal's physical maturity for the type of shockwave study that they are performing. Overall, these results suggest that global flexure of the skull may contribute to the mechanism behind how the brain is injured during primary blast exposure.

Acknowledgments

We would like to acknowledge the Department of Defense (award no. W81XWH-08-2-0207), and the Office of Naval Research (award no. N00014-08-1-0585) for funding this project.

We would especially like to thank Blake Mathie, James Kopacz, and Dr. Bin Wu, for their indispensable contributions during testing, as well as to Dr. Bulent Ozkan for his vital advice during the statistical analysis.

Author Disclosure Statement

No competing financial interests exist.

References

Bhattacharjee, Y. (2008). Shell shock revisited: solving the puzzle of blast trauma. Science 319, 406–408.

Celander, H., and Clemedson, C.J. (1954). The use of a compressed air operated shock tube for physiological blast research. Acta Physiologica Scandinavica 33, 6–13.

Cernak, I., Savic, J., Ignjatovic, D., and Jevtic, M. (1999). Blast injury from explosive munitions. J. Trauma 47, 96–104.

Cernak, I., Savic, J., Malicevic, Z., Gordana, Z., Radosevic, P., Ivanovic, I., and Davidovic, L. (1996). Involvement of the central nervous system in the general response to pulmonary blast injury. J. Trauma 40, 100S–104S.

Cernak, I., Wang, Z., Jiang, J., Bian, X., and Savic, J. (2001). Ultrastructural and functional characteristics of blast injury-induced neurotrauma. J. Trauma 50, 695–706.

Chavko, M., Koller, W.A., Pruzaczyk, W.K., and McCarron, R.M. (2007). Measurement of blast wave by a miniature fiber optic pressure transducer in the rat brain. J. Neurosci. Methods 159, 277–281.

Clemedson, C.J., and Jonsson, A. (1961a). Transmission and reflection of high explosive shock waves in bone. Acta Physiologica Scandinavica 51, 47–61.

Clemedson, C.J., and Jonsson, A. (1961b). Transmission of elastic disturbances caused by air shock waves in a living body. J. Appl. Physiol. 16, 426–430.

Clemedson, C.J. (1956). Shockwave transmission to the central nervous system. Acta Physiologica Scandinavica 37, 204–214.

Cooper, G.J., Townend, D.J., Cater, S.R., and Pearce, B.P. (1991). The role of stress waves in thoracic visceral injury from blast loading: modification of stress transmission by foams and high-density materials. J. Biomechanics 24, 273–285.

Courtney, A.C, and Courtney, M.W. (2009). A thoracic mechanism of mild traumatic brain injury due to blast pressure waves. Medical Hypotheses 72, 76–83.

Dal Cengio Leonardi, A., Bir, C.A., Ritzel, D.V., and VandeVord, P.J. (2009). The effects of intracranial pressure sensor location and skull apertures during exposure of a rat model to an air shock wave. The Second Joint Symposium of the International and National Neurotrauma Societies, Santa Barbara, CA, Poster Presentation, September 2009.

Gefen, A., Gefen, N., Zhu, Q., Raghupathi, R., and Margulies, S. (2003). Age-dependent changes in material properties of the brain and braincase of the rat. J. Neurotrauma 20, 1163–1177.

Guy, R.J., Glover, M.A., and Cripps, N.P.J. (2000). Primary blast injury: pathophysiology and implications for treatment. Part III: Injury to the central nervous system and the limbs. J. Royal Naval Medical Service 86, 27–31.

Irwin, R.J., Lerner, M.R., Bealer, J.F., Brackett, D.J., and Tuggle, D.W. (1997). Cardiopulmonary physiology of primary blast injury. J. Trauma 43, 650–655.

Moss, W.C., King, M.J., and Blackman, E.G. (2009). Skull flexure from blast waves: a mechanism for brain injury with implications for helmet design. Phys. Rev. Lett. 103, 108702_1–108702_4.

Romba, J.J., and Martin, P. (1961). The propagation of air shock waves on a biophysical model. Armed Services Technical Information Agency, Arlington Hall Station, Arlington 12, Virginia. U.S. Army Ordnance. Technical Memorandum 17–61. Human Engineering Laboratories, Aberdeen Proving Ground, Maryland, pps. 1–25.

Suneson, A., Hansson, H.A., and Seeman, T. (1990). Pressure wave injuries to the nervous system caused by high-energy missile extremity impact: part II. Distal effects on the central nervous system—A light and electron microscopic study on pigs. J. Trauma 30, 295–306.

Warden, D. (2006). Military TBI during the Iraq and Afghanistan wars. J. Head Trauma Rehabil. 21, 398–402.

Young, M.W. (1945). Mechanics of blast injury. War Medicine 8, 73.

Address correspondence to:
Pamela J. VandeVord, Ph.D.
Department of Biomedical Engineering
Wayne State University
818 W. Hancock
Detroit, MI 48201

E-mail: pvord@wayne.edu

Annals of Biomedical Engineering, Vol. 39, No. 10, October 2011 *(© 2011)* pp. 2550–2559
DOI: 10.1007/s10439-011-0343-0

Skull Flexure as a Contributing Factor in the Mechanism of Injury in the Rat when Exposed to a Shock Wave

RICHARD BOLANDER,[1] BLAKE MATHIE,[1] CYNTHIA BIR,[1] DAVID RITZEL,[2] and PAMELA VANDEVORD[1,3]

[1]Department of Biomedical Engineering, Wayne State University, 818 W Hancock, Detroit, MI 48201, USA;
[2]Dyn-FX Consulting Ltd., 19 Laird Ave N, Amherstburg, ON N9V 2T5, Canada;
and [3]John D Dingell VAMC, Detroit, MI 48201, USA

(Received 6 April 2011; accepted 23 June 2011; published online 7 July 2011)

Associate Editor Stefan M Duma oversaw the review of this article.

Abstract—The manner in which energy from an explosion is transmitted into the brain is currently a highly debated topic within the blast injury community. This study was conducted to investigate the injury biomechanics causing blast-related neurotrauma in the rat. Biomechanical responses of the rat head under shock wave loading were measured using strain gauges on the skull surface and a fiber optic pressure sensor placed within the cortex. MicroCT imaging techniques were applied to quantify skull bone thickness. The strain gauge results indicated that the response of the rat skull is dependent on the intensity of the incident shock wave; greater intensity shock waves cause greater deflections of the skull. The intracranial pressure (ICP) sensors indicated that the peak pressure developed within the brain was greater than the peak side-on external pressure and correlated with surface strain. The bone plates between the lambda, bregma, and midline sutures are probable regions for the greatest flexure to occur. The data provides evidence that skull flexure is a likely candidate for the development of ICP gradients within the rat brain. This dependency of transmitted stress on particular skull dynamics for a given species should be considered by those investigating blast-related neurotrauma using animal models.

Keywords—Blast, Injury, Mechanism, Explosion.

INTRODUCTION

Due to the current military campaigns and social unrest around the world, the exposure of humans to explosions continues to take place.[10,11,15] A classification system has been invented to describe the manner in which a specific pathology will develop as a result of the trauma caused by the explosion.[12,13,16] The manner in which the shock wave from the explosion causes trauma (primary blast injury) remains a major concern to researchers investigating this injury pattern because of its ambiguous nature.[19]

Multiple hypotheses describing how this injury may result have been suggested. Courtney and Courtney[7] have recently summarized the major hypotheses of the mechanism of primary blast injury. One hypothesis is that the blast wave will compress the thorax and a resulting pressure surge to the head will cause brain injury.[1,3] This hypothesis has been discussed as early as 1916.[18] A second injury mechanism that is hypothesized states that a combination of rotational and translational accelerations resulting from shock wave interaction with the head will be great enough to cause injury.[8,21]

A third hypothesis provided by Courtney and Courtney[7] involves the transmission of the blast energy directly through the cranium. However, the physics of direct stresswave transmission should be distinguished from waves imparted by skull flexure. Direct wave transmission (trans-osteal wave propagation) in this case concerns the processes by which an air-borne shock wave interacts with the material interface of the skull and transmits a 'through-thickness' stress by direct compression of the skull material. The deformations caused by this mode of energy transfer will result in high frequency, low amplitude perturbations, similar to acoustic transmission. The development of the reflected pressure on the skull surface can also transmit enough energy to cause skull flexure. This deformation, in turn, may also cause changes in the pressure environment within the brain. Computer models have observed this transmission of blast energy in humans, but have yet to validate the results against experimental data.[4,17,22]

Courtney and Courtney[7] reference the work from Chavko *et al.*[5] which reports that ICP records within the cranium are very similar in pressure to the external

Address correspondence to Pamela VandeVord, Department of Biomedical Engineering, Wayne State University, 818 W Hancock, Detroit, MI 48201, USA. Electronic mail: dt8583@wayne.edu, blakemathie@gmail.com, cbir@wayne.edu, dritz@dyn-fx.com, pvord@wayne.edu

0090-6964/11/1000-2550/0 © 2011 Biomedical Engineering Society

static pressure condition. However, Leonardi *et al.*[14] compared records from unsealed and completely sealed intracranial pressure (ICP) sensors from rodents exposed to a shock wave which indicated that the observation by Chavko may have been an artifact of an unsealed ICP gauge. The study by Leonardi *et al.* indicated that by creating a fully sealed testing environment, mimicking the actual physiological environment, peak ICP profiles exceeding the external static pressure environment will develop. The unsealed environment produced similar recordings to those of the external pressure measurements since the enhanced fluid pressurization was able to be relieved through the leaking seal. They also noted distinct ICP oscillations taking place in the signal following the initial pressure rise, the amplitude, and frequency of the imparted ICP was likely linked to skull dynamics.

Other researchers have also observed an oscillatory ICP response following an initial rise in pressure, with the response depending on the dampening of the tissues tested.[6,20] In order to determine the source of ICP oscillations, Romba and Martin[20] investigated the effect of shielding the thorax of the Rhesus monkey while subjecting the head to blast exposure. Their results indicated that ICP oscillations were found regardless of the presence of thorax protection. Recently, similar results demonstrated that strong blast-induced ICP was inflicted in swine despite being fitted with thoracic protection.[2] A pressure pulse was generated in the inferior vena cava during exposure, but the delay was approximately two ms with a much longer rise time to peak pressure. Additionally there was no parallel increase in the ICP profiles relative to this pulse.

In the case of head exposures to shock waves, it is hypothesized that the dynamic structural response modes of the skull, with the associated viscoelastic brain mass acting as a coupled mechanical system, controls the stress (pressure) imparted to brain tissue under shock wave loading. The dynamic response modes of the skull, and hence imparted ICP, will relate to its particular geometry and material characteristics.

An experiment was designed to confirm this hypothesis will provide valuable information to identify particular modes of the coupled skull/brain response and their correlation with the ICP waveforms developed. Components of the imparted high strain rates in the form of ICP profiles may contribute to the cellular injury reported after blast exposure. The goal of this study was to examine and identify the critical biomechanical contributions of the shock wave interactions using a rodent model of blast neurotrauma. Independent methods for measuring skull strain and ICP were applied. Subsequent analysis of the rodent skull was used to further characterize potential areas of skull flexure. Currently information regarding the response of the rat head to shock wave exposure is lacking in the literature and this series of experiments will provide much needed insights into the underlying biomechanics of blast neurotrauma.

METHODS

Wayne State University (WSU) Shock Wave Generator

The WSU shock wave generator is a shock tube system that is based on a commonly employed system for the generation of well formed, controlled shock waves.[9] The system has a driver section that is separated from the driven chamber by a frangible membrane and is pressurized with compressed helium. Upon membrane rupture, the rapid expansion of gas in the tube drives an air shock wave into the test section. The event is measured by pressure sensors (Model 102A06, PCB Piezotronics Inc.) at positions along the length of the shock tube. Shock wave amplitude is controlled by varying the thickness of the frangible membrane. As the thickness of the membrane increases, the pressure within the driver will increase prior to rupture of the diaphragm. The increased pressure during rupture of the diaphragm will generate greater shock wave amplitudes. Specific details of the WSU shock wave generator are documented in Leonardi *et al.*[14]

Animal Testing

Approval of all experiments was obtained from the Wayne State University Institutional Animal Care and Use Committee (IACUC) prior to testing. A total of ten male Sprague–Dawley rats, age 65–70 days old, were procured. All animals were given food and water *ad lib*. Animals were randomly assigned to one of two groups based on instrumentation used during the testing: strain gauge (SG) or ICP sensor mounted to the top of the skull (IC).

Animal Preparation and Sensor Installation for SG Testing

Five SG rats were sacrificed immediately prior to testing. The dermal tissue was removed from the medial dorsal surface of the head exposing a 1.5 cm wide region of the skull extending from 1 cm rostral to the bregma to 1 cm caudal to the lambda. The skull surface was then cleaned using acetone to ensure a solid and durable mechanical bond with the strain gauge. A 3-axis rectangular Rosette-style strain gauge (FAER-25B-35SX, Vishay Micro-measurements Inc.) was then attached to the skull surface using

cyanoacrylate and allowed five minutes to cure. To limit motion of the rat's head during exposure and prevent mechanical stress on the instrumentation wires, the nose was secured such that the head was pitched down at approximately 45° to the shock front. The channels were named rostral, medial, and caudal (Fig. 1a).

Animal Preparation and Sensor Installation for IC

Five IC designated rats were anesthetized using a ketamine/xylazine mixture (80 mg/kg/10 mg/kg; I.P.) and immobilized in a stereotaxic frame. A longitudinal incision was made along the dorsal medial surface of the head, exposing the skull from the bregma to the lambda. A 1.5 mm diameter hole was drilled using a stereotaxic high-speed drill at the following location: +3.0 (A-P (mm) from Bregma), −2.0 (M-L (mm)), and −1.0 (D-V (mm)), exposing the frontal cortex.

A plastic guide cannula (18 gauge; 1.2 mm, CMA Microdialysis Inc.) with a small pedestal was implanted through the hole and fixed to the skull using two small stainless steel screws inserted at 45° angles from the horizontal into the skull adjacent to the cannula. Cranioplastic cement was applied to fix the pedestal to the skull and was anchored by the screws. The surgical wound was closed with sutures, as needed. A dummy cannula insert with a threaded cap was inserted in the guide cannula until shock exposure; the rats were allowed five days recovery time.

Prior to testing, rats were anesthetized using a ketamine/xylazine mixture (80 mg/kg/10 mg/kg; I.P). The cannula was then filled with a sterile saline solution. The cannula cap was filled with petroleum jelly and the fiber optic pressure sensor (FOP-MIV, Fiso Inc.) was inserted into the cannula and threaded onto the cannula pedestal. Figure 1b provides a sketch of the technique applied.

Shock Wave Exposure

The rat was affixed to a trolley-mounted stage using a nylon harness, and inserted into the shock tube, such that its nose was positioned 114 cm inside the end of the Lexan® tube opposite to, and facing, the driver (Fig. 2). The harness maintained the rat's longitudinal axis perpendicular to the shock front and in fixed proximity to a side-on pressure sensor. The trolley system reduced the effects of post-shock dynamic pressure flow on the rat.

Once placed in the harness, the SG rats were subjected to three exposures each at 69, 97, 117, and 172 kPa static shock pressure or until sensor failure, thus a total of 12 exposures per animal. The IC rats were exposed to three repeated exposures at three intensities (69, 97, and 117 kPa). In order to conserve the integrity of the ICP sensors, the highest pressure

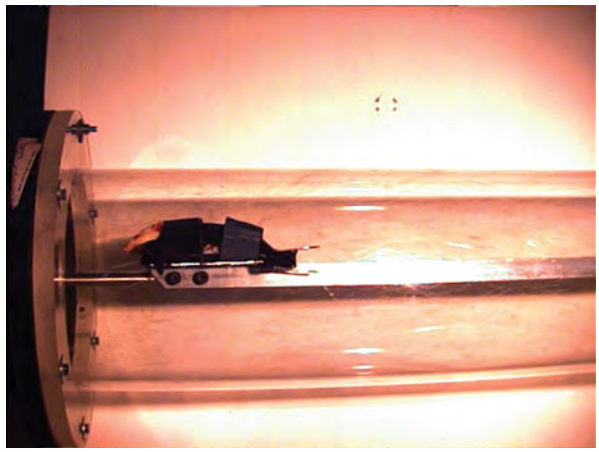

FIGURE 2. The rat was placed 114 cm within the shock tube and was placed on a trolley system to reduce the level of dynamic pressure shifts that are not representative of a free field shock wave.

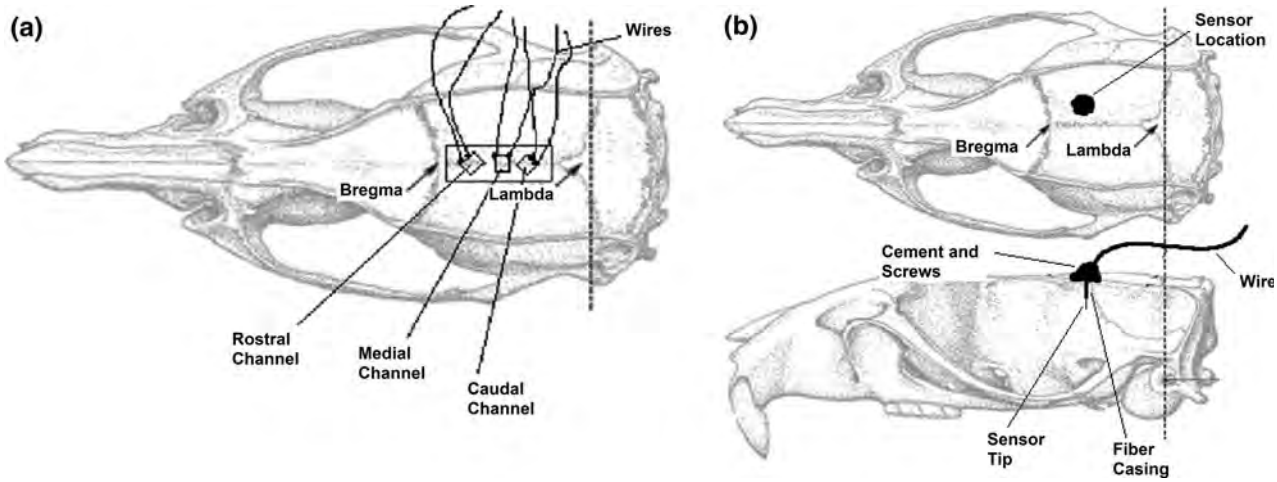

FIGURE 1. Placement of strain gauge on surface of the rat skull (a). Fiber optic pressure sensor installation on a rat skull (b).

intensity (172 kPa) was not applied. The intensities used in the protocol were determined from previous tests to maximize the amount of useful data. The time in between exposures was approximately two minutes for both groups of animals.

Both ICP and strain data were collected at 400 kHz using the Dash 8HF data acquisition system (Astromed Inc.). The data was then post-processed completely using Diadem 11.0 (National Instruments Inc.). Calculations of maximum principal strain were made using the formula below; the rostral channel was measured as ε_1, the medial channel was measured as ε_2, and the caudal channel was measured as ε_3.

$$\varepsilon_{P,Q} = \frac{\varepsilon_1 + \varepsilon_3}{2} \pm \sqrt{\left[(\varepsilon_1 - \varepsilon_2)^2 + (\varepsilon_2 - \varepsilon_3)^2\right] / 2}$$

The data was then reported in microstrain, and the magnitude of the first compressive peak was recorded. The IC pressure data was also analyzed, including peak pressure and rate of pressure change. Data was grouped by shock wave intensity and responses were compared using ANOVA with *post hoc* Tukey HSD used to determine significant differences ($p < 0.05$) between groups.

Computer Tomography (CT) Imaging

Following the experimental test series, computed tomography (CT) scans were obtained for the SG rats by means of a microCT device (Scanco VivaCT, Scanco Medical Inc.). ICP rats were not scanned as the instrumentation installed into the skull made it difficult to measure bone thickness. Variability of SG rat skull thickness throughout the skull was determined to help identify structural weaknesses that could be considered candidates for flexure. Skulls were scanned using a voltage of 70 kVp and current of 114 μA at a 30 μm resolution with a 320 ms integration time. Thickness measurements were calculated by using microCT analysis software (Scanco Medical Inc.). Measurements were taken at the midpoint between the lambda and bregma sutures. Three-dimensional reconstruction of the skull was undertaken to appreciate the skull geometry.

RESULTS

SG Measurements

The data collected from the strain gauges was useful for determining the flexural response of the superior braincase to shock wave loading. There were characteristic superimposed response patterns that were observed consistently as follows: (1) A strong and rapid compression with an associated damped oscillation at relatively high frequency (less than 3 kHz). (2) A quasi-steady decompression closely following the decay of the external static overpressure condition that developed as the strain returned to pre-blast levels. (3) A waveform of lower frequency with its pulse beginning in tension following the rapid compression. These responses were present for all the rats tested and are shown in Fig. 3.

The waveforms from two different rats are presented in Fig. 3, and the characteristic responses described prior are observable for both series. The first trace in each series is from the side-on (static) pressure sensor exposed to the incident shock wave. Within both series, following the incident shock, reflections from the fixture holding the specimen develop and create pressure artifacts on the sensor's surface that are not representative of the environment to which the specimen is exposed. This effect is expected from theory; the arrival and amplitude of the perturbation coincides with those expected of that reflection disturbance; confirmation of this phenomenon is also demonstrated by the fact that the shock reflections are similar between series, while the strain response is specific to the specimen being tested.

The peak compression was reported for all exposures. In Fig. 4a, it is shown that as the incident shock wave intensity increased, the calculated maximum principal strain also increased. The means were significantly different between groups ($^*p < 0.05$).

ICP Measurements

For the ICP profiles, two response patterns were observed consistently between specimens. (1) The peak compression wave will rebound and oscillate in a dampened harmonic motion. (2) There was a rapid increase in pressure that approximates the external loading environment and then returns to pre-exposure conditions. In Fig. 4b, 4c it is shown that as the incident shock wave intensity increased, the peak pressure and maximum rate of pressure change both increased.

The pressure response profiles for a 249 gm rat are shown in Fig. 5. The three profiles have been time shifted to begin at the same point. The increase in peak pressure as a function of an increase in incident side-on pressure can be observed for this series of wave forms. The duration of the rise times is also a function of intensity, where the greatest intensities resulted in the shortest rise times. To further this point, the 97 kPa ICP wave form was time shifted so that its pressure profile could be compared to a 97 kPa incident shock wave without the shock reflections that were observed in Fig. 5 (Fig. 6). The rise times between the incident wave as measured by the side-on pressure sensor and the ICP wave is of interest (27 compared to 195 μs). Although the rise time of the shock front is

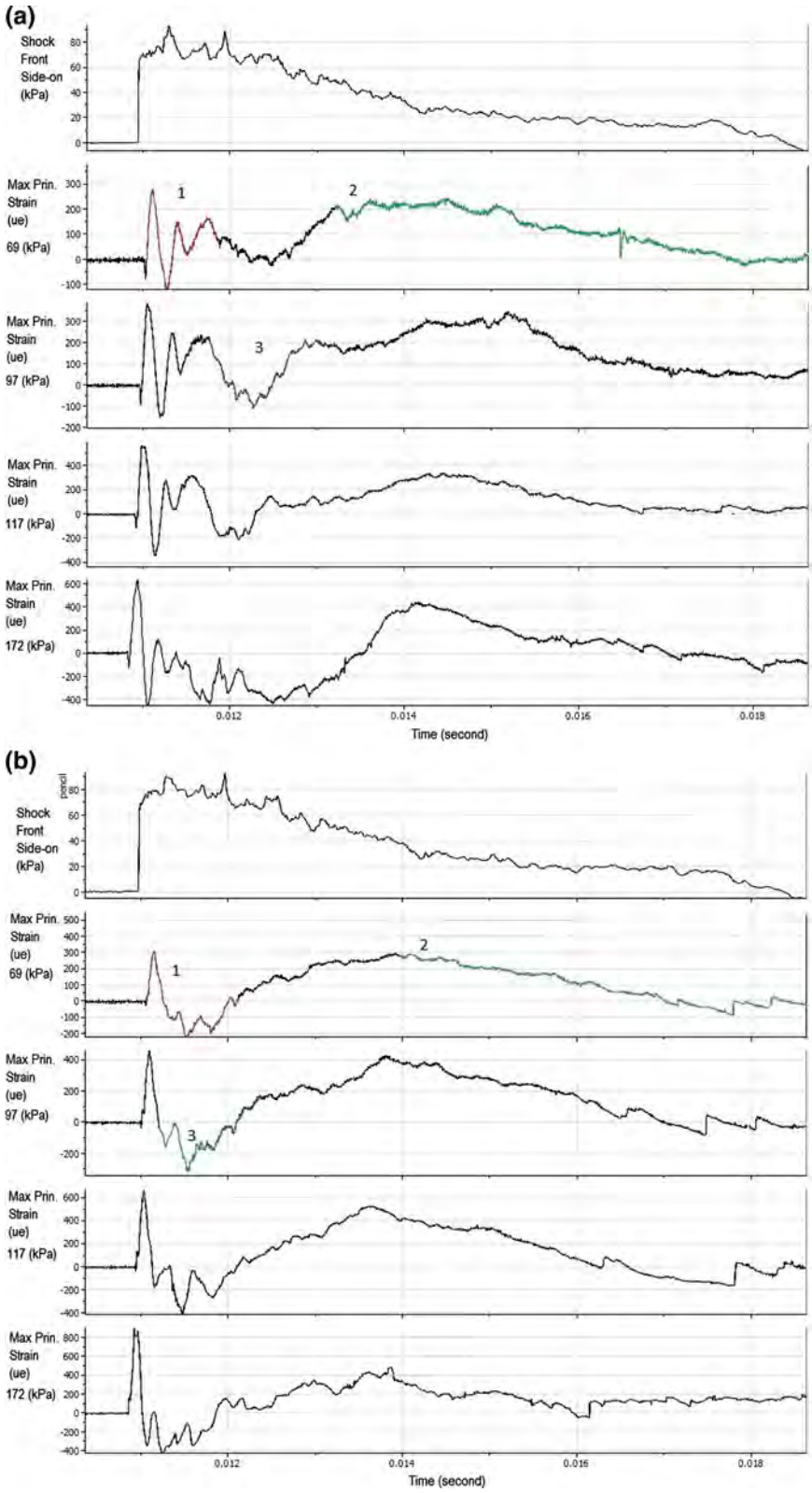

FIGURE 3. The principal strain response profiles of the superior brain case for both a 262 and 247 gm rat when exposed to shock waves of increasing intensity. The magnitude for each profile is adjusted so that the frequency content is observable. For the presented data, tension is negative and compression is positive. (1) A strong and rapid compression with an associated damped oscillation at relatively high frequency (less than 3 kHz). (2) A quasi-steady decompression closely following the decay of the external static overpressure condition that developed as the strain returned to pre-blast levels. (3) A waveform of lower frequency with its pulse beginning in tension following the rapid compression.

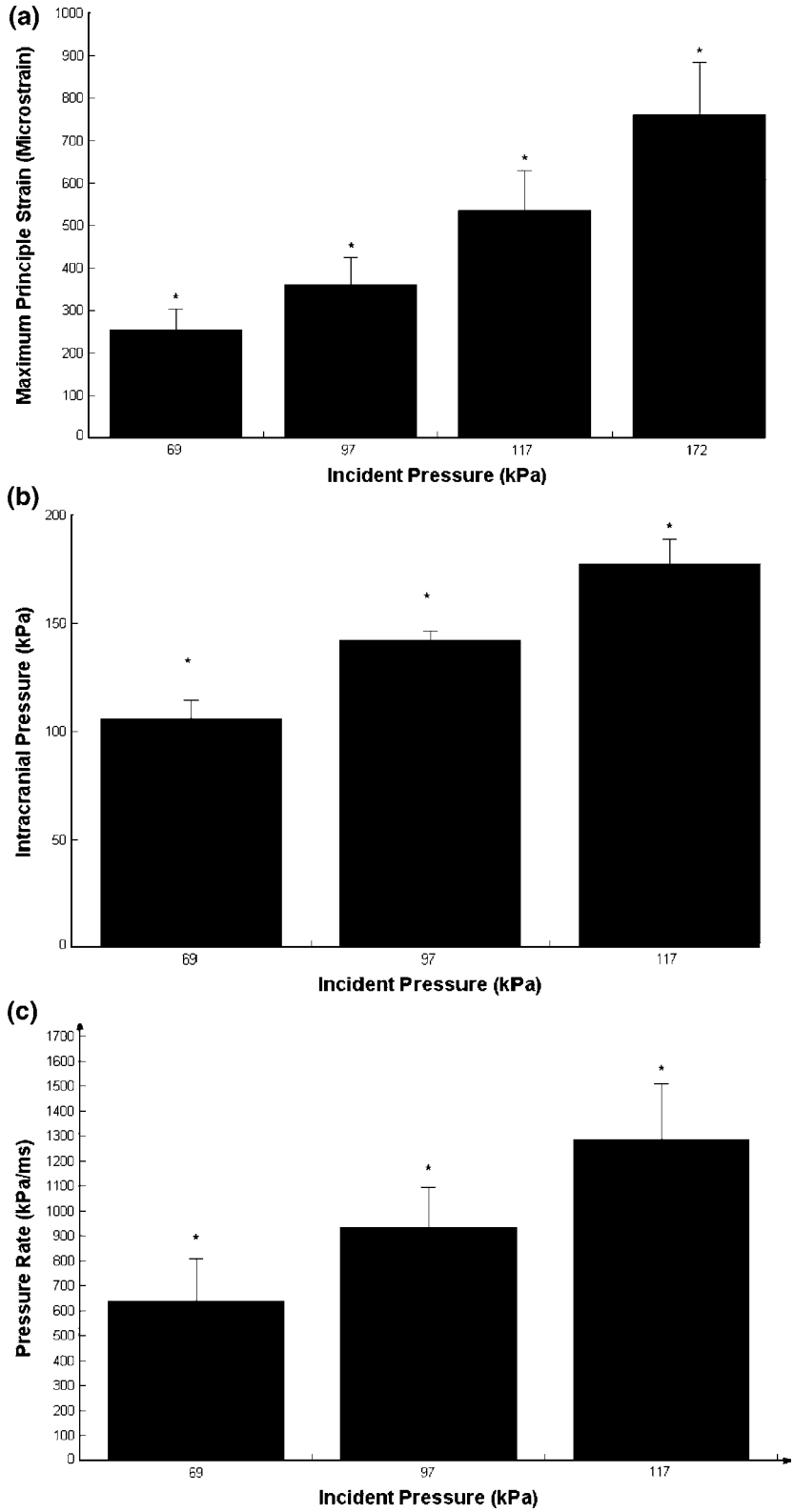

FIGURE 4. (a) The initial compression of the skull is dependent on intensity of the incoming shock wave. The largest magnitude shock waves caused the greatest maximum principal strains. All groups were significantly different from each other (*$p < 0.05$). (b) The ICP will increase beyond that of the incident shock wave (*$p < 0.05$). (c) The rate of pressure change will also increase with intensity (*$p < 0.05$).

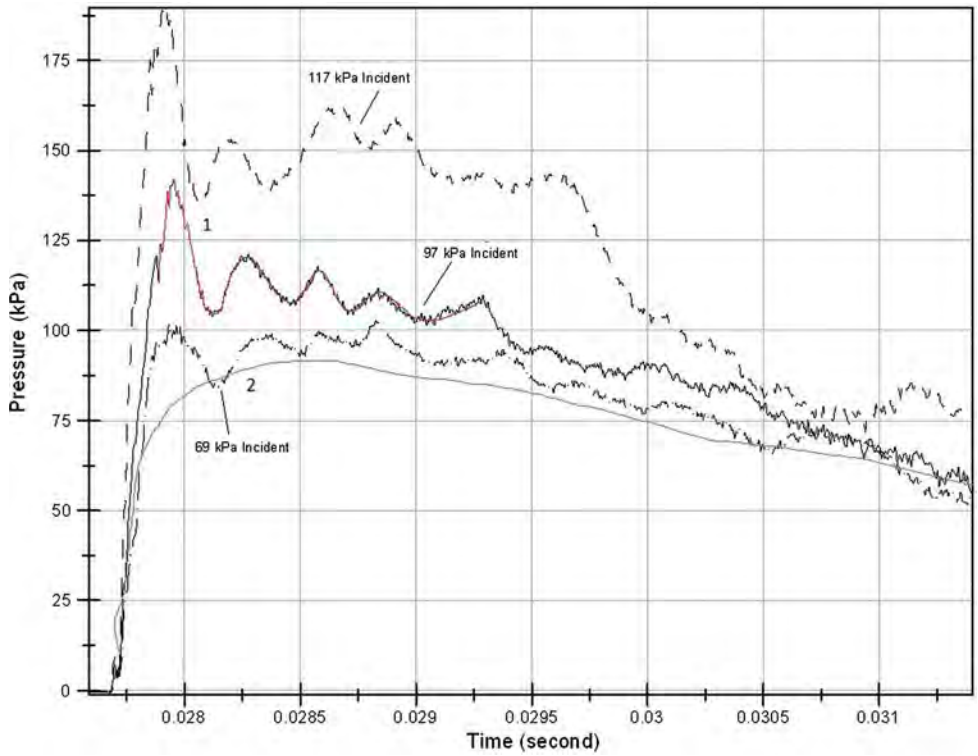

FIGURE 5. The intracranial pressure response of a rat skull is dependent on shock wave intensity. The ICP responses for a 249 gm rat show distinct pressure fluctuations (1) (red) that are present in each of the profiles that last for less than 2 ms. The waveforms will also approximate the external loading response invoked by the shock wave (2) (green).

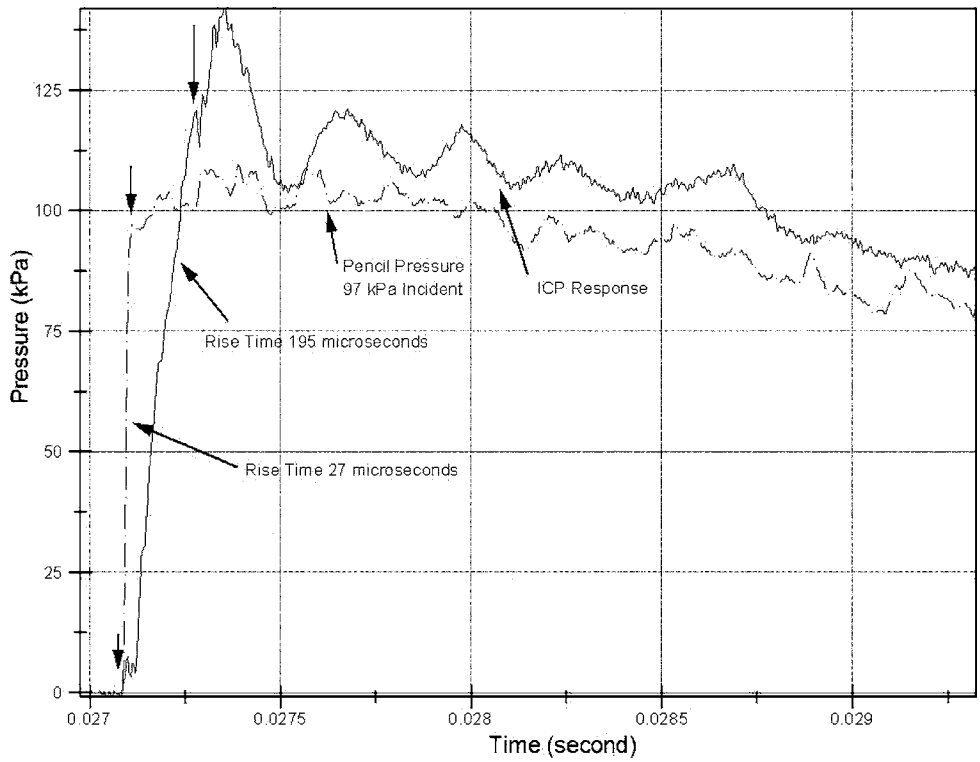

FIGURE 6. The rise time of the external pressure wave is faster than the rise time of the record intracranial pressure for a 249 gm rat. It is hypothesized that this is due to the amount of energy that is required to deform the skull so that a pressure wave can develop within the brain.

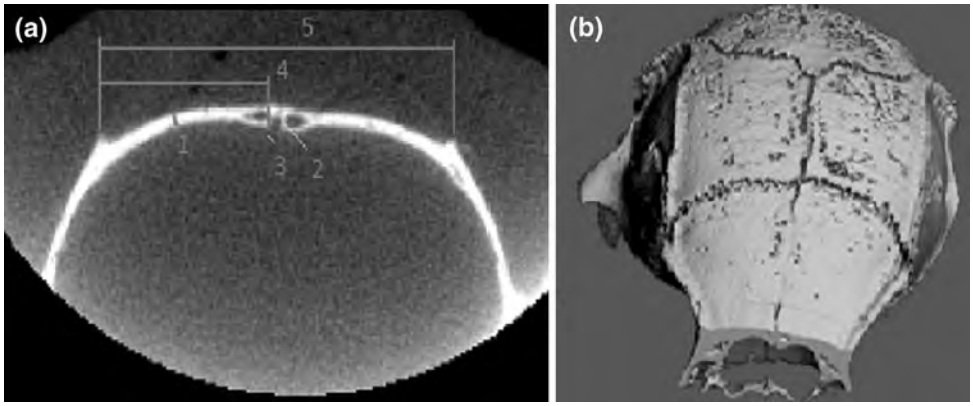

FIGURE 7. (a) Measurements were taken of the MicroCT images of the rat skull to determine key structural elements. (b) A three-dimensional reconstruction of the images depict that there are considerable gaps between the bone plates with significant reinforcement on the lateral bone folds, suggesting that the midline suture will be a probable place for skull flexure to take place.

approximately 1 μs the 27 μs measured is an artifact that is created by displacing the sensing element. It is expected that this delay between the two pressure profiles is caused by the absorption of energy that takes place by causing the skull to flex, thereby increasing ICP.

MicroCT Imaging

The results from the microCT imaging provided information regarding the geometry and thickness of specific bones in the skull (Fig. 7a). The mid-plate thickness between lambda and bregma sutures was approximately 0.354 ± 0.061 mm thick (1) where the thickness increases near the midline suture to 0.630 ± 0.082 mm thick (3). The gap between the suture itself was approximately 0.162 ± 0.016 mm thick (2). At this point the distance from horn to horn was 11.72 ± 0.114 mm (5). Additionally the distance from horn to suture top was 5.78 ± 0.207 (4). A sample of measurement locations are indicated in Fig. 7a. The image is of a cross section of head mid-distance between the lambda and bregma sutures. The term horn is in reference to the folds of bone on the lateral aspects of the skull, acting as reinforcements. Values are reported as (mean $\pm$ SD).

In Fig. 7b a three-dimensional reconstruction of the rat skull is provided. The rostral end was rotated down to the bottom of the graphic; the caudal region is near the top. The locations of the suture lines indicate that inward flexure of the superior bones of the skull case is probable during exposure due to the static pressure as it traverses the head.

DISCUSSION

Recent experimental biomechanical data for the rat suggested that skull flexure contributes to the ICP gradients developed within the brain as a result of shock wave interaction.[14] Results from the current experiments validate the hypothesis by Leonardi *et al.*[14] demonstrating that strain on the skull surface may have a significant effect on the imparted ICP waveform. By applying a series of pressure intensity exposures, it was observed in this study that the ICP response was dependent on the incident shockwave intensity. Further, the rate of pressure change was found to increase while the rise time to peak pressure was found to decrease with intensity.

When the ICP response was compared to the pressure profile of the incident shock wave, a delay in the rise time of the ICP was observed. This suggests that the rat skull is acting as a medium between the external environment and the intracranial contents. Pressure recordings reported by Bauman *et al.*[2] also found a significant delay in the rise time of the ICP profile compared to the incident shock wave during their swine testing. It is hypothesized that the rise time of those ICP profiles within the swine will be longer than that of the rat because of the difference in skull thickness between species. More studies need to be conducted to verify this relationship.

The microCT imaging of the superior braincase of the rat revealed that the bones are not completely fused and the lateral aspects are reinforced with thicker layers of bone. It is hypothesized that when the incident shock wave traverses the surface of the skull, the shock wave is acting as a moving load. This loading will cause the greatest deflections in the regions with the least reinforcement. When examining the specific anatomical features of the rat skull, the region between the lambda and bregma suture appears to offer the greatest amount of deflection as the bone plates may hinge about the major sutures.

The results from the strain gauge data further substantiates the hypothesis that the incident shock wave

is causing the skull to flex. The rapid compression that increases in magnitude with the intensity of the incident shock is believed to be the direct result of the shock wave compressing the skull surface. The damped harmonic oscillation phase that then developed as a result of the compression is hypothesized to be due to the return of the deflected surface regions back to equilibrium. The quasi-steady decompression phase that approximates the external pressure environment is then best observed due to the dispersion of the energy from the rapid compression of the skull case. The nature of the secondary surface wave beginning in tension has yet to be determined. It has been observed that this wave is dependent on the intensity of the incident shock wave. The front of this wave will be steeper as the intensity increases. Research is ongoing to determine the nature of this wave.

Because of these observations in both the strain gauge and ICP responses, it is proposed that there are two major regions in the waveform response. The first is the transient phase which consists of a rapid compression and harmonic oscillations; the other is the quasi-steady decompression phase. It is possible that the most damaging aspect of these waveforms is the initial oscillations that may cause high levels of strain rates in both tension and compression that could be transferred as rapid compression waves within the brain due to the coupling at the skull/dura interface.

Some limitations exist with the current data. The placement of the strain gauge on the skull is problematic because mounting on the suture lines will cause an amplification of the signal. Although the results provided key information, the principal strain calculations were not made on a homogenous surface and the sensors were relatively widely distributed. But, given the consistency of the signals between exposures and that similar responses were observed between species, the data is useful for describing responses of the rat skull to shock wave exposure.

The ICP data was of concern because the skull was modified with small screws and bone cement, modifying the native surface. If the superior skull case is acting as a diaphragm, the additional mass of the sensor cement complex will cause the periodic oscillations to have a response with fewer competing frequencies than what are observed in the strain profiles. This can be seen in Fig. 5, specifically for the 97 kPa incident exposure. Additionally, it still needs to be determined to what extent the fiber optic sensors are mapping the motion of the skull when compared to the environment within the brain. Because of the artifacts of testing with the ICP sensors, direct relationships were not made to the strain gauges. Further studies are required to address this issue.

It is expected that the biomechanical responses of the rat will be unique when compared to other species. It would be ideal to be able to equate injury responses in rats to humans, but scaling for thresholds of injury cannot be conducted until the mechanism of injury is discovered. The human head is much more spherical and thicker in geometry as compared to the rat. These changes may result in different response modes than what are observed in the rat. Because the mechanical inputs into the brain are likely specific to the system, a multi species analysis of skull flexure and ICP will need to be undertaken.

In summary, this article provides key biomechanical data which suggests that skull flexure may be one of the major factors for causing ICP gradients. The superior rat skull is a location where flexure will be exaggerated. Since neuronal injury is dependent on strain rate, it is hypothesized that the first two ms following exposure (the transient phase) is the likely timeframe for causing neurotrauma. This period is composed of extremely rapid shifts in strain that are likely transmitted to the cells within the brain. It is not yet known which aspects of the intracranial pressure profile causes cellular injury. Ultimately, it is of utmost importance to evaluate cellular vulnerability under the particular stress-rate conditions observed. Utilizing appropriate *in vitro* experiments for blast-related neurotrauma will help identify biomarkers of neuropathology and shifts in gene expression occurring as a result of shock wave exposure.

ACKNOWLEDGMENTS

We would like to thank the WSU Bioengineering Center staff and students for assisting with this project. We would also like thank Dr. Amanda Esquivel for obtaining the CT images. This project was partially funded by DOD Award Number W81XWH-08-2-0207 and the Thomas J. Rumble Fellowship.

REFERENCES

[1]Battacharjee, Y. Shell shock revisited: solving the puzzle of blast trauma. *Science* 319:406–408, 2008.

[2]Bauman, R., G. Ling, L. Tong, A. Januszkiewicz, D. Agoston, N. Delanerolle, J. Kim, D. Ritzel, R. Bell, J. Ecklund, R. Armonda, F. Bandak, and S. Parks. An introductory characterization of combat casualty care relevant swine model of closed head injury resulting from exposure to explosive blast. *J. Neurotrauma* 26:841–876, 2009.

[3]Cernak, I. Penetrating and blast injury. *Restor. Neurol. Neurosci.* 23:139–143, 2005.

[4]Chafi, M., G. Karami, and M. Ziejewski. Biomechanical assessment of brain dynamic responses due to blast pressure waves. *Ann. Biomed. Eng.* 38:490–504, 2010.
[5]Chavko, M., W. Koller, W. Prusaczyk, and R. McCarron. Measurement of blast wave by a miniature fiber optic pressure transducer in the rat brain. *J. Neurosci. Methods* 159:277–281, 2007.
[6]Clemedson, C., and C. Criborn. Mechanical response of different parts of a living body to a high explosive shock wave impact. *Am. J. Physiol.* 181:471–476, 1955.
[7]Courtney, M., and A. Courtney. Working toward exposure thresholds for blast-induced traumatic brain injury: thoracic and acceleration mechanisms. *Neuroimage* 54:S55–S61, 2011.
[8]Finkel, M. The neurological consequences of explosives. *J. Neurol. Sci.* 249:63–67, 2006.
[9]Henshall, B. Shock tube–versatile tool of aerodynamic research. *J. Royal Aeronaut. Soc.* 58:541–546, 1954.
[10]Hicks, R., S. Fertig, R. Desrocher, W. Koroshetz, and J. Pancrazio. Neurological effects of blast injury. *J. Trauma* 68:1257–1263, 2010.
[11]Hoge, C., D. McGurk, J. Thomas, A. Cox, C. Engel, and C. Castro. Mild traumatic brain injury in U.S. Soldiers returning from Iraq. *N. Engl. J. Med.* 358:453–463, 2008.
[12]Kluger, Y., A. Nimrod, P. Biderman, A. Mayo, and P. Sorkin. The quinary pattern of blast injury. *Am. J. Disaster Med.* 2:21–25, 2007.
[13]Lechner, R., G. Achatz, T. Hauer, H. Palm, A. Lieber, and C. Willy. Patterns and causes of injuries in a contemporary combat environment. *Unfallchirurg* 113:106–113, 2010.
[14]Leonardi, A., C. Bir, D. Ritzel, and P. VandeVord. Intracranial pressure increases during exposure to a shock wave. *J. Neurotrauma* 28:85–94, 2011.
[15]Ling, G., and J. Ecklund. Traumatic brain injury in modern war. *Curr. Opin. Anaesthesiol.* 24:124–130, 2011.
[16]Luks, F. Blast injuries—and the pivotal role of trauma surgeons. *Acta Chir. Belg.* 110:517–520, 2010.
[17]Moss, W., M. King, and E. Blackman. Skull flexure from blast waves: a mechanism for brain injury with implications for helmet design. *Phys. Rev. Lett.* 103:108702, 2009.
[18]Mott, F. On the effects of high explosives upon the central nervous system. *Lancet* 187:331–338, 1916.
[19]Risling, M. Blast induced brain injuries—a grand challenge in TBI research. *Front. Neurol.* 8:1, 2010.
[20]Romba, J., and P. Martin. The propagation of air shock waves on a biophysical model. US Army Ordinance Technical Memorandum, pp. 17–61, 1961.
[21]Stuhmiller, J., K. Ho, M. VanderVorst, K. Dodd, T. Fitzpatrick, and M. Mayorga. A model of blast overpressure injury to the lung. *J. Biomech.* 29:227–234, 1996.
[22]Taylor, P., and C. Ford. Simulation of blast-induced early time intracranial wave physics leading to traumatic brain injury. *J. Biomech. Eng.* 131:061007, 2009.

Journal of Biomechanics 45 (2012) 2595–2602

Contents lists available at SciVerse ScienceDirect

Journal of Biomechanics

journal homepage: www.elsevier.com/locate/jbiomech
www.JBiomech.com

Head orientation affects the intracranial pressure response resulting from shock wave loading in the rat

Alessandra Dal Cengio Leonardi [a,b], Nickolas J. Keane [a], Cynthia A. Bir [a], Anne G. Ryan [c], Liaosa Xu [c], Pamela J. VandeVord [a,b,*]

[a] Department of Biomedical Engineering, Wayne State University, 818 W. Hancock, Detroit, MI 48201, United States
[b] John D. Dingell VA Medical Center, Research & Development Service, 4646 John R, Detroit, MI 48201, United States
[c] Department of Statistics, Virginia Tech, VA 24061, United States

ARTICLE INFO

Article history:
Accepted 1 August 2012

Keywords:
Blast
Traumatic brain injury
Skull flexure
Orientation
Intracranial pressure

ABSTRACT

Since an increasing number of returning military personnel are presenting with neurological manifestations of traumatic brain injury (TBI), there has been a great focus on the effects resulting from blast exposure. It is paramount to resolve the physical mechanism by which the critical stress is being inflicted on brain tissue from blast wave encounters with the head. This study quantitatively measured the effect of head orientation on intracranial pressure (ICP) of rats exposed to a shock wave. Furthermore, the study examined how skull maturity affects ICP response of animals exposed to shock waves at various orientations. Results showed a significant increase in ICP values in larger rats at any orientation. Furthermore, when side-ICP values were compared to the other orientations, the peak pressures were significantly lower suggesting a relation between ICP and orientation of the head due to geometry of the skull and location of sutures. This finding accentuates the importance of skull dynamics in explaining possible injury mechanisms during blast. Also, the rate of pressure change was measured and indicated that the rate was significantly higher when the top of the head was facing the shock front. The results confirm that the biomechanical response of the superior rat skull is distinctive compared to other areas of the skull, suggesting a skull flexure mechanism. These results not only present insights into the mechanism of brain injury, but also provide information which can be used for designing more effective protective head gear.

© 2012 Elsevier Ltd. All rights reserved.

1. Introduction

With the increasing number of military personnel returning from conflicts with neurological manifestations of traumatic brain injury (TBI), there has been a great focus on the effects resulting from blast exposure (Hicks et al., 2010; Okie, 2005; Warden, 2006). The incidence of TBI and psychological health issues in the current veteran population is at the forefront when planning for the long-term healthcare of our wounded soldiers (Hoffman and Harrison, 2009). Furthermore, blast trauma is also becoming more common among civilians subjected to terrorist attacks, so much that blast injury has been proposed as the fourth weapon of mass destruction because of its increasing prevalence in the tactics of terrorists (Born, 2005).

Although there has been a rise in the number of blast neurotrauma reports, the exact mechanism of how the brain is injured remains a topic of debate. Proposed theories on the injury mechanism vary from transosteal propagation (Clemedson, 1956; Clemedson and Jonsson, 1961), which hypothesized that the shock wave enters the brain by propagating directly through the skull, to a thoracic mechanism, by which the overpressure squeezes the thorax and transmits pressure to the brain through the vasculature (Bhattacharjee, 2008; Cernak et al., 2001; Courtney and Courtney, 2009; Young, 1945). Studies that had the ability to measure intracranial pressure (ICP) indicated that there was little evidence to support a significant transmission of pressure through the body vasculature (Bauman et al., 2009; Clemedson, 1956; Dal Cengio Leonardi, 2011; Romba and Martin, 1961; Saljo et al., 2008).

Recently, experimental studies have been reported which investigate the biomechanical response of the head exposed to a shock wave (Bolander et al., 2011; Dal Cengio Leonardi et al., 2011). The results indicated that the imparted shock wave may induce multiple response modes of the skull, including global flexure, which may have a significant contribution to the mechanism of injury.

* Corresponding author at: School of Biomedical Engineering and Sciences, Virginia Tech University, Blacksburg, VA 24061, United States.
Tel.: +540 231 1994; fax: +540 231 9738.
E-mail addresses: adc.leonardi@gmail.com (A. Dal Cengio Leonardi), nickolasjkeane@gmail.com (N.J. Keane), cbir@wayne.edu (C.A. Bir), agryan@vt.edu (A.G. Ryan), liaosax@vt.edu (L. Xu), pvord@vt.edu (P.J. VandeVord).

0021-9290/$ - see front matter © 2012 Elsevier Ltd. All rights reserved.
http://dx.doi.org/10.1016/j.jbiomech.2012.08.024

While evidence has demonstrated that shock wave induced stresses injure the brain, the question of whether head orientation could play a role in the level of energy imparted on the brain is still of concern. Thus, the goal of this study was to quantitatively measure the effect of orientation on ICP of rats exposed to a shock wave. It is hypothesized that skull flexural modes dominate the ICP response, hence varying head orientation would be expected to alter this imparted stress waveform. The head orientation affects not only the shape and size of the "presented area" exposed to the incident wave, but the degree and nature of the response of the individual skull plates due to the variance of skull physiology. As such, this will have a significant influence on the stress that the shock wave imparts on the brain due to changes in skull dynamics.

Moreover, research has shown significant differences in peak ICP values for rats of dissimilar size/age (Dal Cengio Leonardi et al., 2011). Therefore, this study further investigated how skull maturity affects ICP response at various orientations. The results provide insight into the mechanism of brain injury from blast.

2. Methods

2.1. Shock wave generation and shock wave profile in air

A custom built shock tube (ORA Inc., Fredericksburg, VA) located at Wayne State University (WSU) was used to produce simulated blast waves (Fig. 1). It consists of two sections: the driver (0.76 m long; 0.31 m in diameter), filled with highly pressurized helium; and the driven section open to ambient air. The sections are separated by a membrane, which is ruptured to generate a shock wave. The driven section had two distinct parts: a cylindrical part (2.46 m long; 0.31 m diameter), and a conical expansion (4.70 m long; expanding to 0.91 m in diameter at the open end). This expanded configuration is used so that the apparatus holding the specimen covers no more than 15% of the cross-sectional area of the conical driven (Dal Cengio Leonardi 2011). This is done to avoid disrupting the shockwave natural flow; otherwise, transverse reflections will affect the response and the restricted airflow would adversely affect the relationship between dynamic and static pressures loading the target. Thus, the tube ceases to simulate a free field shock wave environment and data would be corrupted.

The animal was placed inside the conical section and its head was consistently positioned at 1.25 m from the open end of the tube. This position assured that the air overpressure positive phase was not affected by the anomalous effect of the rarefaction wave coming from the open-end of the tube. Calibrations were performed to determine the shock wave profile in air using a side-on pressure sensor (PCB Piezotronics, Model 137A22) placed at the same location where the rat head was positioned. This side-on pressure sensor captured the static pressure changing in time and the peak pressure measured at 1.25 m from the open end of the tube was approximately 70 kPa (Fig. 2). An additional side-on pressure sensor (PCB Piezotronics, Model 102A06) was installed on the cylindrical driven section to monitor the development of the shock wave along the test section. This sensor (R-wall) was placed at 1.83 m from the frangible membrane (Fig. 1) and was utilized as the trigger for the event. The sampling rate for all pressure sensors was 500 kHz with an anti-aliasing filter at 200 kHz.

2.2. Animal preparation

Approval from the WSU Institutional Animal Care and Use Committee was obtained. All animals were purchased from Harlan Laboratory (Indianapolis, Indiana) and kept under similar housing conditions. Eight male Sprague-Dawley rats were divided into two groups of four based on their ages. Group 1 was 68 days old on day of testing with an average weight of 274.8 g (Standard Deviation (SD) $\pm$ 1.7 g). Group 2 was 158 days old with an average weight of 453.5 g (SD $\pm$ 4.4 g). The difference in animal weight allowed for assessing the effects of skull maturity on ICP.

Rats were anesthetized and an incision was made along the midline suture of the head to expose the superior and caudal portions of the skull. A 1 mm-diameter hole was drilled into the occipital bone 1 mm right of the midline to allow for

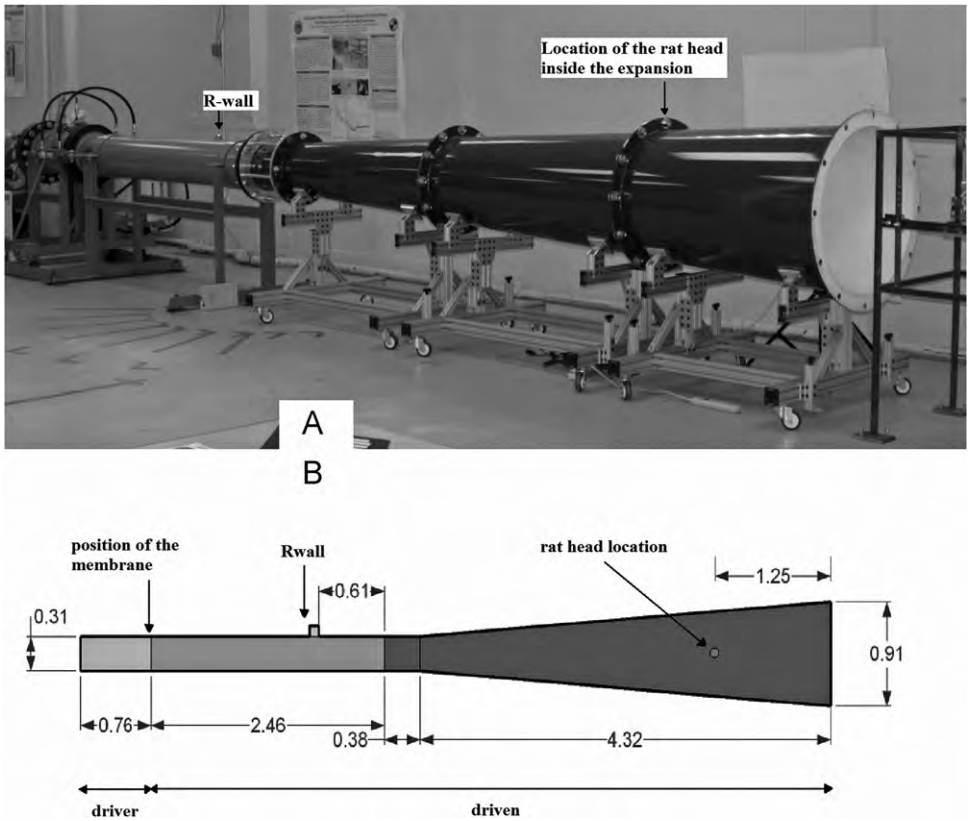

Fig. 1. WSU shock wave generator with conical expansion. (A) Photo of the apparatus which identifies the position of the trigger (R-wall) and the location of the rat's head. A steel structure with trolley system is positioned in front of the tube open-end. All fixtures were mounted to the trolley system to minimize mechanical stresses imparted to the animal due to its restraint in the shock wave flow. (B) Drawing of the same apparatus which identifies the location of the rat's head, the position of the trigger (R-wall) and the membrane's placement. Measurements are in meters.

insertion of a guided cannula (16-gage with hypodermic steel tubing) to reach the right forebrain area (Fig. 3). The occipital mounting method was necessary to preserve the physiological response of the skull top. Screws were placed around the cannula to help anchor it to the skull once bone cement was applied. For group 1, a 10 mm long cannula was mounted to the occipital bone; for group 2, the cannula length was increased to 14 mm in order to measure ICP in analogous locations in the brain. Once the cement had cured, the incision was sutured to minimize direct skull exposure.

Prior to testing, saline solution was administered into the cannula to reduce the possibility of introducing air in the system, which hampers the rise of ICP. Then an optic pressure sensor (FISO Technologies, model FOP-MIV-PK) was inserted into the cannula and locked into position. The sensor optic cable was adapted to screw into the cannula in order to seal the skull/brain system (Dal Cengio Leonardi et al., 2011).

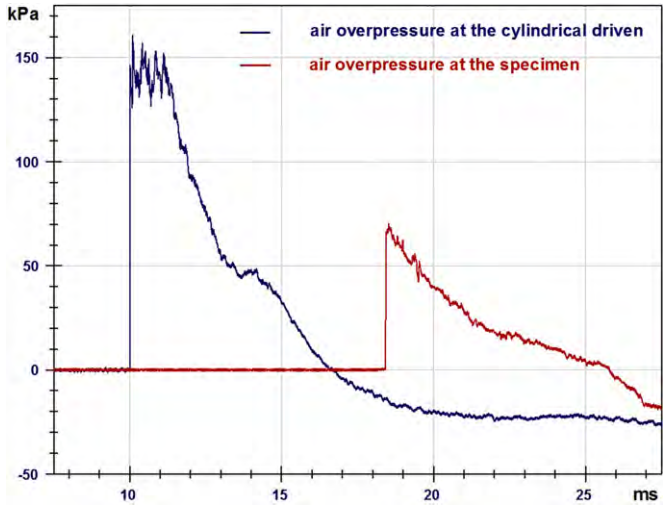

Fig. 2. Static air overpressure profiles captured at the cylindrical driven (R-wall) and at the specimen's head location. Notice how the pressure profile develops into a more proper Friedlander wave as it moves further away from the membrane. The dramatic decrease in peak pressure from the trigger position to the specimen is the natural consequence of the conical expansion.

2.3. Testing schedule and fixtures

Each rat was exposed to a series of shock waves with its head in one of four different orientations: front, side, top, and back (Fig. 4). For each orientation the rat was placed in a custom-built restraint fixture that shielded the body and exposed only the head in each orientation. The animal's muzzle was secured to the fixture to prevent rotation of the head due to the blast wind. The animal was exposed to three separate shock waves of equal intensity; subsequently the orientation was changed. The frontal exposure was repeated at the end of the series to verify that the results remained consistent: this brought the total number of exposures to 13 trials per rat (Table 1). Importantly, the head remained at 1.25 m from the open end for all orientations. Fixtures were designed to maximize the aerodynamic profile in order to minimize the creation of anomalous turbulence and shock reflections (Fig. 4). For side and top orientations the same fixture was used (Fig. 4C and D). During side exposure, the left side of the rat head made the initial contact with the shock front.

2.4. Histological validation of sensor position

All animals survived the testing series. After which, they were perfused with 4% paraformaldehyde. Brains were processed for post-fixation, sectioned and stained with hematoxylin and eosin to confirm sensor placement (right forebrain region of the cerebrum) (Fig. 5).

2.5. Statistical analysis

The dependent variables considered were peak ICP (maximum pressure in the first 0.3 ms) and peak rate (rate of change of ICP from 5% of the peak ICP value to the peak point) (Fig. 6). The time frame of 0.3 ms was chosen to capture the initial response to loading.

A two-way ANOVA with repeated measures was used to determine the effect of orientation and size of the rodent on peak ICP and peak rate. Average values were calculated for the 3 trials per position, with the exception of the frontal position in which 4 trials were averaged. Statistical significance was assumed at $p\text{-value} < 0.05$. Statistical analyses were performed using SAS (SAS Institute Inc., NC).

3. Results

ICP profiles between animal groups were very consistent and repeatable (Fig. 7). However, each orientation demonstrated some

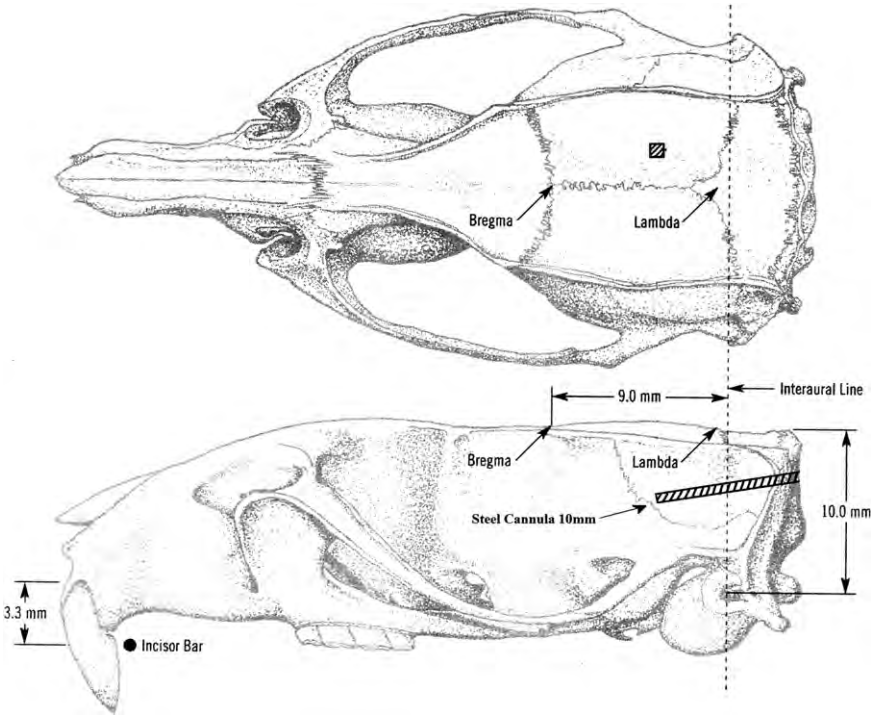

Fig. 3. Illustration of ICP sensor positioning and cannula mounting through occipital bone. The top figure shows the position of the ICP sensor using a superior view of the rat skull. The bottom figure shows the cannula insertion using a lateral view of the rat skull. The ICP sensor is located at the end of the steel cannula. The figure shows the measurements used for a small rat; therefore the cannula was 10 mm long. For the large rats the cannula was 14 mm long.

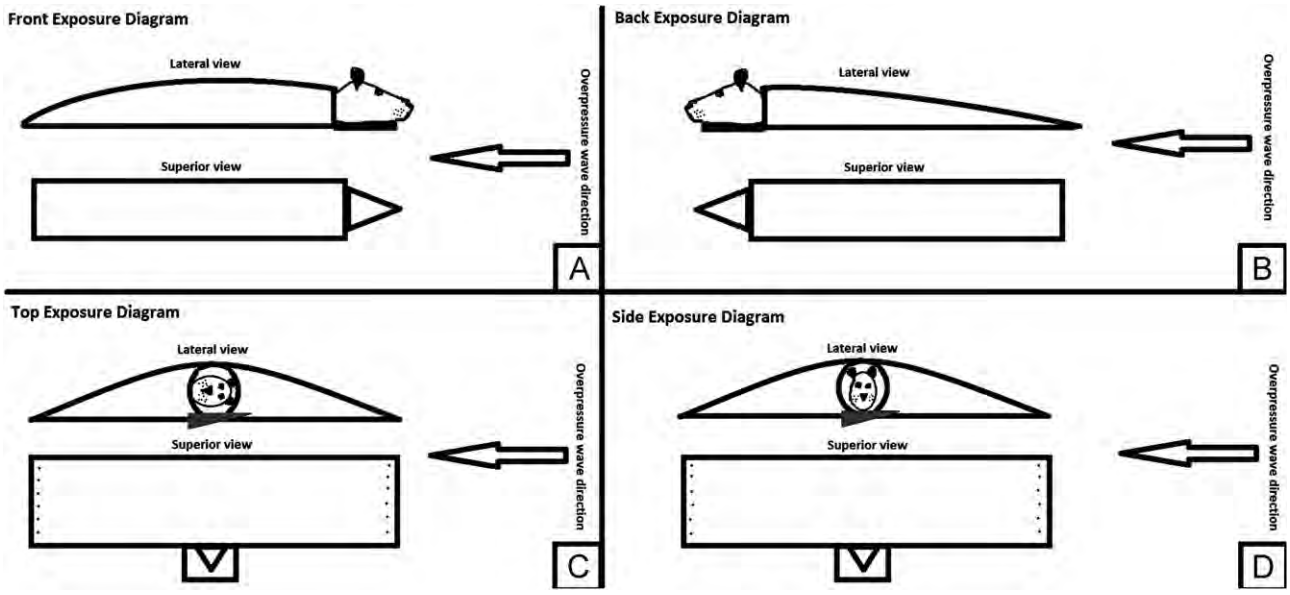

Fig. 4. Representation of the fixtures used in the 4 orientations (superior and lateral views): (A) front; (B) back; (C) top; and (D) side.

Table 1
Sample of data collected in animals in groups 1 (rat D) and 2 (rat E).

Group/ Rat	Orientation	Trial #	Peak pressure (kPa)	Peak rate (kPa/ms)
1/D	Front	1	86.3	870.6
		2	78.2	656.8
		3	79.1	770.6
	Side	1	61.2	412.0
		2	69.9	467.6
		3	69.9	457.8
	Top	1	66.9	833.7
		2	66.7	792.0
		3	66.5	930.0
	Back	1	79.1	436.1
		2	79.3	407.2
		3	83.2	401.5
	Front	4	77.3	863.0
2/E	Front	1	159.4	734.6
		2	157.1	777.6
		3	151.5	698.5
	Side	1	120.5	246.6
		2	117.1	252.3
		3	116.3	267.9
	Top	1	115.6	1344.4
		2	122.5	1327.6
		3	124.9	1708.1
	Back	1	140.0	511.3
		2	145.9	458.1
		3	141.2	427.5
	Front	4	139.6	485.3

unique features that may contribute to varying cellular injury patterns. The averages for peak ICP and peak rate are displayed in Table 2. When quantifying peak ICP, it was determined that significant differences existed due to both size/age and orientation of the rodent at time of exposure (Fig. 8). The pair-wise comparisons of peak ICP for different orientations based on size of the rodent are presented in Table 3. For both sizes of rodents, the average peak ICP at the side orientation is significantly lower as compared to the front and back orientations. For the small rodents, the average peak ICP at the side orientation is also significantly lower than the peak ICP at the top position. The same trend of lower average peak ICP at the side position was found for the large rodents as well, but the difference is not

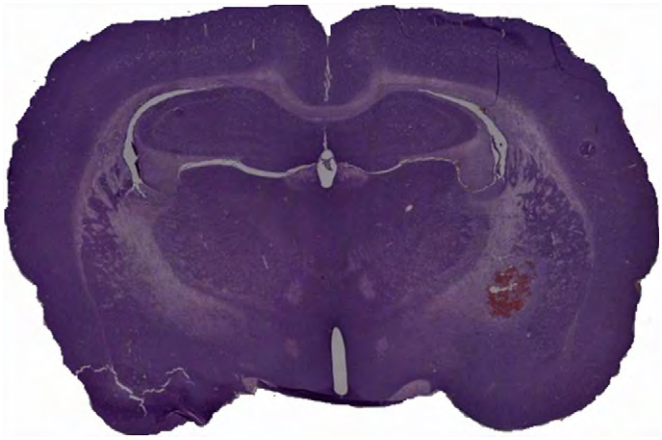

Fig. 5. H&E histological staining of the brain was used in order to determine the position of the ICP sensor in the brain. ICP sensors were found to be located in the forebrain region of the cerebrum.

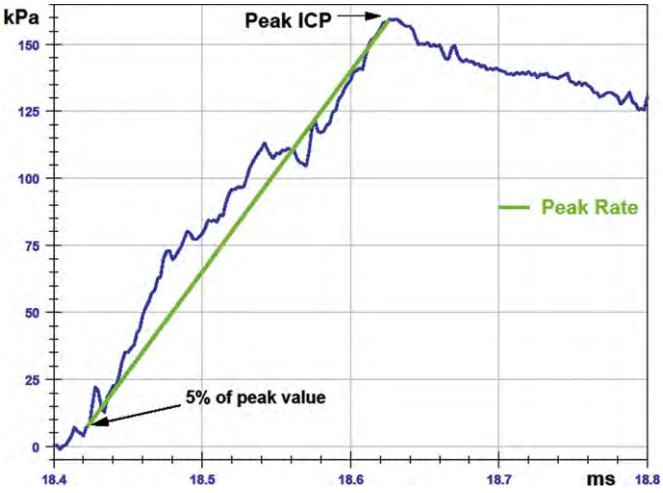

Fig. 6. Quantitative values that were acquired in each test. Peak ICP is the highest pressure value reached within the first 0.3 ms of inception of the ICP profile. Peak rate is the rate obtained from the pressure differential between peak ICP and 5% of the peak ICP over the rise time between these two points.

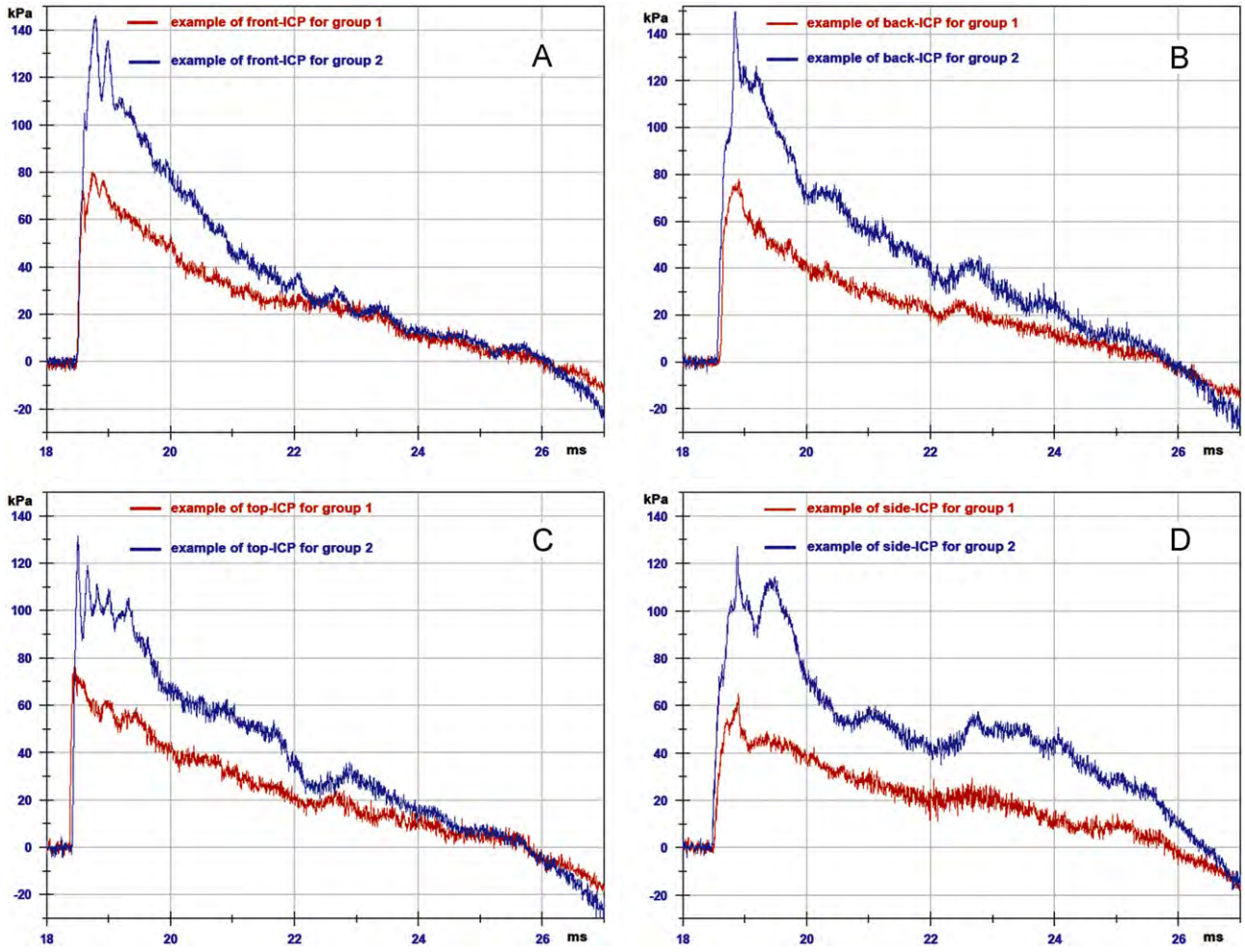

Fig. 7. Examples of ICP profiles for each orientation. Both examples for Group 1 (small rats) and Group 2 (large rats) are shown together. Although the full positive phase of the ICP profiles are provided, this study only focuses on the initial response to loading, which corresponds to the pressure increase to peak value. (A) front; (B) back; (C) top; and (D) side.

Table 2
Averages of data collected for each rat.

Group number/rat	Days old	Rat weight (g)	Cannula length (mm)	Target air overpressure (kPa)	Peak ICP average (kPa)				Peak rate average (kPa/ms)			
					front	side	top	back	front	side	top	back
1/A	68	274	10	70	76.3	69.5	74.4	75.3	660.0	383.7	357.6	373.6
1/B	68	275	10	70	76.0	58.5	71.7	65.9	807.5	320.8	923.4	318.3
1/C	68	273	10	70	74.5	65.2	75.7	72.8	724.7	361.3	646.6	347.5
1/D	68	277	10	70	80.2	67.0	66.7	80.5	790.2	445.8	851.9	414.9
2/E	158	456	14	70	151.9	117.9	121.0	142.4	674.0	255.6	1460.0	465.6
2/F	158	448	14	70	114.3	103.4	133.2	153.1	967.3	709.4	1511.3	530.9
2/G	158	458	14	70	151.7	103.3	113.2	143.2	546.2	428.0	1052.3	471.4
2/H	158	452	14	70	142.5	92.6	148.5	112.7	503.9	344.1	903.5	356.6

statistically significant with the *p-value* being slightly above 0.05. It was also noted that for all orientations, larger rodents have significantly higher peak ICP levels on average compared to smaller rats (Table 4).

Comparisons of peak rate based on orientation and size are given in Table 5 and illustrated in Fig. 9. When looking within each group, the peak rate averages for side and back orientation are similar and lower than the front and top values. Unlike the peak pressure result, the size of the animal does not seem to have as much of an effect of the mean peak rate. For the larger rodents, the average peak rate at the top orientation was significantly higher than the front orientation. As seen in Table 6, the top orientation is the only orientation where the mean peak rate is significantly higher for large rodents compared to small rodents.

Since this testing method required repeated testing on one animal, statistical analysis was used to verify that results were not compromised from the series of tests. Using a nonparametric paired *t*-test, the Wilcoxon Signed-Rank test, the average of the initial three front ICP measurements was compared to the fourth final measurement. The *t*-test indicated that there is not sufficient

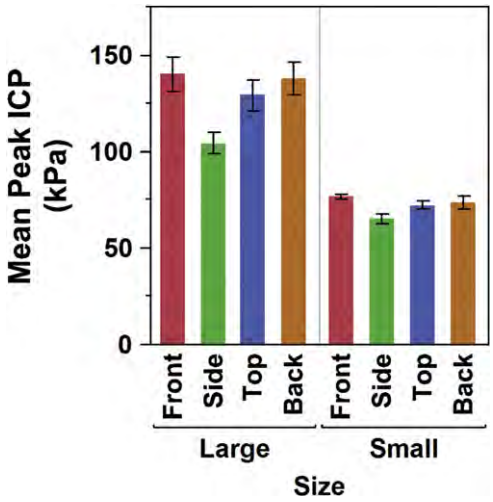

Fig. 8. Peak ICP comparisons across the four orientations for large and small rats. Results demonstrated that for each orientation larger rats had significantly higher peak ICP levels compared to smaller rats. Also in each group the average peak ICP at the side orientation is significantly lower as compared to the front and back orientations. Each error bar is constructed using 1 standard error from the mean and indicates the variability associated with the average peak ICP.

Table 3
Peak ICP comparisons. The estimated difference column is the average difference in peak ICP for two orientations.

	Orientation effect	Estimated difference	Standard error	*p-value*
Large	Front vs. Side	35.78	12.27	0.0171*
	Front vs. Top	11.12	12.27	0.3882
	Front vs. Back	2.26	12.27	0.8580
	Side vs. Top	−24.66	12.27	0.0753
	Side vs. Back	−33.53	12.27	0.0231*
	Top vs. Back	−8.86	12.27	0.4884
Small	Front vs. Side	11.79	2.92	0.0029*
	Front vs. Top	4.71	2.92	0.1405
	Front vs. Back	3.19	2.92	0.3019
	Side vs. Top	−7.08	2.92	0.0381*
	Side vs. Back	−8.60	2.92	0.0162*
	Top vs. Back	−1.52	2.92	0.6149

* $= p\text{-values} < 0.05$.

Table 4
Peak ICP comparisons of orientations for size. For all orientations, larger rodents have significantly higher peak ICP compared to smaller rats.

Position	Estimated difference (Small–Large)	Standard error	*p-value*
Front	−63.26	8.09	< 0.0001
Side	−39.27	8.09	0.0004
Top	−56.85	8.09	< 0.0001
Back	−64.20	8.09	< 0.0001

evidence from the data to suggest a significant difference between the average of the first set of three tests and the last test. Similar conclusions were reached when the peak rate results for front exposures were compared.

4. Discussion

The main goal of this preliminary research was to establish the fundamental phenomenology of shock wave interaction with the rat head in different orientations. This study investigated the initial ICP response of rats with two different size/age groups that were exposed to a simulated free-field blast wave.

Table 5
Peak rate comparisons.

	Orientation effect	Estimated difference	Standard error	*p-value*
Large	Front vs. Side	238.54	65.57	0.0033*
	Front vs. Top	−558.94	115.29	0.0017*
	Front vs. Back	216.70	60.81	0.0086*
	Side vs. Top	−797.49	115.32	0.0002*
	Side vs. Back	−21.85	60.58	0.7297
	Top vs. Back	775.64	128.25	0.0010*
Small	Front vs. Side	364.28	65.57	0.0001*
	Front vs. Top	47.31	115.29	0.6934
	Front vs. Back	378.57	60.81	0.0004*
	Side vs. Top	−316.97	115.32	0.0280*
	Side vs. Back	14.28	60.58	0.8208
	Top vs. Back	331.26	128.25	0.0425*

* $= p\text{-values} < 0.05$.

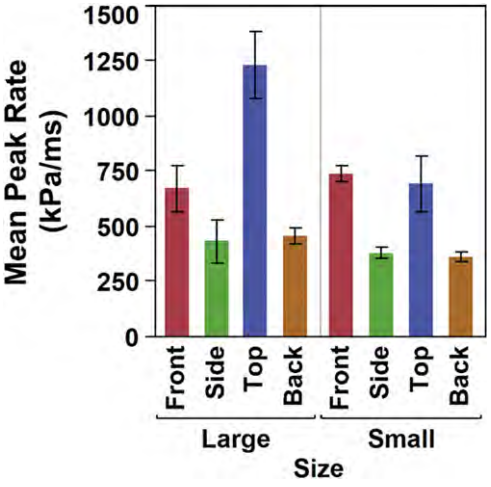

Fig. 9. Peak rate comparisons across the four orientations for large and small rats. Results demonstrated that the top orientation was significantly higher for large rats compared to small rats. Each error bar is constructed using 1 standard error from the mean and indicates the variability associated with the average peak rate.

Table 6
Peak rate comparisons of orientations for size. Only the top orientation has a significant increase in rate from small to large rats.

Position	Estimated difference (Small–Large)	Standard error	*p-value*
Front	69.34	104.63	0.5299
Side	−56.40	104.27	0.6083
Top	−536.91	203.60	0.0397*
Back	−92.53	41.75	0.0676

* $= p\text{-values} < 0.05$.

Gefen et al. (2003) noted that the rat skull thickness increased significantly with age and that aging simultaneously decreased the water content and increased the myelin content of the brain, changing its mechanical characteristics. Dal Cengio Leonardi et al. (2011) proposed that ICP results were linked to the maturity of the rat head, with larger, older rats experiencing higher ICP. Since age directly influences the skull's size and thickness, it was suggested that the skull's dynamics was related to the skull maturity. The current results confirmed that peak ICP values are higher in older, larger animals as compared to the younger group and this outcome held true at all orientations of the head.

Jaslow (1990) proved that sutures have a different response to loading than bone. In particular, sutures can absorb much more energy per unit volume during impact loading. The rat skull is an oblong structure in which sutures are not evenly distributed. It is

reasonable to hypothesize that different biomechanical responses could be excited according to the position of the head in relation to the incident shock front. When examining the peak ICP results in both groups, the side position was found to have significantly lower peak pressures compared to all the other orientations. Currently, it is not clear how the side orientation creates such a different ICP response compared to the other orientations; nonetheless the same outcome is consistent in animals of different maturity. This result seems to confirm the hypothesis that geometry of the skull and location of sutures are important parameters when understanding the stress imparted on the brain by the shock wave. Although different in size, the animals share a geometry that maintains similar proportions and sutures. This finding underscores the importance of skull dynamics in explaining possible injury mechanisms during blast, giving support to the skull flexure theory. Further investigations are needed to explore diverse regions of the brain to verify this finding; however, results from a separate study examined the effect of front and side orientation in a complex shock wave environment and showed a similar decreased ICP response during side exposure (data in preparation).

When analyzing the rate of ICP change, only the top orientation was found to have a significant increase. This outcome indicates that animal maturity has a significant effect predominantly at the superior rat skull. These findings supports what was suggested by Bolander et al. (2011) that the superior rat skull is a location where flexure is exaggerated creating bigger deformations as the bone plates may hinge about the major sutures, also explaining the faster rate results compared to the other orientations.

Additionally, this data set was used to explore possible mechanisms of blast brain injury. The fact that the thorax was shielded in all cases yet high peak ICP values were recorded seems to discount the role of thoracic or "systemic" compression being a major biomechanical mechanism for primary blast TBI. Further, the peak ICP for front exposures are similar to results from another study in which the thorax was not shielded (Dal Cengio Leonardi et al., 2011). The ICP sensor location in relation to the arrival of the shock wave on the skull (coup site) was investigated for each orientation. The sensor positioning in the brain is such that the distance from the coup site is similar in all orientations. However, the front, back and top orientations provide peak ICP values that are comparable and higher than the side. If transosteal propagation were the primary injury mechanism all pressure recordings should be similar. Thus, results from this study discount the role of transosteal propagation. Moreover, in the case of transosteal propagation, the amplitude should be diminished relative to the incident wave by the impedance mismatch, which is opposite to what was recorded. Instead, the skull flexure theory suggests that deformation of the skull can create ICP values that surpass the overpressure of the surrounding environment (Dal Cengio Leonardi et al., 2011). Furthermore, the results of the peak rate analysis point out that the biomechanical response is linked to the particular geometry of the skull and suture lines, which strengthen the support for the skull flexure theory.

This study provides important data and is the first to attempt to quantify the results of orientation, however, there are limitations. It is unknown if FISO pressure sensors are affected by their orientation. Ground breaking work in our lab demonstrated that the sensors did not show sensitivity to orientation when placed in tissue, yet more studies are needed to validate their response to shock waves. A second limitation could be the timeframe chosen for data analysis. The current results focused on the first 0.3 ms of data collected at the initial loading in the ICP-time profile curve. This decision was made to focus the analysis on the initial moments which are suspected to be extremely injurious. However, it is possible that further investigations focusing on different timeframes of the ICP-time profile curve could reveal knowledge that may contribute to a better understanding of the injury mechanism.

5. Conclusions

Results of this study demonstrated a significant increase in ICP for larger rats in all orientations. It also showed a relation between ICP and orientation of the head due to geometry of the skull and location of sutures. These findings accentuate the importance of skull dynamics in explaining the possible injury mechanism during blast. Furthermore, the rate of pressure change confirmed that the initial biomechanical response of the superior rat skull is distinctive compared to other areas of the skull. How the pressure response observed in the rat brain will translate to the human injury is still unknown. Nevertheless, this data provides clues as to how geometry, bone thickness and skull sutures play a role in the pressure transfer. This knowledge can ultimately help understand the injury occurring to the human brain and help design strategies to protect against it.

Conflict of interest statement

No conflicting financial interest exists. This article has been neither published nor submitted for publication, in whole or in part, either in a serial, professional journal or as a part in a book that is formally published and made available to the public.

Acknowledgments

We would like to thank the WSU Bioengineering Center Staff for assisting with this project, and especially Dr. Wu, Mr. Mathie, and Mr. Ritzel. This project was partially funded by the Department of Defense (Award No. W81XWH-08-2-0207).

References

Bhattacharjee, Y., 2008. Shell shock revisited: solving the puzzle of blast trauma. Science 319, 406–408.

Bauman, R.A., Ling, G., Tong, L., Januszkiewicz, A., Agoston, D., Delanerolle, N., Kim, Y., Ritzel, D., Bell, R., Ecklund, J., Armonda, R., Bandak, F., Parks, S., 2009. An introductory characterization of a combat-casualty-care relevant swine model of closed head injury resulting from exposure to explosive blast. Journal of Neurotrauma 26, 841–860.

Bolander, R., Mathie, B., Bir, C., Ritzel, D., VandeVord, P., 2011. Skull flexure as a contributing factor in the mechanism of injury in the rat when exposed to a shock wave. Annals of Biomedical Engineering 39 (10), 2550–2559.

Born, C.T., 2005. Blast trauma: the fourth weapon of mass destruction. Scandinavian Journal of Surgery 94, 279–285.

Cernak, I., Wang, Z., Jiang, J., Bian, X., Savic, J., 2001. Ultrastructural and functional characteristics of blast injury induced neurotrauma. Journal of Trauma 50, 695–706.

Clemedson, C.J., 1956. Shockwave transmission to the central nervous system. Acta Physiologica Scandinavica 37, 204–214.

Clemedson, C.J., Jonsson, A., 1961. Transmission and reflection of high explosive shock waves in bone. Acta Physiologica Scandinavica 51, 47–61.

Courtney, A.C., Courtney, M.W., 2009. A thoracic mechanism of mild traumatic brain injury due to blast pressure waves. Medical Hypotheses 72, 76–83.

Dal Cengio Leonardi, A., Bir, C.A., Ritzel, D.V., VandeVord, P.J., 2011. Intracranial pressure increases during exposure to a shock wave. Journal of Neurotrauma 28, 85–94.

Dal Cengio Leonardi, A., 2011. An Investigation of the Biomechanical Response From Shock Wave Loading to the Head. Ph.D. Thesis. Wayne State University Dissertations, Paper 306, 521 pp.

Gefen, A., Gefen, N., Zhu, Q., Raghupathi, R., Margulies, S., 2003. Age-dependent changes in material properties of the brain and braincase of the rat. Journal of Neurotrauma 20, 1163–1177.

Hicks, R.R., Fertig, S.J., Desrocher, R.E., Koroshetz, W.J., Pancrazio, J.J., 2010. Neurological effects of blast injury. Journal of Trauma 68 (5), 1257–1263.

Hoffman, S.W., Harrison, C., 2009. The interaction between psychological health and traumatic brain injury: a neuroscience perspective. The Clinical Neuropsychologist 23 (8), 1400–1415.
Jaslow, C.R., 1990. Mechanical properties of cranial sutures. Journal of Biomechanics 23 (4), 313–321.
Okie, S., 2005. Traumatic brain injury in the war zone. New England Journal of Medicine 352 (20), 2043–2047.
Romba, J.J., Martin, P., 1961. The Propagation of Air Shock Waves on a Biophysical Model. Armed Services Technical Information Agency, Arlington Hall Station, Arlington 12, Virginia. US Army Ordnance. Technical Memorandum 17–61. Human Engineering Laboratories, Aberdeen Proving Ground, Maryland, pp. 1–25.
Saljo, A., Arrhen, F., Bolouri, H., Mayorga, M., Anders, H., 2008. Neuropathology and pressure in pig brain resulting from low-impulse noise exposure. Journal of Neurotrauma 25, 1397–1406.
Warden, D., 2006. Military TBI during the Iraq and Afghanistan wars. Journal of Head Trauma Rehabilitation 21, 398–402.
Young, M.W., 1945. Mechanics of blast injury. War Medicine 8, 73–81.